Investigating the causal effects of oscillations on intrinsic brain activity

Dissertation
for the award of the degree

“Doctor of Philosophy” (Ph.D.)
of the Georg-August-Universität Göttingen

submitted by
Kathleen Anne Williams

from Tulsa, USA

Göttingen 2018.

Thesis Committee

Prof. Dr. Melanie Wilke (Supervisor & Thesis reviewer 1)
Department of Cognitive Neurology
University Medical Center, Göttingen (UMG)

Prof. Dr. Jens Frahm (Thesis reviewer 2)
Research Group Leader, Head of the Biomedical NMR
Max Planck Institute for Biophysical Chemistry

Dr. Igor Kagan
Decision and Awareness Group
German Primate Center (DPZ)

Prof. Dr. Mathias Bähr
Director
Department of Neurology
University Medical Center, Göttingen (UMG)

Further members of the Examination Board

Dr. Roberto Goya-Maldonado
Systems Neuroscience and Imaging in Psychiatry Lab
University Medical Center, Göttingen

Dr. Arezoo Pooresmaeili,
Group Leader, Perception and Cognition Group
European Neuroscience Institute, Göttingen

I hereby declare that this thesis has been written independently and with no other sources and aids than quoted.

_____

Kathleen Anne Williams

Göttingen

14 of January

2018

Index

Chapter 1

General Introduction

Oscillations are ubiquitous in the human brain, and oscillation-based communication represents an efficient mechanism upon which neural systems could function (Buzsáki and Draguhn, 2004). Frequency bands naturally occur in cortical activity, a phenomenon which has been recorded in mammalian brains, from the rat to the human (Buzsáki and Draguhn, 2004). Thanks to empirical evidence from laboratory experiments as well as clinical cases of neurological insult or dysfunction, some associations have been made between different frequencies and different behaviors or regions of the brain, however no clear relationships have been defined between specific brain functions and the range of frequencies that have been recorded locally and globally in the brain. Additionally, multiple frequencies have been associated with more than one region and more than one task, leaving a bounty of questions to be clarified concerning the mechanisms of frequency-based neural activity and its relationship to cognitive function (Uhlhaas et al., 2008).

As such, the use of transcranial alternating current stimulation (tACS) as a causal intervention to study the role of oscillations in brain function has surged in the last decade and begun to contribute to resolving the relationship between oscillatory brain activity and cognition (Antal and Paulus, 2013). TACS is a noninvasive electrical brain stimulation technique in which a rhythmic current is applied at low amplitudes through one or more electrodes placed on the scalp. It provides a frequency-specific method of exogenously influencing the field potentials of cortical neural networks (Antal et al., 2008; Zaehle et al., 2010). TACS has been shown to modulate sensory perception as well as behavioral performance, ranging from motor to memory (Herrmann and Strüber, 2017). More recently, due to advances in methods overcoming technical challenges, an increasing number of combined tACS-neuroimaging experiments have allowed for analysis of brain signals acquired during stimulation. Examples of combined imaging studies range in complexity from EEG measuring aftereffects of stimulation to simultaneous tACS-functional magnetic resonance imaging (fMRI) to nesting stimulation frequencies in order to measure MEG in a frequency of interest.

The body of experimental evidence shows exciting promise for the use of tACS in researching the roles of brain oscillations and eventually applications in clinical populations with neurospychiatric or neurologic disorders of oscillatory dysfunction. However, comprehensive guidelines of specific applications for its use has not been defined, partially due to lack of clear knowledge of exactly where, how, and when tACS affects the brain. To take knowledge and experience from other brain stimulation techniques, it is clear that there are a number of factors that influence effective brain stimulation (Chew et al., 2015; Ziemann and Siebner, 2015). Physiologically relevant stimulation parameters, state and timing dependence, and variability due to inter- and intra-individual differences are all elements that should be taken into account to elicit desired effects of tACS. It is important to identify the most influential factors and learn to what degree we have control over each of them in order to establish best practices for the successful application of tACS.

The work in this thesis takes advantage of recent advances in neuroimaging technology, brain stimulation techniques, and analysis methods to characterize tACS modulation of intrinsic brain activity measured with fMRI. To give a general overview of the thesis, **Chapter 1** establishes perspective for the experiment by giving an overview of relevant research topics. Three subsections of the general introduction of Chapter 1 explore important topics for the context of the current study, however the introduction is not an attempt to be exhaustive in any topic. The subsections include the following: knowledge supporting the importance of the role of neural oscillations in brain function and human cognition, an explanation of some relevant neuroimaging measurement and analysis techniques that help to define the current state of the fields of intrinsic brain activity and functional connectivity, and a description of notable studies employing noninvasive brain stimulation in oscillations research. **Chapters 2-4** focus on different methods of evaluating changes in intrinsic brain activity measured with fMRI due to different combinations of tACS stimulation frequency (10Hz, 16 Hz, or 40 Hz) and electrode montage (Cz-Oz and P5-P6). **Chapter 5** summarizes the work in a general discussion of the findings of each chapter and their collective context in the current body of literature regarding brain stimulation.

Oscillations in the brain

In 1929, Hans Berger published the first measurements of oscillations in the human

brain, in which he used electroencephalography (EEG) to show a dominant low frequency rhythm around 10 Hz, which he termed the alpha rhythm (Berger, 1929). Since then, researchers have identified multiple patterns of neural oscillatory activity using scalp recordings, which measure the field generated by transmembrane currents of local neuronal populations that represent cyclic changes in their excitability (Thut et al., 2012). In fact, recordings from mammalian brains exhibit oscillatory bands, spanning frequencies from 0.5 Hz to 500 Hz, that are phylogenetically preserved across species (Buzsáki and Draguhn, 2004). In a time-frequency decomposition of neural signals, that is, EEG or low field potentials (LFP), as recorded invasively, the mean frequencies of the oscillatory bands are distributed linearly on a logarithmic scale, thus maintaining a constant ratio between neighboring frequencies (Buzsáki and Draguhn, 2004). Rhythms arising from different neural populations, or networks, have been associated with different brain states, and have been found to coexist or interact in time and space (Buzsáki and Draguhn, 2004; von Stein and Sarnthein, 2000). Additionally, the power density of an EEG or LFP signal is inversely related to the frequency (f). A 1/f power distribution is a well-known characteristic of physical systems of complex oscillator networks (Buzsáki and Draguhn, 2004). The physical architecture of the brain and its speed-limited neuronal communication (e.g., synaptic delays and axon conduction) give rise to a self-organizing system that exhibits properties of neuronal oscillators (Buzsáki and Draguhn, 2004). Justified by these naturally occurring features, considering the brain as a system of neuronal harmonic oscillators allows us to draw many implications from theories and principles of dynamic physical systems.

For numerous reasons, oscillations represent an excellent mode of temporal-based communication. The repeating cycles of their sinusoidal signal provide a recurrent temporal reference frame in which time points of each cycle can be identified by the phase (Thut et al., 2012). Upon the temporal framework, neural elements can code information for coordination and communication. Cell assemblies coordinate through synchrony, that is, in a given temporal window, two signals will interact and an event retained in one signal alters the response of a subsequent event in the other signal (Buzsáki and Draguhn, 2004). Observed as temporal coherence arising across neural networks, oscillation-based synchrony represents the most energy-efficient physical mechanism for temporal communication (Buzsáki and Draguhn, 2004). Different spatial scales of neural integration are related to frequency such that the size of the neuronal

pool determines the period of the signal. This means that cells in short ranges communicate in high frequencies while larger neuronal pools fluctuate together in the low frequency ranges (Kopell et al., 2000; von Stein and Sarnthein, 2000). Oscillations can be exploited to efficiently bind cell assemblies for functional specialization, giving rise to dynamic segregation and integration of necessary neural networks (Buzsáki and Draguhn, 2004).

The 1/f power distribution of the signal implies that low frequency perturbations can cause a cascade of energy dissipation into high frequencies, thus widespread slow oscillations modulate faster local activity (Buzsáki and Draguhn, 2004). On a macroscopic level, networks appear to have phase-governed excitability states, such that cell firing rates increase and decrease on a population level, as the measured membrane potentials decrease and increase, respectively. Importantly, this phase excitability is a dynamic time frame, subject to reset by external stimuli, top-down, or bottom-up processes (Thut et al., 2012). Cross-frequency coupling, or interaction between different frequency bands, is another property of oscillatory communication that the brain exploits through many mechanisms that will further discussed in Chapter 2 (Jensen and Colgin, 2007).

Utilizing these physical characteristics allows for simultaneous multi-scale communication on a temporal and spatial basis (von Stein and Sarnthein, 2000). This dynamic and modular system allows brain regions to interact and synchronize for specific behavioral goals, making oscillations and their synchronization important correlates of neuronal processing (Thut et al., 2012). For different classes of oscillations, there are behavioral correlates preserved throughout mammalian evolution (Buzsáki and Draguhn, 2004). Such universality of these physical principles across scales means that the function of a supporting system likely evolved to select its best-fitting benefits from oscillation-based communication. Binding of cell assemblies for perception, input selection and plasticity, consolidation of learned information, and phase representation of information are each functions utilizing different aspects of oscillatory communication (Buzsáki and Draguhn, 2004). In the following sections, we shift perspectives to brain function and cognition and relay some associations established between neuronal processing and oscillations or synchrony. It should also be emphasized that there is not yet a clear understanding of the role of oscillations and their synchronization in human brain function and cognition.

Oscillations in brain function and cognition

Of the oscillatory bands which currently receive the most focus in neuroscience and human cognition research, we introduce the alpha (8-12 Hz), beta (12-30 Hz), and gamma (>30 Hz) rhythms and include some known cognitive associations or physiological features for each rhythm described (Uhlhaas et al., 2008). We restrict our focus to these three frequency bands, as each range includes one of the stimulation frequencies chosen for the experiments of this thesis (10, 16, and 40 Hz tACS). The scope of this section includes examples of studies from the field that allow us to draw specific relationships between brain function and rhythmic activity.

The alpha rhythm, as the first discovered, is probably the most famous of the brain rhythms. It is generally a prominent peak centered around 10 Hz and its power is known to increase distinctively in the occipital cortex when the eyes are closed (Berger, 1929). Alpha results from the reciprocal interplay of excitatory and inhibitory neurons, its synchronization stabilized by gap junctions among inhibitory neural networks (Hughes et al., 2004; Lörincz et al., 2008). Besides its dominance in the occipital cortex, alpha is also prominent in the thalamus, and cortical alpha appears to result from interactions of re-entrant thalamo-cortical-thalamic networks (Uhlhaas et al., 2008). Such recurrent loop networks and reciprocal interactions support a multitude of theories regarding top-down and bottom-up processing in the brain (Stein et al., 2000). For example, alpha has been demonstrated to be involved in inhibition of task-irrelevent processing and attention (Jensen and Mazaheri, 2010). Alpha shows long range coherence, and has been associated with communication between distant brain regions for facilitation of perceptual and cross-modal binding (von Stein and Sarnthein, 2000). Alpha also has a relationship to external stimuli; by averaging event-related potentials (ERP) it has been demonstrated that alpha is subject to phase-resetting in response to stimuli (Makeig et al., 2002). It is not clear, however, if these measurements capture merely a transient response to stimuli or if the ERPs are superimposed upon ongoing alpha activity (Notbohm and Herrmann, 2016; Sauseng et al., 2007). It has been proposed that there may be more than one alpha rhythm, upon which different functions hinge. For example, the rolandic mu rhythm (7.5-12.5 Hz) has been recorded from the sensorimotor cortex and decreases when a subject is moving or observing movements of others (Muthukumaraswamy and Johnson, 2004; Pfurtscheller and Aranibar, 1979).

Beta rhythms fall between 12 and 30 Hz and are found in all cortical areas as well as

many regions of the subcortex (Uhlhaas et al., 2008). Beta-band activity shows enhanced synchrony prior to motor activity and during steady holds following movement (Engel and Fries, 2010). In Parkinson's disease, the reciprocal desynchronization of beta during movement is abnormal due to impairments in dopamine modulation in the basal ganglia, subthalamic nucleus, and the motor cortex. In addition to movement, beta plays a role in learning , novelty detection, sensory gating, and reward evaluation (Uhlhaas et al., 2008). Alongside other slower frequency bands recorded from the brain, like alpha and theta (4-8 Hz), beta facilitates long range synchrony of neuronal populations (Fries, 2005; Schnitzler and Gross, 2005).

Gamma rhythms, that is, all measurable oscillations faster than 30 Hz, are also found in all brain structures and have been found to be dependent on several neurotransmitter systems (Uhlhaas et al., 2008). Gamma has been measured in the visual cortex during feature binding, or the grouping of different stimulus elements into a coherent object representation (Tallon-Baudry and Bertrand, 1999). This evidence shows the importance of gamma in small neuronal pools for perception, but gamma's role extends to correlations with consciousness, as perceived stimuli induce transient long-range gamma synchronization across separated regions (Rodriguez et al., 1999). Gamma also appears to play an important part in language processing as well as motor coordination (Miltner et al., 1999).

For the sake of brevity, more experimental evidence of oscillatory activity and its functional correlates will be described as discovered through brain stimulation techniques.

Intrinsic oscillations and functional connectivity (measured with neuroimaging)

In conjunction with the rise in attention to brain oscillations, the neuroimaging community has shifted attention from merely averaging event-related evoked responses to investigating underlying oscillatory activity and its interaction with external stimuli. Measuring spontaneous fluctuations of brain signals, that is, when the brain is not actively engaged in a specific task, allows for quantification of intrinsic activity (Gusnard and Raichle, 2001). Ongoing oscillations can be analyzed to better understand the brain's neural networks and their dynamic interactions with both internal and external activity. Using whole-brain imaging techniques, long-range interactions, or

coherence, of intrinsic brain fluctuations can measure functional connectivity (FC) of neural networks. Functional connectivity is a term used to describe temporal synchrony between signals of spatially distinct areas of the cortex (K. J. Friston et al., 1993). As oscillatory synchrony represents an efficient method of communication for harmonic oscillators, which characterize some physical properties of neural networks, there is much motivation to quantify FC using neuroimaging tools such as EEG, MEG, and fMRI (Cabral et al., 2011; Stam et al., 2007). Although EEG and MEG measure brain signals at acquisition speeds of the cortical oscillations which we have described in the previous section, measuring intrinsic brain activity with fMRI offers insight for the physiological effects of tACS. The temporal resolution of fMRI and the hemodynamic changes that it measures are limited to the range of seconds, but as we describe in the following section, blood-oxygenation-level-dependent (BOLD) activity fluctuations remain physiologically relevant in the study of the role of cortical oscillations (Nir et al., 2007; Ogawa et al., 1990). First, for the case of relevance to this thesis combining tACS with task-free fMRI, it is important to understand some of the quantification and analysis techniques that allow us to draw conclusions regarding brain activity using resting-state fMRI measurements. Then, we bridge these lower temporal resolution measurements to the faster oscillations described in the previous section by relating EEG and MEG measures to fMRI measures as elucidated from recent studies.

Though functional connectivity studies originate from positron emission tomography (PET), the promise of resting-state studies for widespread applications arose through scientific advances in MRI techniques: faster acquisition methods paired with the discovery of the metabolism-mediated BOLD contrast (K. J. Friston et al., 1993). The BOLD effect was introduced for use as a functional imaging tool because the signal fluctuation varies in a correlative fashion with neural activity mediated through blood-oxygen metabolism (Ogawa et al., 1990). Magnetic resonance signal intensity fluctuations of about 2% in the brain during periods of rest were observed, and these fluctuations, found in the lower frequencies around 0.08 Hz, are presumed not to be associated with system noise or cardiac or respiratory peaks. In a later study, Bharat Biswal analyzed the low-frequency oscillations in voxels from the two hemispheres of the motor cortex of a resting human brain, finding temporal correlations between them and other remote areas also believed to be associated with motor function (Biswal et al., 1995). A number of resting-state FC studies followed revealing evidence of connectivity

within additional known functional-anatomical networks of the brain, such as the somatosensory and visual cortices (Cordes et al., 2000; Lowe et al., 1998). In addition to these functionally defined networks that cooperate during specific behaviors, resting-sate fMRI experiments unveiled a network in the brain that becomes more active during the task-free periods. Furthermore, this “default mode” network (DMN) is anticorrelated to networks that are task positive and often attention driven. The BOLD signal underlying FC has neurophysiological origin (Logothetis, 2003; Logothetis et al., 2001; Nir et al., 2007) and the spatially distant but synchronous regions are found to be structurally constrained using diffusion tensor imaging (DTI), which is an MRI technique that allows reconstruction of white matter tracts (van den Heuvel et al., 2009; Honey et al., 2009). Application of analysis methods beyond a simple correlation has led brain mapping with resting-state fMRI to contribute a bounty to knowledge about brain function, synchrony, and organization in health and disease.

Initially in fMRI, the primary statistical approach to functional connectivity studies was seed-based cross correlation. Cross correlation analysis begins with selecting a set of voxels, or a seed, from a hypothesis-motivated region of interest (ROI) of the brain in the image sequence. A Pearson's correlation is then computed between the average time series of that seed and time series of each other voxel in the brain. Alternatively, employing model-free analysis methods rather than the simple pairwise cross correlation allows for data-driven analysis without the need for a priori hypotheses. Independent component analysis (ICA) is an example of a model-free signal decomposition method that, when applied in a group fashion, has identified as many as ten consistent and reliable RSNs that can further divide into sub-networks (Beckmann et al., 2005; Damoiseaux et al., 2006; De Luca et al., 2006). Chapter 2 of this thesis explains the application and findings of ICA analyses in more detail. More recently, multivariate methods for characterizing higher order global organization and dynamics include graph theory techniques (van den Heuvel and Hulshoff Pol, 2010; Park and Friston, 2013; Sporns, 2013). We have presented evidence for oscillation-based functional segregation and integration of the brain for information transmission. These physical properties of harmonic oscillators that are employed for synchrony between neurons give rise to complex self-organizing networks (Sporns, 2013; Sporns et al., 2004). Graph theory uses mathematical principles to describe global and local properties of a network comprised of a set of nodes and their interactions. The application of graph

theory principles to brain networks has led to a number of discoveries about the topological properties of brain structure and function in health as well as disease (Sanz-Arigita et al., 2010; Stam, 2014). In chapter 4 of this thesis, we explore graph theory in further detail.

Aside from quantifying FC between spatially distant regions in the brain, measures of local brain activity can also be computed with resting-state fMRI data. Regional homogeneity (ReHo) measures the functional coherence between a voxel and its nearest neighbors (Liu et al., 2008; Zang et al., 2004). The spatial patterns of resting-state ReHo maps closely resemble those of resting-state PET studies, with corresponding regions that deactivate during tasks (Liu et al., 2008; Raichle et al., 2001). Another local measure of brain activity that can be computed from resting-state fMRI data is the amplitude of low frequency fluctuations (ALFF). ALFF measures the regional intensity of the spontaneous fluctuations in the slow (~0.01-0.08 Hz) frequency range that constitutes most of the neurophysiologically relevant temporal coherence of FC (Yu-Feng et al., 2007). Computed as the square root of the mean power spectrum in the low frequency band, ALFF and its normalized version fractional ALFF (fALFF) shows increased activity during rest in localized regions corresponding to those in the DMN (Yu-Feng et al., 2007; Zou et al., 2008). Both ReHo and f/ALFF have been applied in studies with clinical populations, with differences from healthy populations found in agreement with those found with other neuroimaging techniques employing robust local measures of brain activity (Liu et al., 2008; Yu-Feng et al., 2007; Zou et al., 2008).

Further evidence of the neurophysiological underpinnings of intrinsic activity measured with fMRI allows for making valid associations between fast brain oscillations and whole brain neural dynamics. Additionally, any definitive relationships between specific frequency bands and resting-state fMRI measures motivate the ability to capture meaningful tACS-induced modulations of spontaneous BOLD activity. Combining information from resting-state fMRI with EEG or MEG through either separate or simultaneous measurements, a number of studies have attempted to rectify the spatial and temporal scale differences between modalities to understand how high frequency neural activity correlates to resting-state BOLD signal fluctuations (Deligianni et al., 2014; Mantini et al., 2007; Tagliazucchi et al., 2012). This question can be approached in multiple ways, with options to compare measures in either modality on the local, connectivity, or network organization level. Some example studies relating EEG/MEG

frequencies to intrinsic BOLD activity on different levels are outlined below, however the topic will be covered more thoroughly in Chapter 2. Overall, the most information relating EEG and MEG activity to spontaneous BOLD fluctuations is in the alpha range, likely due to its prominent history in the field.

To derive EEG/MEG relationships arising from localized BOLD activity, power from the different frequency bands has been correlated with BOLD signal fluctuations. In EEG-informed fMRI studies, alpha power has been negatively correlated with the BOLD signal in the occipital (DiFrancesco et al., 2008; Goldman et al., 2002; de Munck et al., 2007), temporal (Goldman et al., 2002), parietal (Laufs et al., 2003; de Munck et al., 2007), and frontal cortices (Goldman et al., 2002; Laufs et al., 2003). When comparing BOLD fluctuations to lower alpha (8.5-10.5 Hz) global field synchronization, which measures zero phase-lag correlations between electrodes, Jann and colleagues found positive correlations in the anterior and posterior cingulate cortices as well as orbitofrontal and parietotemporal regions, whereas negative correlations were found with superior frontal gyrus, insula, supramarginal gyrus, and supplementary motor areas (Jann et al., 2009). These regions correspond to anatomical nodes of the DMN. Upper alpha (10.5-12.5 Hz) was found positively correlated with regions belonging to the task-positive dorsal attention resting state network (Jann et al., 2009). In regard to other EEG rhythms and their relationship to spontaneous BOLD activity, Laufs and colleagues employed a general linear model using occipital theta, alpha, and beta power as predictors and found positive correlations between beta (17-23 Hz) power and the DMN (Laufs et al., 2003). Another study relating RSN-specific BOLD fluctuations to EEG power included global averages of delta, theta (4-8 Hz), alpha (8-13 Hz), beta (13-30 Hz), and gamma (30-50 Hz) bands (Mantini et al., 2007). Each of the six RSNs considered was found to have a specific electrophysiological signature combining all frequencies (Mantini et al., 2007). In simultaneous intracranial electrophysiology and fMRI experiments in monkeys, spontaneous BOLD fluctuations were most informed by alpha, beta, and gamma band LFP power to be informative about low frequency, with gamma contributing to both amplitude and latency of the signal (Magri et al., 2012).

At the level of functional connectivity, several studies have correlated the strength of interaction between regions measured with resting-state fMRI to EEG or MEG band power. In a simultaneous EEG-fMRI study that focused on visual cortex FC, alpha

power increases were found to be correlated to decreased connectivity between the visual cortex and regions in the occipital cortex, decreased connectivity between visual cortex and anterior-medial thalamus, and decreased connectivity between visual cortex and ventral-medial prefrontal cortices (Scheeringa et al., 2012). Simultaneous EEG-fMRI has also revealed negative alpha power correlation to FC between subcortical areas, primary, and association cortices and positive gamma power correlation to FC within primary, subcortical, and association networks (Tagliazucchi et al., 2012). In a study investigating RSN FC, both within and between networks, alpha power was found negatively correlated connectivity between the dorsal attention network (DAN) and DMN (Chang et al., 2013). Using seed-based correlation analysis for fMRI and MEG data for comparison, de Pascuale and colleagues found theta, alpha, and beta band connectivity to inform resting-state fMRI connectivity (Pasquale et al., 2010). Spatial agreement between MEG FC and and fMRI connectivity has been shown, with the closest resemblance between the two modalities occurring in the beta band (Brookes et al., 2011). In a study using inctracranial surface electrode recordings in humans, Hacker and colleagues measured the spatial correspondence between RSNs and band-limited electrophysiology power. They found widespread gamma band power correspondence throughout the brain. Stronger specific correspondence was found for theta power in DMN and fronto-parietal control networks as well as alpha in the somatomotor and dorsal attention resting state networks (Hacker et al., 2017).

Finally, graph theory measures offer insight about network organization. Using simultanously acquired data, Deligianni and colleagues compared connectivity networks, or connectomes, between fMRI and EEG across frequency bands, found that the connectomes derived from delta, theta, and alpha rhythms best resembled fMRI connectomes (Deligianni et al., 2014). Through adding nonlinear and cross-frequency interactions of MEG data into a predictive model for fMRI-based RSNs, Tewarie and colleagues demonstrated that it is likely that BOLD FC does not simply rely on specific electrophysiology power bands, but is comprised of overlapping connectivity profiles in the brain, spread across frequency bands (Tewarie et al., 2016).

The studies mentioned above illustrate a relationship between EEG and MEG frequency power and intrinsic BOLD fluctuations, with the strongest indication that low frequency bands, especially alpha, most closely relate to fMRI connectivity, mostly in the occipital regions. There are an increasing number of studies employing multi-modality

measurements of spontaneous neural activity and inspecting different aspects of agreement between them, from local activity to network organization, from stationary to dynamic (Foster et al., 2016; Pasquale et al., 2010). In Chapter 1, we discuss in greater detail the associations between spontaneous BOLD activity and electrophysiological measures.

Researching oscillations through perturbing the network – brain stimulation

It is clear that functionally relevant rhythms pervade throughout the human brain, but it also stands to say that the exact relationships between brain oscillations and their functions are not entirely understood. We have discussed that oscillations represent excitability states of neurons on a local scale, that their physical properties allow for multi-scale modulation of signal gating and communication, and that they play a role in organization and plasticity of neuronal networks. We also know that oscillations play a role in many different behavioral and cognitive functions. Through specific interference with oscillatory activity, causal interventions allow for delineating clearer associations between the brain's function and its rhythms(Herrmann and Strüber, 2017). Noninvasive, rhythmic brain stimulation is an ideal tool for investigating the role of oscillations in human brain function (Thut et al., 2017). Accomplished through various possible mechanisms, controlled intervention of brain oscillations is possible using frequency-specific noninvasive techniques such as transcranial magnetic stimulation (TMS), transcranial electrical stimulation (TES), or even rhythmic sensory inputs, like flashing light (Schutter and Wischnewski, 2016). A number of studies employing noninvasive brain stimulation in healthy populations have shown causal evidence implicating specific rhythmic activity for specific functions, as we describe in the following paragraph. Afterwards, we narrow focus to tACS, introducing what it is, in terms of controllable parameters, and then presenting evidence of what we know about its effects and mechanisms, as gathered from recent studies.

The overall goal of enhancing or driving neural oscillations through a periodic external drive is known as entrainment. Given the multiple mechanisms of oscillatory communication, there are various ways to use noninvasive brain stimulation to interact with ongoing neural oscillations, with targets either behaviorally associated or derived using neuroimaging methods. Entrainment, or phase-coupling the intrinsic frequency to

an external rhythm, can be achieved through the use of pulsed discrete events or continuous repeating waveforms (Thut et al., 2017). TMS uses current induction through a coil placed over the scalp to produce electromagnetic pulses in the brain with high spatial specificity. Studies employing repetitive (or rhythmic) TMS (rTMS) can time pulses to endogenous oscillations or behavioral stimuli. Motivated by links between individual peak alpha frequency and memory performance and the fact that task-related alpha desynchronization depends on resting alpha amplitudes preceding task performance, Klimesch and colleagues applied rTMS to the mesial frontal and right parietal cortices of subjects at their own individual alpha frequency (IAF) during the reference interval of a mental rotation task (Klimesch et al., 2003). RTMS applied at IAF was found to enhance cognitive performance, and additionally, EEG measured a large event-related desynchronization prior to improved performance. Explained through successful manipulation of alpha power in the reference period relative to the test period, the results of this experiment implicate the functional relevance of alpha oscillations in implementing cognitive tasks. To investigate the causal relevance of beta desynchronization in memory formation, Hanslmayr and colleagues used combined EEG-TMS to apply TMS to the inferior frontal gyrus at different frequencies during memory encoding, and found selective encoding impairment with beta (18.7 Hz) stimulation, but not with that in other other frequency bands (theta, 6.8 Hz and alpha, 10.7 Hz) (Hanslmayr et al., 2014). Additionally, EEG measures showed only beta stimulation to induce an entrainment echo, which outlasted the stimulation period by about 1.5 seconds. In another study, applying 20 Hz rTMS to the dorsolateral prefrontal cortex during a working memory task produced differential effects between healthy subjects and patients with schizophrenia (Farzan et al., 2012). In the patients, accompanying improved cognitive performance, EEG measurements showed that the beta stimulation reduced excessive gamma inhibition associated with a working memory task. This study demonstrated both the presence of dysfunctional gamma oscillations during working memory in schizophrenia and the ability to indirectly modulate brain activity in frequency bands with stimulation through cross-frequency coupling mechanisms. Jaegle and colleagues used rTMS to the posterior parietal cortex (PPC) or the occipital cortex at 10 Hz paired with simultaneous EEG recording during a visual perception task to demonstrate entrainment of alpha activity that induced a phase-specific enhancement of target detection (Jaegle and Ro, 2013). Together, these studies show compelling evidence connecting frequency-specific, phase-specific, and cross-

frequency mechanistic properties of neural oscillations to particular cognitive functions in health as well as disease. With frequency-specific behavioral consequences of stimulation as well as measured causal effects measured with EEG reflecting entrainment, the studies represent the tremendous potential of going beyond mere brain-behavior correlations by using combined rhythmic stimulation and neuroimaging alongside behavioral readouts.

tACS

While rTMS can successfully entrain neural networks with pulsed, supra-threshold stimulation of the brain, recently there is increasing use of continuous, low amplitude current stimulation through the scalp to influence field potentials of neurons below their firing threshold with TES (Antal et al., 2008). The family of non-invasive electrical stimulation techniques includes tACS, transcranial direct current stimulation (tDCS), transcranial random noise stimulation (tRNS), and oscillatory tDCS (otDCS), in which the amplitude of a direct current is slowly modulated with a sinusoidal offset (Anna Fertonani and Carlo Miniussi, 2017). In the following discussion, we focus on tACS, first describing setup and implementation, then laying out behavioral and neuroimaging evidence of its effects, and finally addressing outstanding questions regarding mechanisms of its effects.

Applying tACS

To begin with, tACS is a technique with properties that vary across applications. Stimulation usually consists of a battery-operated machine programmed to output a sinusoidal current, meanwhile modulating voltage in relation to impedance changes measured between two or more electrodes placed on the scalp (Antal and Paulus, 2013). As the timing aspect of tACS presents its greatest strength, timing parameters are likely the most important to consider when considering desired effects of tACS. As with all rhythmic stimulation, investigations of oscillatory communication can be based on interaction with power in a chosen frequency band or on the phase relationships between signals (Thut et al., 2017). Phase experiment design can be considered through the relative timing of two signals, whether the stimulation signal phase relates to another stimulator-generated signal (Polanía et al., 2012), the presentation of stimuli (ten Oever et al., 2016), or to instrinsic oscillations (Gharabaghi et al., 2014). Experiments testing

both frequency and phase relationships of stimulation will be discussed in greater detail in the following section. Considering timing of stimulation, it should additionally be noted that measured effects of rhythmic stimulation can be categorized as online, or immediate effects of stimulation, and offline, or after-effects of stimulation. There is discussion and research about the mechanisms of action that support each of these two aspects of stimulation effects, and whether the mechanisms for each are different (Notbohm and Herrmann, 2016; Romei et al., 2016; Veniero et al., 2015). Namely, the question is whether online effects are generated through entrainment, stochastic resonance, or simply the super-position of transient steady state evoked potentials (SSEP) over ongoing oscillatory activity (Notbohm et al., 2016; Veniero et al., 2015). Following that, how does entrainment interact with intrinsic networks offline to produce plasticity-induced changes, either through long-term potentiation or long-term depression (Veniero et al., 2015; Vossen et al., 2015; Zaehle et al., 2010)? For both questions, it is likely that there are contributions from multiple mechanisms, and determining which we can best interact with through brain stimulation would help to optimize tACS effect specificity (Veniero et al., 2015).

In addition to the critical timing-specific parameters, tACS experiment design includes choosing the type and number of stimulation electrodes, choice of electrode montage, and stimulation intensity. Electrode types vary in materials and include saline-soaked sponges, rubber, solid gel, and silver chloride. Except for the sponges, electrodes are typically applied with various types of conductive gel in order to facilitate current flow from the electrodes to the scalp. Electrodes vary in shape and size, both of which strongly effect direction of current flow through the head, and should be chosen appropriately (Opitz et al., 2015). Electrode montage describes the number and placement of electrodes on the scalp. An electrode montage can be comprised of two electrodes, which would be anti-phase during tACS, to mulitple-electrode montages that allow greater manipulation of stimulation phase timing through the use of multiple stimulation waves or return electrodes. By adding a third return electrode, two regions can be stimulated in-phase (Polanía et al., 2012). Additional electrodes allow for higher spatial specificity and targeting stimulation to multiple regions in various phases relative to one another (Helfrich et al., 2014a). Placement of the montage over functionally-identified regions of the brain typically will induce high electric field in cortical regions below electrodes, however the use of finite-element method simulation

models, which we discuss further in the body of this thesis, has proven to be useful and accurate in predicting field spread induced by transcranial brain stimulation (Neuling et al., 2012; Opitz et al., 2013; Ruffini et al., 2014; Thielscher et al., 2015). A framework has been proposed to categorize tDCS montages into four groups, including unilateral, bilateral, and midline, and dual channel, which further subdivide into 12 subgroups, based on features of the targets, such as symmetry or direction of current flow (Nasseri et al., 2015). Though anode/cathode labels specific to tDCS electrodes would not carry over, and phase and frequency relationships should be described for standardizing tACS, such a classification serves as an applaudable effort to standardize experimental design and allow for easier consolidation of findings across studies when specific regimes are maintained.

Stimulation is usually applied with current amplitudes in the range of 1-2 mA, peak-to-peak. With high enough stimulation strengths, TES induces phosphenes, or temporary perception of flickering light, as well as cutaneous sensations such as tingling, or burning in extreme cases (Antal and Paulus, 2013). For tACS, both phosphene and somatosensory perception vary in a frequency- and intensity-specific manner (Turi et al., 2013). For this reason, it is common to assess the sensation thresholds associated with tACS to determine stimulation strengths that are undetectable for each subject in the study. Aside from temporary dizziness or perception of pressure or burning, no persistent adverse effects due to tACS have been found (Matsumoto and Ugawa, 2017).

Behavioral evidence of tACS effects

One of the first studies to present promising evidence of tACS as a method to modulate behavior in a frequency-specific manner showed that stimulation of the primary motor cortex with 10 Hz, but not other frequencies (1 Hz, 15 Hz, 30 Hz, 45 Hz), improved response times of healthy subjects in an implicit motor learning task (Antal et al., 2008). Following this study, an increasing number of studies have built a substantial body of evidence that tACS is a reliable method for frequency-specific brain-behavior modulation in motor performance, perception, and cognitive domains. Another study stimulating the motor cortex during a visuomotor task showed beta range (20 Hz) tACS to slow voluntary movement in healthy subjects (Pogosyan et al., 2009).

As already mentioned, tACS effects perception in a frequency-specific manner. Feurra and colleagues demonstrated that stimulation over the primary somatosensory cortex of

subjects induces tactile sensation in the contralateral hand for physiologically relevant frequencies within alpha and gamma ranges, and to a less degree with beta band tACS (Feurra et al., 2011). Another early study of phosphene perception importantly showed that modulation due to tACS depends on ongoing brain activity in addition to stimulation frequency (Kanai et al., 2008). To evaluate tACS-induced perception changes in relation to differences in baseline, Kanai and colleagues stimulated the occipital cortex of healthy subjects with frequencies ranging from theta to gamma in either dark or light conditions. In light conditions, tACS resulted in increased subjective ratings and decreased threshold measurements of phosphenes with beta stimulation, while in dark conditions, phosphene perception was modulated in a similar way, but with alpha tACS.

While there has been some controversy about whether phosphenes perceived during tACS are generated through retinal stimulation rather than cortical stimulation (Schwiedrzik, 2009), studies modulating higher cognitive functions correlated to specific frequency bands suggest tACS successfully modulates cortical computations. In an investigation of the lateralization of theta-band oscillatory balance in the prefrontal cortex and its involvement in risk-taking behavior, Sela and colleagues showed theta tACS applied to the left hemisphere, but not the right, to increase risky choices in volunteers (Sela et al., 2012). Interhemispheric gamma-band coherence as a mechanism for motion perception was demonstrated in a study in which bi-hemispheric tACS was applied to occipito-parietal cortices either phase-matched or with a 180-degree phase difference (Strüber et al., 2014). Anti-phase 40Hz tACS increased vertical motion versus horizontal motion perception in an ambiguous stimulus perception task, while 6 Hz tACS and in-phase 40 Hz tACS had no effect on motion perception. Applying tACS at frequencies belonging to theta, alpha, beta, and gamma bands during performance of a visuospatial abstract reasoning task that gauges fluid intelligence, Santarnecchi and colleagues found that only 40 Hz tACS selectively enhanced performance specifically in more complex logic-related tasks, indicating the importance of gamma activity in higher-order cognition (Santarnecchi et al., 2013). Each of the previous studies demonstrates the ability of tACS to modulate behavior in a frequency-specific manner. Pairing tACS with neuroimaging techniques allows for investigation of the neurophysiological underpinnings of tACS effects. It follows that the ability to measure causal influences of tACS on brain activity that accompany behavioral modulation is of

critical importance to close the loop of brain-behavior oscillation relationships.

Neuroimaging evidence of tACS effects

Measuring tACS-induced modulation of brain activity is important for determining exactly how the stimulation interacts with neural oscillations to give rise to behavioral effects. Using electrophysiological measurements in combination with electrical stimulation is a technical challenge regarding stimulation-induced artifacts generated in the measured signal, especially in frequencies of interest (Herrmann and Strüber, 2017). However, recent advances in the field of artifact removal have allowed for an increasing number of EEG and MEG studies to make interesting findings about interactions of tACS with oscillatory activity (Dowsett and Herrmann, 2016; Neuling et al., 2017). Additionally, despite the temporal resolution mismatch between stimulation and measurement, combined tACS-fMRI studies have been equally informative about tACS effects on brain activity. In this section, we highlight notable studies combining neuroimaging methods with tACS to probe oscillatory activity.

Some of the first evidence of tACS interacting with brain oscillations was demonstrated measuring EEG activity immediately following ten minutes of tACS applied at IAF bilaterally to (Zaehle et al., 2010). Compared to subjects receiving sham stimulation, post-stimulation EEG measured an increase in subjects who were stimulated at their IAF. Demonstrating successful removal of tACS artifact in simultaneously acquired EEG signal, Helfrich and colleagues measured alpha band power to increase during 10 Hz tACS applied to the occipital cortex (Helfrich et al., 2014b). Additionally, target stimuli presented at different phases of the tACS signal were detected in a phase-dependent manner, implying a causal role for alpha oscillations in visual perception. In a following study, the same group employed bi-hemispheric high-definition tACS with simultaneous EEG to show that in-phase gamma tACS applied to occipito-parietal cortices was found to increase hemispheric coherence while anti-phase tACS decreased it (Helfrich et al., 2014a). Hemispheric synchrony modulation due to tACS was correlated to accompanying perceptual changes in an ambiguous motion task. To investigate cross-frequency-coupling mechanisms of oscillatory function, Alekseichuk and colleagues recorded EEG before and after simultaneously delivering two tACS waveforms at frequencies in the theta and gamma bands during a spatial working memory task (Alekseichuk et al., 2016). Timing of the waveforms was designed in a

cross-frequency-coupling protocol, with gamma stimulation superimposed on the trough or the peak of the theta stimulation wave. When gamma stimulation was coupled to the peak of theta waves, working memory performance improved and functional connectivity was found to be increased after stimulation.

Using beamforming reconstruction techniques, Neuling and colleagues demonstrated that MEG recordings during tACS can be successfully reconstructed even at the frequency of stimulation (Neuling et al., 2015). Source space signal showed an increase in alpha power in the occipital cortex after 10 Hz tACS that could not be detected when analyzed in sensor space. Beamforming techniques applied to MEG data acquired during tACS applied at IAF in subjects with eyes closed and eyes open conditions demonstrated state-dependency of tACS (Ruhnau et al., 2016). Amplitude modulation of tACS, by using a fast carrier frequency with an amplitude envelope waveform of the desired stimulation frequency, has also proven a novel method for reliable mapping of tACS entrainment, as demonstrated with simultaneous tACS-MEG experiments (Witkowski et al., 2016).

Combining tACS with fMRI offers whole brain imaging with high spatial resolution, and tACS does not produce artifacts detrimental to the measured BOLD signal (Antal et al., 2014). Applying IAF tACS to the occipital cortex concurrently during a visual vigilance task, Vosskuhl and colleagues showed a task-related BOLD response reduction in tACS periods compared to stimulation-free baseline periods (Vosskuhl et al., 2016). Given the inverse relationship between BOLD signal and alpha amplitude, the response reduction was interpreted as an alpha increase in the occipital cortex. Simultaneous tACS-fMRI has also provided supporting evidence that effects of tACS are task- , intensity- , and frequency-dependent (Cabral-Calderin et al., 2016a). Cabral-Calderin and colleagues also showed in their study that the greatest effects of tACS are not always directly below the electrodes, but sometimes in regions distant from the electrodes, implying network modulation through functional connectivity. More recently, using simultaneous tACS-fMRI, Violante and colleagues demonstrated tACS-induced enhancement of working memory performance that correlated with increased activity in the parietal cortex (Violante et al.). The study also showed tACS effects to be dependent on relative phase of stimulation and cognitive demand, highlighting the role of phase synchronization in cognition.

Animal and computer models of tACS effects

Experimental findings outlined from the human studies above help to make a clear association between neural oscillations and behavior through causal interactions. However, in order to elucidate putative mechanisms of tACS and its effects, direct measures of neural activity are limited to clinical cases in humans. Supporting evidence of tACS-induced modulation of oscillations can also be taken from animal and computer modeling studies investigating the effects of exogenous oscillations on neural networks. Although direct comparisons cannot usually be made between animal studies reporting voltage gradients and studies in humans reporting noninvasive measurements, animal studies as well as simulations offer insight about parameters required for successful entrainment as well as the mechanisms of sinusoidal stimulation effects.

Applying weak sinusoidal electric fields to in vitro slices of rat cortex during recordings, Fröhlich and colleagues characterized interactions of endogenous network activity with stimulation (Fröhlich and McCormick, 2010). Field applied at strength matching in vivo endogenous measurements entrained slow cortical oscillations, demonstrated through an acceleration of oscillations during stimulation and small depolarization in the membrane potential (Fröhlich and McCormick, 2010). Activity in the network modulated interactions of endogenous activity with applied fields, theoretically through positive and negative feedback loops between neuronal activity and intrinsic field potentials, adding evidence of state dependency of stimulation effects (Fröhlich and McCormick, 2010). Another group simulated a large-scale network of spiking neurons, and confirmed their findings with multichannel extracellular recordings of multiunit firing activity in anesthetized ferrets (Ali et al., 2013). They found phase-locking to occur fastest when stimulation is aligned to the peak of intrinsic oscillations and sparse global stimulation to more effectively entrain networks than localized stimulation (Ali et al., 2013). Hyperpolarizing-only stimulation was more effective than depolarizing-only stimulation, which may be related to the fact that inhibitory networks are more easily effected by stimulation than excitatory ones, which may be attributable to the cellular morphology in the cortex (Ali et al., 2013). Importantly, stimulation effects were nonlinear in a frequency and intensity-dependent manner, characterized by an Arnold tongue, which predicts the degree of success of entrainment of a signal based on its intrinsic oscillating frequency (Ali et al., 2013). For further information regarding the Arnold tongue, see Chapter 3. In vivo experiments

measuring intracellular and extracellular activity in the cortex and hippocampus of anesthetized rats applied slow frequency (0.8, 1.25 or 1.7 Hz) stimulation through the surface of the skull (Ozen et al., 2010). Transcranial stimulation was found to reliably entrain neurons throughout the brain with voltage gradients as low as 1 mV/mm (Ozen et al., 2010). More phase-locking was induced with increased stimulation intensity, which was greater during sleep than active awake periods, corroborating intensity and state-dependency of stimulation effects found in humans (Ozen et al., 2010). Additionally, both subthreshold field potentials and spiking activity could be modulated by stimulation (Ozen et al., 2010). Recently, intracranial field recordings in anesthetized humans and monkeys revealed that electric fields induced by tACS result in negligible phase shifts across space and a frequency-dependent attenuation of induced field potentials, with lower frequencies (below 15 Hz) having a greater increase in magnitude than high frequencies, in a testing range of 1-150 Hz stimulation (Opitz et al., 2016). Additionally, maximum induced electric field strengths were found in the superficial regions and measured to reach about 0.5 mV/mm (Opitz et al., 2016).

Taken together, it can be concluded that the stimulation parameters applied to humans can reach voltages required to successfully entrain a network of oscillators. Stimulation effects are governed by underlying network properties, including cellular and gyral morphology of excitatory and inhibitory neural assemblie, intrinsic oscillating frequency of the network, the state of the network, and the extent of the network – that is, long-range entrainment is possible in spatially distributed networks.

Towards a better understanding of tACS

Even after combining insights from studies in animal and computer models with what we know from behavioral and neuroimaging experiments in humans, there is still controversy about the reliability of transcranial electrical stimulation in its applications and the possibility of reproducible results (Antal et al., 2015; Horvath et al., 2015). The controversy highlights the bounty of outstanding questions regarding effects and mechanisms of online and offline tACS. High variability and small effect sizes in results across studies and fundamental problems of artifact removal in electrophysiology remain persistent (Herrmann and Strüber, 2017). Currently, the main limitations of tACS and other transcranial brain stimulation techniques include a clear understanding of how stimulation interacts with brain activity to give rise to behavioral effects, how

the effects can be optimized, and how inter- and intra-individual factors influence stimulation effects (Thut et al., 2017).

Combining tACS with fMRI is one method of measuring brain signals without detrimental artifacts in the data due to stimulation (Antal et al., 2014). In the introduction, we have described a few studies employing simultaneous tACS-fMRI experiments, however in this thesis we specifically evaluate intrinsic BOLD fluctuations and their interactions with stimulation. With the advantage of combining the two, we can measure the causal effects of tACS on intrinsic activity in a number a ways, which we do herein. The next three chapters describe the implementation and analysis of a simultaneous tACS-fMRI experiment to evaluate effects of externally applied oscillations on intrinsic brain activity. Each chapter includes relevant literature and attempts to avoid redundant content from the introduction. Specifically, we applied tACS to healthy resting (eyes open, centrally fixated) subjects with varied combinations of frequency (10 Hz, 16 Hz, or 40 Hz) and electrode montage (EEG International 10-20 System: Cz-Oz or P5-P6), while additionally acquiring fMRI data before, during, and after the stimulation. We investigated changes induced by tACS using multiple analysis techniques. **Chapter 2** reports group-level tACS parameter-dependent differences in intrinsic BOLD brain activity. **Chapter 3** revisits the data by considering variance factors attributable to inter- and intra-individual differences. **Chapter 4** offers a methods focus, in which we exploit tACS-modulated differences in the fMRI data to demonstrate the feasibility of using novel functional connectivity measures in graph analysis techniques. The aim of the thesis is to provide evidence that tACS effects are frequency, electrode montage, and subject specific and that these effects are detectable with fMRI measurements. We show that intrinsic neural activity as well as underlying connectivity networks are important factors in attaining successful, specific tACS effects. This work contributes to establishing an overall framework for tACS to be effective for individual brain stimulation.

Scope of this thesis (Thesis at a glance):

Chapter 2-

Objective: To characterize the effects of different tACS parameters, varied by frequency and electrode montage, on intrinsic low frequency fMRI signal fluctuations.

Methods: We employed simultaneous fMRI-tACS in 20 subjects during resting state (eyes open with central fixation for ~8 min). Subjects received tACS at different frequencies (10, 16, 40 Hz) and with different electrode montages (Cz-Oz, P5-P6) previously used in behavioral studies.

Results: Electric field simulations showed that tACS over Cz-Oz directly stimulates occipital cortex, while tACS over P5-P6 primarily targets parietal cortices. Group-level simulation-based functional connectivity maps for Cz-Oz and P5-P6 resembled the visual and fronto-parietal control resting-state networks, respectively. The effects of tACS were frequency and partly electrode montage dependent. In regions where frequency-dependent effects of tACS were observed, 10 and 40 Hz tACS generally induced opposite effects. Most tACS effects on functional connectivity were observed between, as opposed to within, resting-state networks. The left fronto-parietal control network showed the most extensive frequency-dependent modulation in functional connectivity, mainly with occipito-parietal regions, where 10 Hz tACS increased and 40 Hz tACS decreased correlation values.

Conclusion: TACS modulates local spontaneous low frequency fluctuations and their correlations with more distant regions, which should be taken into account when interpreting tACS effects on brain function.

Keywords: tACS, brain stimulation, fMRI, oscillations, entrainment, fALFF/ALFF, intrinsic functional connectivity, resting state, cross-frequency coupling

Chapter 3 –

Objective: To highlight methods practices that take into account individual differences whose variability influence group level analyses.

Methods: We used FEM model simulation-derived subject-specific seeds for computing correlation maps. Additionally, at the group level, we compare a linear mixed effects model with covariates to the traditional ANOVA employed in our previous study.

Results: Group level LME analysis of subject-specific seed-based correlation maps and covariates yield results that are in better agreement with our original hypotheses.

Conclusion: Accounting for variance factors attributable to subjects in subject-level and group-level analyses gives more informed results for scientific studies, however in order to make conclusive statements, more data is needed for statistical significance.

Keywords: linear mixed effects, FEM model, SimNIBS, ANOVA, tACS, resting-state fMRI

Chapter 4 –

Objective: To gain insight into using graph measures to detect effects of transcranial alternating current stimulation (tACS), we addressed the question of whether phase lag index (PLI) or coherence as a functional connectivity measure of blood-oxygenation-level-dependent (BOLD) functional magnetic resonance imaging (fMRI) time series better captures the changes in brain network topology induced by two different tACS electrode montages.

Methods: We used simultaneous tACS-fMRI to acquire resting-state fMRI data in 20 subjects before and during tACS applied with two different electrode montages (Cz-Oz and P5-P6) on different days. To characterize network topology in an unbiased fashion, minimum spanning trees were constructed from PLI and coherence adjacency matrices, and their topological characteristics were compared using degree, eccentricity, betweenness centrality, diameter, leaf fraction, and mean functional connectivity.

Results: We found that PLI-based betweenness centrality can best detect electrode montage-dependent differences in network topology due to stimulation. Additionally, group average MSTs for coherence and PLI exhibit cross-hemisphere and anterior-posterior connectivity backbones, respectively.

Conclusion: Differences in network organization due to different tACS setups are detectable using PLI betweenness centrality. Evaluating MST topology based on both PLI and coherence is feasible and, together, the two offer complementary information about network organization.

Keywords: graph analysis, resting-state fMRI, tACS, minimum spanning tree, functional connectivity, phase lag index, coherence

Chapter 2

The reader is referred to: Appendix A

Transcranial alternating current stimulation modulates spontaneous low frequency fluctuations as measured with fMRI

Manuscript as accepted by NeuroImage

On 2 of July 2016

Chapter 3

Main topic: Considering and controlling for subject-specific variability in evaluating effects of tACS.

Abstract

objective – To highlight methods practices that take into account individual differences whose variability influence group level analyses.

Methods – We used FEM model simulation-derived subject-specific seeds for computing correlation maps. Additionally, at the group level, we compare a linear mixed effects model with covariates to the traditional ANOVA employed in our previous study.

Results – Group level LME analysis of subject-specific seed-based correlation maps and covariates yield results that are different when compared to the previous chapter. Implications of differences are discussed.

Conclusion – Accounting for variance factors attributable to subjects in subject-level and group-level analyses gives more informed results for scientific studies.

Keywords: linear mixed effects, FEM model, SimNIBS, ANOVA, tACS, resting-state fMRI

Introduction

Just like we know from treating patients in medicine, and as we learn in more relevant detail with other neuromodulatory brain stimulation techniques, there are a number of inter- and intra-individual factors that influence efficacy of a treatment. In Chapter 2, we showed how varying stimulation parameters can exert different effects on the intrinsic activity of the brain. As has been shown more extensively with tDCS applications, even when using identical stimulation parameters applied in healthy populations, effects are considerably heterogeneous (Horvath et al., 2015; Li et al., 2015; Opitz et al., 2015; Ziemann and Siebner, 2015). When searching for compelling evidence of tACS modulation, it should be considered that neglecting effect variability that can be accounted for during the experiment or analysis leads to small effect sizes on a group level. A large portion of effect variability can be attributed to individual differences.

Neurodiversity-producing factors, intra-individual baseline factors, and methodological factors are all components that should be considered in tACS studies (Tavakoli and Yun, 2017; Yavari et al., 2017). In the following paragraphs, we consider each these aspects, review examples from supporting literature, and specify a modification in analysis for our simultaneous tACS-fMRI experiment data to control for inter- and intra-individual differences. The overall goal of this chapter is to exemplify that accounting for sources of variability arising from individual differences influences results, even within the same data set. Using the same seed-based correlation approach employed in Chapter 2, we repeat the individual analysis using subject-specific seeds constructed from the SimNIBS FEM model. Additionally, on the group level, we employ a linear mixed effects analysis, a statistical test that allows a vast amount more flexibility than a traditional ANOVA model, such as handling within subject variability from multiple runs and continuous explanatory variables (Chen et al., 2013). We show that, while additionally including mean electric field spread as a between-subject covariate, the results of the modified analyses divert a fair amount from the group-level results in Chapter 2. We emphasize that individual differences are key features in the effectiveness of tACS and advise that care should be taken to control for the most influential of these differences when possible.

Variability: Individual differences

Contributing sources of experimental differences in tACS experiments can be classified into categories constituting the intra- and inter-individual aspects of the source. These categories are neurodiversity-producing factors, intra-individual baseline factors, and methodological factors. There are a number of neurodiversity-producing factors that may remain relatively stable during non-longitudinal experiments, however their levels certainly influence tACS efficacy. Some factors in the list are cranial and brain anatomy – including head size and brain lesions – , neurochemistry, genetics, age, and functional organization of local circuits (Li et al., 2015).

As we introduced in Chapter 2, with the present data set and SimNIBS (http://simnibs.de/), we can use individual brain anatomy to construct finite element models for predicting electric field spread during tACS. The simulations predict electric field spread for a specific electrode montage and current strength using each subject's anatomical MRI data to quantify skin, skull, CSF, gray matter, and white matter

conductivities for accurate current flow modeling (Opitz et al., 2015; Windhoff et al., 2013). Although we introduced a subject-based simulation for determining target stimulation areas, for simplicity we combined subject-specific ROIs into one that could be generalized the group. This can be justified as a first step to determine parameter-dependent tACS effects that could be generalized to a larger population. However, gyral folding patterns and other brain anatomical features can have a greater influence on the field spread than electrode placement, thereby sometimes preventing maximal current to stimulation targets (Opitz et al., 2015). Our investigation of simulation-informed seed-based FC centers around the idea that regions that are maximally stimulated by tACS will affect intrinsic correlations with distant, functionally connected areas in a frequency-dependent manner. Given the influence of anatomical differences on current flow, using a group-based seed risks calculating FC for a given subject while completely overlooking the maximally-stimulated regions predicted in that subject's brain. A strength of individualized FEM models is the ability to account for these differences across subjects, especially when using the models for further steps in analysis of individual-specific data, such as seed-based rs-fMRI approaches. As such, when it is possible, subject-specific predictions should be utilized to their maximum benefit.

Methodological factors

Analysis techniques constitute an important second tier in approaching experiments in which variance in the data can be accounted. Ongoing technological advances allow tools and techniques in science to quickly develop and improve, enabling design of more complex experiments and measurement of any number of explanatory variables. The spatial resolution of fMRI and its increasing acquisition speeds, combined with simultaneous physiological and behavioral measurements and any of the aforementioned sources of variance in and across individuals all sum up to a tremendous amount of data that can be used, appropriately or inappropriately, when assessing effects at the group level. A limitation of most current fMRI software is its inability to handle a number of aspects when it comes to increasing amounts of experimental data (Chen et al., 2013). Typically, fMRI studies employ a traditional ANOVA or ANCOVA for group level analysis of experimental data with multi-level factors. However, the model cannot handle within-subject variability from data with multiple runs or sessions, or the addition of continuous explanatory variables (i.e.,

covariates). If data is inappropriately entered into the AN(C)OVA, violated assumptions in the model lead to inflated statistical power. By employing a linear mixed effects (LME) analysis, we can take advantage of strengths in the data set such as repeated scans within subjects and explanatory variables (Chen et al., 2013). The LME expands on the simplified general linear model case of the AN(C)OVA by including both a fixed effects design matrix and a random effects design matrix in the model. With such a model, subject variability can be allocated to random effects variables and thus taken into consideration on the group level (Chen et al., 2015).

In this chapter, we generate subject-specific seeds for FC analysis based on each subject's individual FEM head model simulation of Cz-Oz stimulation. Using the ROIs transformed to fMRI space, for each subject, an Oz-specific seed is used to calculate FC maps and mean electric field for that seed. We used fMRI data acquired before and during stimulation from the Cz-Oz tACS (3 sessions: 10 Hz, 16 Hz, and 40 Hz) sessions only. We show that the use of individualized ROIs changes results in a group level ANOVA. Additionally, on the group level, we employ a LME analysis incorporating subject-specific ROI size and mean electric field spread as random explanatory variables and compare results to the traditional ANOVA results presented in Chapter 2. We show that selection of group level models appreciably changes analysis outcomes, and advise that appropriate choices should be made depending on the data set being analyzed.

Methods

Data used in the subject-based analyses are the same as that acquired for the group analyses described in Chapter 2. Refer to the methods section of Chapter 2 for experimental setup, fMRI, and participant details.

Data analysis

Finite element method model

FEM modeling was accomplished using SimNIBS 2.0 (Windhoff et al., 2013). As mentioned, due to a mesh generation error with one of the anatomical datasets, one subject was excluded from the electric field simulations. For each of the remaining 19 subjects, T1- and T2-weighted images (with and without fat suppression) were used to

create an individualized mesh for modeling the electric field for the electrode montages used in the experiment. Inconsistencies in head meshes resulted from electrode gel signal near that of the skin in some anatomical images and were corrected manually. Using customized Matlab scripts (Matlab R2011b, www.mathworks.com, Natick, MA), electrode position coordinates were determined using a virtual 10-20 cap placed on the mesh of each subject based on anatomical landmarks on the head mesh (inion, nasion, left ear canal, right ear canal). Electric field simulations were generated in SimNibs for Cz-Oz and P5-P6 electrode montages for all subjects using standard tissue conductivities of σ_{skin}= 0.465 S/m, σ_{skull}= 0.010 S/m, σ_{CSF}= 1.654 S/m, σ_{GM}= 0.275 S/m, σ_{WM}= 0.126 S/m, for skin, skull, CSF, GM and WM, respectively (Thielscher et al., 2015; Windhoff et al., 2013). To generate the Oz region of interest (ROI) for seed-based FC, the normal component of the electric field (norm E) for the Cz-Oz simulations were transformed to corresponding subject gray matter masks segmented from original subject MRI space. The resulting MR-space simulation data were normalized to MNI space using the transformation matrices applied to subject anatomical data during preprocessing. Voxel data values in each transformed electric field map were ranked, and values greater than 3 standard deviations above the mean of the histogram of the data were truncated and reassigned to the new maximum value. This step was performed in order to remove extreme values resulting from fraction estimation errors in the FEM model. From the remaining ranked electric field values, the 400th value was chosen as a threshold cutoff (arbitrarily selected with the goal of ~500 voxels per mask per subject) for making seed masks. For each subject, the electric field value threshold below that value was set to zero, and all values equal or higher were set to one. The resulting thresholded Cz-Oz masks were constrained to only the Oz ROI by applying a mask constructed of the occipital cortical regions in MNI space provided in the AFNI package. For each subject, the mean electric field of the volume within the seed mask was computed along with the mask voxel count for use as quantitative variables in the group level analyses.

Preprocessing

All data preprocessing was performed in AFNI (Cox, 1996). The first 10 volumes were discarded to align stimulation start time to functional data. Preprocessing steps included: despiking, slice timing correction, deobliquing, motion correction, transformation to MNI space using each session's T1-to-MNI152 standard template

transformation, 6.0 mm FWHM-kernel Gaussian smoothing. Temporal preprocessing steps included 4th-order polynomial regression (equivalent to demeaning, linear trend removal, and high-pass filtering), regression of motion parameters and the first derivative of the motion parameters, bandpass filtering between 0.01 and 0.1 Hz, and nuisance regression of white matter (WM) and cerebral spinal fluid (CSF) signals (See Chapter 2 Methods).

Subject-based Oz seed functional connectivity analysis

For each stimulation-associated run of each subject (pre-, during, and post-stimulation), whole brain FC was computed using that subject's simulation-based Oz seed. For each subject, the Oz seed was resampled into functional data resolution (3 x 3 x 3 mm^3) and used as a mask to extract the average time course for the Oz ROI. The resulting time course was then correlated with that of every other voxel in the brain using Pearson's correlation coefficient. Correlation maps were Fisher's r-to-z transformed prior to statistical analysis. One subject's anatomical data were corrupted by artifacts, and a mesh could not be constructed for the subject, so subject-based analyses included 19 subjects unless otherwise noted.

Statistical Analysis

All group level volume statistics were conducted in AFNI on z-transformed FC maps. Two-way ANOVAs with the factors frequency (10 Hz, 16 Hz, 40 Hz) and time (pre, stim, and post) were performed on three sets of FC maps, including group-based Oz seed FC maps from Chapter 2 for comparison within the analysis package. Statistical maps of group ANOVAs on 1) the subject-based Oz FC maps of 19 subjects, 2) group-based Oz FC maps of the same 19 subjects, and 3) group-based Oz FC maps of the original 20 subjects from Chapter 2 were generated for qualitative comparison. LME analysis was performed only on the subject-based Oz FC maps. First, the model was conducted using the fixed effects frequency and time, as well as the additional random effect variable of ROI size in voxels per subject. A second LME analysis was run by constructing the model with mean electric field as an additional random variable to be included as a covariate of interest in the interaction of the main effects. Given the low power of the data set and the exploratory nature of this comparison, statistical maps were not corrected for multiple comparisons. In order to compare our results to the

original group level analysis of Chapter 1, we evaluated the main factor interaction (frequency x time) statistical maps. Regions reported are based on a voxel-wise p-value threshold of 0.05, filtered for clusters of five voxels (unless otherwise noted) touching faces, sides, or corners. Voxel-wise post-hoc t-tests were performed in the LME model between stimulation and pre-stimulation time points within each frequency. For visualization, statistical maps were projected onto the MNI surface using BrainNet Viewer (http://www.nitrc.org/projects/bnv/) (Xia et al., 2013), with thresholding chosen for illustration and qualitative evaluation.

Results

FEM Simulations

Figure 1 shows simulations displaying electric field spread predicted for Cz-Oz stimulation in each of the 19 subjects for whose data successfully produced a FEM mesh head model. The figure illustrates variability of the field distribution across individuals within electrode montage, positioned using the standard EEG 10-20 system. Figure 2 shows the Oz seed used for correlation analysis from two representative subjects.

Group level analysis using the traditional ANOVA

To assess the impact of using subject-specific ROIs for seed-based correlation analysis, we employed the traditional 3 x 2 (frequency-by-time) ANOVA used in Chapter 2. Because we switched analysis packages for this study in order to implement the LME, we repeated the original analysis from Chapter 2 in AFNI. Figure 3A displays statistical maps of group ANOVAs conducted using group-based Oz FC maps of the original 20 subjects from Chapter 2. Figure 3B shows ANOVA results from group-based Oz FC maps of the 19 subjects whose data were used in subject-specific ROI analyses. Finally, Figure 3C shows the ANOVA results from subject-based Oz FC maps of 19 subjects. Using a cluster threshold of 10 voxels at an uncorrected voxel-wise $p > 0.05$, allows for qualitative comparison of results across the different analyses. Regions passing the threshold for the 20-subject group-based Oz seed FC, displayed in Figure 3B, include right inferior frontal gyrus (IFG), left superior medial gyrus (SMG), right IFG (triangularis), right superior frontal gyrus (SFG), left middle temporal gyrus (MTG),

and left middle orbital gyrus. The 19-subject group-based Oz seed FC analysis displayed in Figure 3B was conducted to ensure that the excluded subject from the subject-based portion of the group level analysis did not disproportionately skew group results. Regions passing the same cluster threshold scheme employed in Figure 3A include right IFG, left SMG, right SFG, left precuneus, left MTG, and right middle orbital gyrus. Finally, the subject-based Oz seed FC maps were used for a third ANOVA, and clusters passing the threshold scheme employed previously include left precentral gyrus/SFG, caudate nucleus (more WM), right cerebellum, right IFG (triangularis), left precuneus, right precuneus, and left middle frontal gyrus (FG) .

Group level analysis using LME model

Figure 4 shows for qualitative comparison the maps of statistical results from the three variations of group level analysis using subject-based Oz FC maps from 19 subjects. Figure 4A shows the results of the traditional 3 x 2 ANOVA. Figure 4B shows results of the LME model including ROI sizes in number of voxels as quantitative random variables to be regressed out, as its interaction with results is not specifically of interest but should be controlled for differences across subjects. Figure 4C displays results of the LME when including electric field means for the Oz seed of each subject, specifically as a covariate of interest, as well as ROI size as random quantitative variables. For the 19-subject LME in which ROI size is controlled for in the regressors, a threshold of $p>0.05$ was set, and clusters passing a 20-voxel size threshold are reported for comparison to other group-level results. Surviving clusters include left precentral gyrus, left inferior temporal gyrus (ITG), left middle frontal gyrus, left precuneus, left cerebellum, and right paracentral lobule. Results passing the same voxel-wise p threshold and a cluster size threshold of 10 for the LME model including mean electric field as a covariate of interest are as follows: right middle FG, left middle FG, right hippocampus, right IPL, right IFG (pars opercularis), left middle occipital gyrus (MOG), left calcarine gyrus, right SFG, right clacarine gyrus, right insula, right middle cingulate cortex, left middle cingulate cortex, right IFG (pars opercularis), left ITG, and left middle temporal gyrus.

Figure 5 displays results from t-tests conducted within the LME model framework, which allows to control for the random quantitative variables, however analyzing with covariates of interest at this level is a complicated mathematical principle not yet

implemented in AFNI's LME functionality. Panels 5A, 5B, and 5C respectively display whole-brain group level t-tests between pre- and stimulation runs within 10 Hz, 16 Hz and 40 Hz frequency stimulation conditions.

Discussion

In this chapter, we assessed tACS-modulated FC based on subject-specific seeds generated from each subject's individual FEM head model simulation of Cz-Oz stimulation. Using individualized ROIs changed results from the group level ANOVA. Additionally, on the group level, we employed a LME analysis incorporating subject-specific ROI size and mean electric field spread as random explanatory variables.

SimNIBS simulation results

The FEM model simulations can be evaluated qualitatively by considering the spatial distribution of the electric field. Figure 3.1 shows that predicted current flow varies considerably across subjects. After thresholding and normalization, the seeds generated for the subjects show similar variability, as illustrated with the representative subject seeds shown in Figure 3.2. The field spread for the subject in the upper panel appears to extend ventrally along the occipital cortex in comparison to that of the subject in the lower panel, which shows current to travel more medially through the cuneus. This spatial variability across subjects should illustrate the importance of selecting seed regions of interest that fit the hypothesis. That is, in our case, we are interested to see how the brain connectivity changes relative to the stimulated regions. If a group-based seed does not cover the stimulated region of one subject, the additional data could perhaps be considered just noise.

Subject-based versus group-based correlation seeds in traditional ANOVA

The results from the original ANOVA model and group-based seed correlation maps with one subject excluded shows overall the same regional effects as the original 20 subject group test. However, the interesting aspect of the comparison is that, even when applying the same ANOVA, using a subject-specific correlation seed considerably changes results on a group level. While there may be some spatial overlap between the two results maps, one notable regional change is the significantly modulated regions

below the location of the Cz electrode. If tACS successfully affects regions directly below stimulation electrodes, a high functional correlation would be expected between their signals. It should be noted that some significantly affected regions remain the same, so the previous results could still be considered to offer information about how tACS parameters effect intrinsic activity, such as the opposite effects from 10 Hz and 40 Hz stimulation, but perhaps the modulation regarding specific regional effects should be approached with caution.

LME compared to traditional ANOVA

Considering the group level results in Figure 3.3, the models applied increased in complexity through addition of the subject-specific variables mean electric field and ROI size. Complex data – in this case, multiple within-subject runs and subject-specific covariates can be considered and modeled as a nonlinear system arising from the presence of multiple variance parameters, which the LME can handle specially from both theoretical and numerical perspectives (Chen et al., 2013). By offering modeling flexibility through the use of a fixed/random effects dichotomy, variables assigned in the random effects design matrix of the LME represent the deviation of each subject from the population average. This allows controlling for inter- and intra-individual variability through allocating subject contributions to levels of the random effects component. In Chapter 2, all analyses were considered using a group level ANOVA model. The LME offers a framework under which most analyses can be performed under a single numerical scheme while accounting for cross-run variability, unequal correlations and unequal variance across factor levels (Chen et al., 2013). As such, given the present data set consisting of multiple subject runs and sessions, explanatory variables of no interest such as ROI size, and quantitative covariates of interest such as electric field estimations, we consider the LME model to reflect differences in group level statistics that better pinpoint specific effects of tACS. One important rule of thumb to consider when applying such a complex model to experimental data, is that an increasing number of explanatory variables requires more measurements to fit the model accurately. It is recommended that at least five measurements should accompany each explanatory variable in the model (Chen et al., 2013). Also, acquiring data from a sufficient number of subjects is required to make reliable estimations on a group level, with 20 subjects as a guideline for a minimum (Chen et al., 2013).

Within frequency stimulation comparison to baseline in LME

Traditionally, post-hoc t-tests are conducted and reported to show direction of effects, however, restricting those t-tests to significant clusters ignores the possibility detecting changes in the whole spatial configuration of connectivity. Taking the whole volume into consideration and comparing the spatial distribution of the statistics can be informative about the frequency-specific effects of stimulation condition. Evaluating the frequency-specific modulation due to tACS on a spatial level, 10 Hz stimulation changes appear different from 16 Hz and 40 Hz. A time-specific effect like fatigue should have similar spatial distribution when comparing subjects in different conditions, so it could be considered to rule out that the effect is that of typical scan-to-scan variance. As such, it is interesting that two of the three within-frequency results resemble two typical resting-state networks, DMN and DAN, resulting from 10 Hz and 16 Hz stimulation, respectively. Considering the strong association between alpha and DMN, this preliminary result motivates further validation with additional measures or proper sham control data (Jann et al., 2009). In contrast, 40 Hz tACS induces decreased FC in a few regions that are considered part of DMN, but effects are not as clearly exclusive to the DMN as 10 Hz stimulation effects. Note the decrease in these regions of DMN compared to increases in FC with those regions seen in the 10 Hz pre-stimulation versus stimulation comparison, which follows the trend of opposite 10 Hz versus 40 Hz effects we reported in Chapter 2 (Cabral-Calderin et al., 2016b). Also, while particular nodes of DMN decreased FC with the Oz seed region, nodes belonging to task-active networks, like IPL to DAN, decreased as well. Overall, it could be considered that modulation effects relate to the theory that in the brain, slow frequencies are reserved for long-range communication between spatially distant cell assemblies, while gamma-band activity is associated with local communication (von Stein and Sarnthein, 2000; Uhlhaas et al., 2008). Ultimately, for this experiment, there is no sham data for use in the analysis, so no conclusive statement can be made, however the maps provide enough interesting differences that motivate further investigation into 10 Hz and 16 Hz stimulation using matched frequency and electrode montage shams.

Variability: intra-individual baseline factors

In light of the modifications we made in our analyses to control for sources of individual variability, we now discuss additional variability factors to consider in tACS

experiments. As we discussed in the introduction, employing subject-derived seed-based correlation is one way to account for inter-individual variability when analyzing the data. Head shape and brain morphology contribute to inter-individual differences in a constant manner over time. In addition to more stable neurodiversity-producing factors across individuals, intra-individual differences are also likely to play a role in how reliably tACS can affect brain activity. Such differences arise from baseline factors that lay both beyond and within experimental control, that is, to take it further, tACS effects are conclusively state-dependent (Cabral-Calderin et al., 2016; Feurra et al., 2011; Kanai et al., 2008). Accounting for these factors by measuring relevant baselines prior to stimulation or optimizing design of analysis and experiments is likely to best capture crucial aspects of the experimental modulation. For example, baseline level of motor function has been associated with extent of stimulation-induced modulation, as demonstrated through measurement of motor evoked potentials in TMS (Silvanto et al., 2008) and tDCS experiments (Pellicciari et al., 2013). Likewise, in experiments of cognitive function, initial skill levels of participants in a given task predict whether or not tDCS or tACS improves task performance. In a study of working memory in older adults, tDCS applied to the either hemisphere of the prefrontal cortex improved task performance only in participants with more education (Berryhill and Jones, 2012). Another study demonstrated that tDCS applied to the parietal cortex biased visuospatial attention as measured through a line bisection task, however, significant effects were dependent on subjects' baseline task performance (Benwell et al., 2015). Gamma (40 Hz) tACS applied to the prefrontal cortex during complex logic problem solving tasks was shown to reduce response latencies, with the slowest participants receiving greatest improvements (Santarnecchi et al., 2016).

Another source of intra-individual variability arises from differences in neurophysiological response to a particular task, which may be related to task ability or a subject's sensitivity to a behavioral paradigm. Experiments with tACS have demonstrated state dependence of sensory systems through frequency-specific modulation of visual (Kanai et al., 2008) and somatosensory (Feurra et al., 2011) perception. In a study employing gamma tACS, subject performance in visuospatial abstract reasoning was found to be selectively enhanced depending on the complexity of the task trial (Santarnecchi et al., 2013). The evidence of tACS response variation arising from behavioral demands and underlying neurophysiological dynamics shows

the impact of an individual's oscillatory patterns profile on stimulation response. For measuring changes in perception, the use of discrimination thresholds represents a method to account for subject-specific task responses (Schutter and Wischnewski, 2016). Additionally, neurophysiological state can influence intra-individual reliability in non-invasive brain stimulation experiments. Baseline neurophysiological states include alertness, metabolic cycles, circadian rhythms, and general subject status (Krause and Cohen Kadosh, 2014; Yavari et al., 2017). Relating to differences in cognitive baselines across subjects, recent evidence shows that individual differences in resting state functional connectivity is predictive of cognitive performance (Mennes et al., 2010; Sala-Llonch et al., 2012). Additionally, resting state BOLD activity has been correlated with arousal, intellectual ability, gender, age (Boveroux et al., 2010; Damoiseaux et al., 2008; Finn et al., 2015; Mennes et al., 2010; Tian et al., 2011). As such, resting state brain activity is useful data for mapping heterogeneity-inducing sources of tACS effects through evaluation of individual-level intrinsic activity and its interaction with stimulation. Moreover, conducting experiments with the same subjects across multiple sessions provides the advantage of capturing within-subject variance and assigning it to particular explanatory variables in analysis at the group level. In addition to some of the transient neurophysiological influences listed, resting-state fMRI data can also provide information about inter-individual heterogeneity of spatial distribution of FC networks in the context of stimulation targets.

Variability: methodological factors

When considering methodological factors and limitations of tACS experiments due to individual differences, it is possible to tailor stimulation parameters to each subject as well as control some state-dependent sources of intra-individual variance during the experiment. For example, depending on whether a participant has eyes closed or open during stimulation, baseline alpha power in the occipital cortex will increase or decrease, respectively, impacting the effectiveness of stimulation in the alpha range (Kanai et al., 2008). Additionally, the temporal location of the alpha peak changes from subject to subject, and it has been shown that EEG-informed, that is, basing stimulation parameters on an individual's EEG spectral information, stimulation improves behavioral performance (Kasten and Herrmann, 2017; Vosskuhl et al., 2015), modulates perception (Cecere et al., 2015), and increases power in the stimulation frequency range

(Kasten and Herrmann, 2017; Ruhnau et al., 2016; Zaehle et al., 2010).

Using subject measurements, optimal parameters for current strength and stimulation frequency can be systematically selected for successful entrainment, as has been demonstrated through the use of rhythmic light stimulation in individuals (Notbohm et al., 2016). Through stimulating subjects with various light intensities at stimulation frequencies at and around their IAF, Notbohm and colleagues showed that plotting the degree of external synchronization as a function of stimulus frequency and intensity produces the triangular shape of the Arnold tongue (Notbohm et al., 2016). The Arnold tongue is a mathematical principle that predicts entrainment of a harmonic oscillator. Characterized by an inverted triangular shape, it illustrates the frequency band in which an oscillator will synchronize with an external signal. Stimulation frequencies matching the intrinsic rhythm require only minimal intensity for entrainment, while if the stimulation frequency is a greater distance from the intrinsic rhythm, higher stimulation intensities are required to achieve entrainment. Frequencies and intensities outside this region will not successfully synchronize the signals (Notbohm et al., 2016). Such application of the Arnold tongue theory illustrates the use of neurophysiological state dependence, in this case, the individual baseline oscillatory brain activity, to optimize stimulation parameters. Consideration for many of the neurophysiological states listed in the previous section can be incorporated into experiment design, and should be prioritized based on the context of the hypothesis. We have already mentioned the use of discrimination thresholds in perception tasks for subject task-response variability, which also serves as a method of accounting for inter-individual differences.

Timing is a crucial element of experiments, especially when considering tACS is a tool for probing temporally-specific mechanisms, and many of these aspects are within design control. The effect of ambient light conditions on alpha power appears to add linearly with tACS effects, which was demonstrated in an experiment that stimulated subjects in dark conditions and ambient light conditions, and measured alpha power for 30 minutes following stimulation (Stecher et al., 2017). This evidence shows the need for specific experimental environment guidelines in regard to room light. Similarly, noting the influence of circadian rhythms on effects of stimulation should guide choices about time of day for stimulation administration, motivated by correlations between baseline cortisol levels and stimulation effectiveness (Sale et al., 2008). Perhaps the most obvious time factors under experimental control involve the design of the task or

behavioral conditions under which stimulation takes place. TACS induces different temporal and spatial effects depending on the task in which a subject is engaged, as demonstrated in a fMRI study comparing effects during finger tapping, movie viewing, or rest (Cabral-Calderin et al., 2016). Attention is a behavioral transient state that can be spatially and temporally directed in relation to stimulation timing for specific experimental hypotheses (Hopfinger et al., 2017). Timing stimulation relative to presented stimuli allows for testing aspects of phase locking due to tACS modulation, as demonstrated in an auditory detection task during theta tACS (Riecke et al., 2015).

Inter-individual state of being or psychological status modulates transcranial electrical stimulation response. For example, a study evaluating the impact of anxiety levels on tDCS effects in subjects performing mathematics exercises showed reduced response times as well as a reduction in cortisol levels in subjects with high mathematics anxiety (Sarkar et al., 2014). In light of these studies, care should be taken that all participants are as comfortable as possible during the experiment and stimulation, or that physiological metrics of stress, like cortisol levels, are considered in the analysis.

Non-state-dependent methodological factors

Task designs should consider not only timing in relation to stimulation, but also the spatial relationship between stimulation targets and task-recruited brain networks. If strategy of approach to a particular task varies across participants, it would accordingly utilize different brain networks across individuals (Berntsen et al., 2017; Fink et al., 2002; Jordan et al., 2004). Similarly, some functional networks, for instance, handedness, vary in their degree of laterality across individuals. The use of brain imaging, like rest- and task-based fMRI, and causal techniques, like TMS, for mapping functional areas in individuals allows for accurate selection of stimulation targets. Functional brain mapping combined with subject-specific head modeling of can guide optimal choice of electrode montage for an experiment (Fox et al., 2014; Ruffini et al., 2014; Saiote et al., 2013).

Limitations

Given the multitude of potential sources of variability in tACS experiments, and measurements of brain-behavior relationships in general, there are several limitations in our study that could addressed. As already mentioned, the lack of a proper sham data set

prevents conclusive statements about comparisons within frequency. A number of covariates could be included in the analysis, for example diffusion coefficients measured with MRI. However, following a rule of thumb of five measures of dependent data for each explanatory variable in the model, the number of fMRI measurements in this experiment cannot afford additional explanatory variables in the model. Also, to be able to make proper corrections for multiple comparisons, more than 19 subjects should be included in the analysis. Importantly, our experiment design did not include measuring a second quantitative readout of brain or behavior activity, such as measuring EEG or other baseline measures to capture modulation due to tACS. Without a second readout of tACS-induced modulations, a clear relationship between stimulation-driven changes in FC and changes in brain function cannot be made.

Conclusion

Taken together, when variance factors attributable to subjects are accounted for in the subject-level and group-level analyses, and as the model becomes more complex through addition of covariates of interest, results change considerably. As with all properly executed science, appropriate hypotheses should drive experiment design and analysis decisions to ensure draw accurate conclusions from the data.

Chapter 4

Main topic: Evaluating phase lag index and coherence functional connectivity-based minimum spanning tree network measures to detect tACS modulation in resting-state fMRI data.

Abstract

Objective: To gain insight into using graph measures to detect effects of transcranial alternating current stimulation (tACS), we addressed the question of whether phase lag index (PLI) or coherence as a functional connectivity measure of blood-oxygenation-level-dependent (BOLD) functional magnetic resonance imaging (fMRI) time series better captures the changes in brain network topology induced by two different tACS electrode montages.

Methods: We used simultaneous tACS-fMRI to acquire resting-state fMRI data in 20 subjects before and during tACS applied with two different electrode montages (Cz-Oz and P5-P6) on different days. To characterize network topology in an unbiased fashion, minimum spanning trees were constructed from PLI and coherence adjacency matrices, and their topological characteristics were compared using degree, eccentricity, betweenness centrality, diameter, leaf fraction, and mean functional connectivity.

Results: We found that PLI-based betweenness centrality can best detect electrode montage-dependent differences in network topology due to stimulation. Additionally, group average MSTs for coherence and PLI exhibit cross-hemisphere and anterior-posterior connectivity backbones, respectively.

Conclusion: Differences in network organization due to different tACS setups are detectable using PLI betweenness centrality. Evaluating MST topology based on both PLI and coherence is feasible and, together, the two offer complementary information about network organization.

Keywords: graph analysis, resting-state fMRI, tACS, minimum spanning tree, functional connectivity, phase lag index, coherence

Introduction

The human brain as a complex network

The human brain is a complex, multi-scaled architecture of neurons that interact to process information in an efficient and specialized manner, allowing basic sensory processing as well as higher-order cognitive functioning. Segregated modules in functional brain networks are observed in basic perceptual and sensory systems, like vision, hearing, and touch. These specialized, and generally localized, systems work together to create an ensemble of long range connections that integrate and process information for higher order organization, yielding systems-level cognition and behavior (Sporns et al., 2004). One can imagine that such functional segregation and integration for information transmission, or connectivity, between neurons arise as complex self-organizing networks (Sporns et al., 2004). Indeed, the brain can be studied as distinct regions with temporally correlated signals that imply how connected one region is to another, and whose correlations change dynamically over time, giving rise to perception, cognition, or action (Fox et al., 2005; van den Heuvel and Hulshoff Pol, 2010). Case studies in patients with brain lesions, psychophysical experiments, and neuroimaging studies have provided empirical evidence that brain networks function in a modular fashion for specific cognitive tasks. Neuroimaging tools such as electroencephalography (EEG) and magnetoencephalography (MEG) have allowed for the recording of brain signals in controlled environments so that stimulus responses can be measured, analyzed, and explained in the context of cognitive functioning. Relatively recently, measuring spontaneous brain activity in order to describe intrinsic brain function and development has emerged, and resulted in the characterization of so-called “resting-state” networks that are formed by temporally correlated (distant) brain regions, giving additional evidence of the modular organization of the brain (Fox et al., 2005; Park and Friston, 2013). This area of research has grown from studying functional connectivity of sets of two nodes and led to characterizing higher order global organization and dynamics using graph theory (van den Heuvel and Hulshoff Pol, 2010; Park and Friston, 2013).

Characterization of brain networks with graph theory

As such, in EEG and MEG resting-state studies, and increasingly magnetic resonance

imaging (MRI) and functional MRI (fMRI), the application of graph theory analysis has greatly contributed to the study of complex networks of the brain (Sporns et al., 2004; Stam, 2014). Combining contributions from studies across brain imaging modalities, evidence shows intrinsic human brain networks to have properties of self-organizing complex networks described in other biological systems. The field has come to view the healthy brain as a network that combines small-world and scale-free properties, such that the system balances between efficiency, flexibility, and robustness. Graph theory can characterize network topology using measures such as clustering coefficient, path length, and centrality (Reijneveld et al., 2007; Sporns, 2013). The application of graph theory to brain networks has led to a number of discoveries regarding the topological properties of brain structure and function in health and disease (Sanz-Arigita et al., 2010; Stam, 2014).

Challenges with application of graph theory to neuroimaging data

Despite the lessons learned about network characteristics and organization of the brain, comparing various clinical populations or across experimental conditions requires subjective decisions for normalization procedures or thresholds, which bias the analysis. Similarly, testing a range of thresholds potentially leads to multiple conclusions that are dependent upon network density (van Diessen et al., 2015; Stam et al., 2014). As such, some controversy surrounds conclusions regarding network disruptions in neurological diseases, such as consensus on dysfunctional hub locations or whether average path length is increased or decreased between certain nodes. One possible solution to this problem is reconstruction of the minimum spanning tree (MST), which is a subgraph that connects all of the nodes in the original graph, without cycles, such that synchronization – or the measure of FC in our case – is maximum between brain areas (Stam et al., 2014; Tewarie et al., 2015). For an undirected graph with uniquely-weighted edges, the minimum spanning tree is unique (that is: there is exactly one minimum spanning tree for that network). Thus, the local and global properties of the MST can be compared across groups and conditions without biases. The MST has been applied successfully to MRI data to characterize structural brain network topology using diffusion data (Tewarie et al., 2015), as well as to task-based functional MRI data (Baumgartner et al., 2001; Çiftçi, 2011). Summarizing network topology with the MST as a backbone of the graph has been shown to maintain topological features of the full

underlying network including small-world organization and scale-free degree distributions (Tewarie et al., 2015). In fact, 50% of the betweenness centrality of an MST has been shown to be preserved in as little as 16% of the nodes of original network (Kim et al., 2004). Thus, MST topology is a not only an unbiased method, but also a robust way to quantify changes in brain network organization using FC measures.

Another challenge in graph analysis pertains specifically to quantifying FC when measuring BOLD signal fluctuations with fMRI. Correlations are commonly used for assessment of functional connectivity in resting-state fMRI. However, because of unavoidable spatial blurring during preprocessing (slice-timing correction, normalization, smoothing), nonbiological sources contribute to local voxel correlations (Power et al., 2011). This is an issue that becomes exacerbated when parcellating data into nodes and constructing graphs, as the local correlations tend to dominate connectivity in the graph. These spurious correlations should therefore be disregarded before constructing the network. As such, there is reason to evaluate FC measures other than correlation for fMRI, for example using metrics that have been developed for analysis of neurophysiological signals, where similar spurious correlations may be introduced due to volume conduction and field spread (Guevara and Corsi-Cabrera, 1996; Stam et al., 2007). One family of metrics ignores zero-lag phase synchrony and only captures delayed connectivity (Stam et al., 2007). A member of this family, phase lag index (PLI), was introduced for use in EEG data analysis to reduce the effect of volume conduction, or blurring at the sensor level. By ignoring zero- and mod pi-phase differences in the two signals, PLI discards zero-lag phase synchrony and quantifies delayed connectivity (Stam et al., 2007). Asymmetry in phase lead or lag reflects the degree of phase locking between two signals that cannot be explained by spurious correlations (Lee et al., 2013). Coherence is a widely used, classically accepted frequency-domain method of analyzing two signal series at a time that describes the simultaneous activation between areas (Baccalá and Sameshima, 2001). Unlike PLI, coherence depends on amplitude in addition to phase relations. As such, each PLI and coherence captures a different aspect of the degree of relative synchrony between two nodes, both different from the typically-used Pearson correlation in fMRI analysis. Though the Pearson correlation could be considered a special case of coherence, coherence more robustly quantifies amount of overlap in structure of two noisy signals and is less sensitive to phase differences in the signals (Guevara and Corsi-Cabrera,

1996).

Study motivation

Graph theory is ideally suited to identify and describe organization of neural networks in temporal- or frequency-based dynamics, so it is also ideal for analysis of data acquired through combining a frequency-specific probe with measurements before, during, and after manipulation of neuronal networks (Reijneveld et al., 2007). Transcranial alternating current stimulation (tACS) is a noninvasive brain stimulation technique that applies a sinusoidally varying current to the scalp at a selected frequency, thus serving as a potential probe for modulation of frequency-specific cortical activity (Antal et al., 2008). If the brain is considered as a composition of neuronal oscillators that dynamically cluster and influence one another based on factors such as connectivity, proximity, and functional cooperation, frequency specific probes could also be regionally or functionally specific in their actions. Some experimental evidence suggests that using tACS, we can influence the ongoing activity of the brain to interact with – boost or entrain, for example – specific frequencies intrinsic to brain function (Helfrich et al., 2014b; Vosskuhl et al., 2016). TACS has demonstrated behavioral effects in applications with working memory (Alekseichuk et al., 2016), attention (Benwell et al., 2015), and other perceptual task-based experiments (Cabral-Calderin et al., 2015), indicating influence on functional networks. A growing number of combined tACS and imaging studies using EEG, MEG, or fMRI have contributed mixed evidence to the of list of online (i.e., during stimulation) and aftereffects of tACS on the human brain, such as boosting alpha power in the visual cortex (Vosskuhl et al., 2016), determining whether such boosts are a result of entrainment or plastic changes (Vossen et al., 2015), mapping regions of tACS entrainment (Witkowski et al., 2016), and detecting network modulation during working memory tasks (Violante et al.). However, tACS can be considered a somewhat newly revived tool in the last two decades, and its effects and their mechanisms are still not well understood (Herrmann et al., 2013; Tavakoli and Yun, 2017). Optimizing analysis techniques for such studies would allow for specific characterization of the direct, global, and lasting effects of tACS on the human brain and would contribute information for building a framework for best practices in its applications (Romei et al., 2016; Yavari et al., 2017).

Experimental setup: tACS-fMRI experiment

Using combined tACS-fMRI, we have acquired repeated measures for 20 subjects at rest (eyes open, central cross fixation) before, during, and after a constant eight-minute stimulation period. The different measures were conducted on six different days, and on each day, stimulation was applied using one of the different combinations of frequency (10, 16, or 40 Hz) and electrode montage (Cz-Oz or P5-P6, according to 10-20 EEG system). Figure 1B describes the six experimental conditions and Figure 1C shows session flow for the six separate scanning days, over which conditions were applied in random order for each subject.

We have previously analyzed this dataset using correlation of fMRI BOLD time series as a functional connectivity measure (seeds: simulation-based stimulation regions and seven resting-state networks), and fractional amplitude of low frequency fluctuations (fALFF), which is an indication of regional metabolic activity derived from power estimation of signal fluctuations in frequencies of interest (e.g., 0.08-0.1 Hz) (Cabral-Calderin et al., 2016b; Zou et al., 2008). We showed that 10 Hz and 40 Hz stimulation typically have opposite effects in regions where both stimulation frequencies significantly change the intrinsic brain activity (Cabral-Calderin et al., 2016b). Additionally, in regions affected by stimulation within a frequency using either electrode position, Cz-Oz stimulation typically has an opposite effect of P5-P6 stimulation. These fingings provide insight into the interactions of tACS with intrinsic brain activity on a regional level and on a functional connectivity level using fMRI.

Given the regional and connectivity differences across stimulation conditions described in our previous study, we hypothesize that, depending stimulation frequency and electrode montage, tACS would bring about condition-specific changes to the overall network topology. Specifically, given that P5-P6 tACS consists of two anti-phase electrodes placed directly above two hubs in bilaterally symmetrical synchronous resting-state networks such as the default mode network and the dorsal attention network, stimulation in this fashion is expected to cause network disruptions, for example decreasing network efficiency by redistributing node degrees or shifting centrality to areas where stimulation is maximal. In contrast, with electrodes positioned at Cz-Oz, stimulation of a central hub in a hemispherically symmetrical network might increase current flow through and strengthen the importance of such a hub node.

Study aims

Our prior study showed that different electrode orientations differently affect intrinsic fMRI BOLD activity in addition to whole brain functional connectivity (Cabral-Calderin et al., 2016b). With the advantage of simultaneous fMRI acquisition during stimulation, this dataset is well suited to use graph theory measures to detect network dynamics manipulated through tACS. However, as mentioned, some methodological issues exist concerning the construction and comparison of brain networks. In this study, we investigate whether electrode position-dependent tACS modulation of functional brain networks measured with fMRI is best detected and characterized using MST topological properties based on PLI or coherence as a functional connectivity measure.

To accomplish the analyses in an unbiased fashion and avoid arbitrary thresholding, the network backbone is constructed with the MST, and topological characteristics of the MST are compared to test for electrode montage-dependent differences in the effects of tACS. Following more typical techniques used in EEG or MEG studies, and motivated by methodological concerns of using temporal correlations from fMRI data to construct graphs , MST calculation is based on two FC measures that capture different aspects of the signal measured: PLI, which quantifies asymmetry in the phase differences between two signals, and coherence, which quantifies linear time-invariant dependence between two signals (Stam et al., 2007).

Methods

Experimental setup and design and data acquisition

The data analyzed in this chapter is the same as that described in Chapter 2. See Chapter 2 Methods for tACS and MRI experimental setup and parameter details.

Data analysis

Preprocessing

All data preprocessing was performed using the CONN toolbox for Matlab (www.conn-toolbox.org). Figure 2 shows a flowchart of the experimental data processing. The first 10 functional volumes were discarded to align stimulation start time to functional data.

Preprocessing steps included: subject motion estimation and correction, slice-timing correction, functional outlier detection of scans for scrubbing (ART), direct functional segmentation and normalization (simultaneous gray matter/white matter/CSF segmentation and normalization to MNI space). Voxel time series were denoised through linear regression of the six motion parameters and their first derivatives, and additionally the first five principle components of signal contribution from each of the white and gray matter segmented time series, followed by linear detrending. All time series were temporally low-pass filtered (0.008-0.09 Hz). The Automated Anatomic Labeling (AAL) atlas was applied to the MNI-normalized brains, and time series of all the gray matter voxels in each of the 78 cortical (12 subcortical and 26 cerebellar parcels from original AAL 116 excluded) regions of interest (ROIs) were averaged to yield 78 nodal time series for every stimulation run of every subject. Average node time series were truncated to 512-timepoint epochs and multiplied by 10000, in order to compute FC measures using integer values, as required by BrainWave software, which was used for graph analyses described in the following subsection.

Graph Analysis

Graph analyses were completed using BrainWave software (https://home.kpn.nl/stam7883/brainwave.html, version 10.32). For each run for each subject, two sets of 78x78 FC matrices were computed from the extracted averaged ROI time series, i.e. one with the phase lag index (PLI) and one with coherence. PLI, which quantifies asymmetry in the phase differences between two signals, is calculated as

$$PLI = |\langle sign[\sin(\Delta\varphi(tk))\rangle| \quad (1)$$

where $\Delta\varphi(tk)$ is a time series of phase differences between two nodes for k=1...N samples, when $-\pi < \Delta\varphi < \pi$ (Stam et al., 2007). Coherence, which quantifies linear time-invariant dependence between two signals, is calculated as

$$C_{12}(f)=|S_{12}(f)|^2/(S_{11}(f)S_{22}(f)) \quad (2)$$

where S_{12} is the cross-spectral density of time series from nodes 1 and 2, and S_{11} and S_{22} are the auto-spectral densities of the time series from node 1 and node 2, respectively.

A 78x78 FC adjacency matrix can be used to construct a weighted, undirected graph

with 78 brain ROIs referred to as nodes and the pairwise FC measure (coherence or PLI) between each node referred to as an edge. Minimum spanning trees were constructed for each matrix. The MST connects all of the nodes in a graph, without cycles, such that the measure of FC is maximum between nodes. This is accomplished by starting at one node in an empty graph, and adding one edge from the original graph at a time, from strong to weak. If the addition of an edge creates a loop, that edge is skipped, and the procedure continues until all node are connected with no loops. (Stam et al., 2014). This procedure leaves a "backbone" of the original graph with only N-1 connecting edges for the original N nodes. MST topology was characterized using MST overlap, MST degree, MST eccentricity, MST betweenness centrality (BC), MST diameter, and MST leaf fraction (Stam et al., 2014). MST overlap quantifies the number of overlapping edges, or the survival rate of the edges, when comparing two MSTs. When two MSTs are compared to a common reference MST, the value of the fraction of surviving edges can quantify differences in global topology. For quantification in PLI and coherence FC topologies, the reference MSTs were constructed from the group average of the FC matrices corresponding to the pre-stimulation runs (run 4) across all conditions (20 subjects x 6 conditions).

Table 1 describes the other MST metrics evaluated in this study. Figure 3, reproduced from (Stam et al., 2014), illustrates example MSTs with some topological features highlighted and others plotted to indicate how the capture network organization and integration. FC mean is quantified by using only the MST edge FC values. The degree of a node is defined as the number of edges connected to it, and its quantity is normalized by dividing by the total number of edges in the graph; MST degree can be considered as a mean value across all nodes, or on a nodal basis. MST eccentricity is defined as the length of the longest path from the current node to any other node; it can be assessed at a nodal level or as a mean value for the MST. Betweenness centrality of a node in an MST is defined as the number of shortest paths in the tree between any two nodes passing through the node, divided by the total number of shortest paths. The centrality of a node is a measure of its importance in the network, and the specific definition of betweenness centrality here is specific to the node's importance for information transmission in the network. This measure can also be evaluated as a global MST mean, or for each node separately. A leaf is a node with only one edge. A tree with many leaves has a more star-like topology and could be considered efficient or

integrated compared to a more path-like tree configuration with few leaves, and thus few connections between nodes. Global MST leaf fraction translates as a measure of network centrality. MST diameter is the longest shortest distance between any two nodes in a tree. MST diameter also indicates whether a tree is more star-like, with many leaves connected to central hub nodes, or more path-like, with few leaves and a chain-like configuration, thus ranging in network efficiency or integration from high to low (van Dellen et al., 2016; Stam et al., 2014).

Statistics

Statistics were carried out in Matlab (MathWorks, Natick, MA.; version R20017a), and Brainwave was used for all pairwise post-hoc tests, as specified below. Because of a systematic difference in temporal signal-to-noise ratio between the first run and all other runs in scanning sessions, only the stimulation runs were used for comparisons. Additionally, to focus on concurrent effects of tACS on brain activity, only pre-stimulation and stimulation runs (run 4 and run 5, respectively) were compared here. Figure 1C highlights in yellow which runs were used for comparison in this study. In order to reduce the comparison to a two-way ANOVA with factors FC measure (PLI and coherence) and electrode position (Cz-Oz and P5-P6), MST-based FC measures were collapsed in time by using the fraction of the measure computed for the stimulation condition and the sum for the two conditions (pre-stimulation and stimulation). To compare the effect of electrode montage, all frequencies were collapsed, and conditions were simply grouped by electrode position. Stimulation fraction values for the seven evaluated MST metrics corresponding to each FC measure were compared across electrode position using a 2 x 2 (electrode position x FC measure) ANOVA. Significantly different measures are reported with and without Bonferroni correction applied for the seven features tested, using alpha of 0.05.

If a particular FC measure's mean MST features were significant in the ANOVA, follow-up tests were conducted within the FC measure to detect time changes particular to the electrode montage, thus carrying out global and then node-wise 2 x 2 ANOVAs with factors electrode position and time. For additional post-hoc tests of significant MST measures, appropriate pairwise comparisons (i.e., within electrode position pre-stimulation versus stimulation) of nodal quantities of the measures were made in BrainWave to identify nodes in the network responsible for reorganization and the

direction of their changes. Comparisons made in BrainWave were permutation tests, and given the exploratory nature of this study, nodal statistics were not corrected for multiple testing.

Visualization

MSTs were visualized in BrainNet Viewer (Xia et al., 2013). To summarize electrode position-specific changes visually, for each electrode montage used, an MST was constructed from the absolute time difference matrix resulting from subtraction of the pre-stimulation adjacency matrix from the stimulation adjacency matrix. Such an MST should capture the backbone of what changes during stimulation, with no particular knowledge of the direction of the changes. Finite-element method models were created from the anatomical scans of each subject using SIMNIBS, as described in further detail in our previous study, and simulations of the electric field induced by tACS were referenced for qualitative evaluation (Cabral-Calderin et al., 2016b; Thielscher et al., 2015; Windhoff et al., 2013).

Results

PLI-based versus coherence-based MSTs

We evaluated whether electrode montage effects were picked up by PLI-based MSTs and coherence-based MSTs. Figure 4 shows group mean MSTs based on PLI and coherence, constructed from the pre-stimulation runs (run 4) across all scanning sessions. The PLI-based MST shows primarily anterior-to-posterior connectivity between nodes in the network, while the coherence-based MST reflects cross-hemisphere synchrony, namely between functionally homologous regions in the two hemispheres. Table 2 displays the ANOVA results for each MST measure considered. Only MST betweenness centrality showed an electrode montage effect, and MST reference overlap showed a significant effect of FC measure. Figure 5 displays plots of mean MST BC (Figure 5A) and MST reference overlap (Figure 5B) based on PLI and coherence, compared across electrode montages. The upper panels in Figure 5 show mean measures, while the lower panels show each individual subject's stimulation fraction data value for PLI and coherence for both BC (Figure 5C) and overlap (Figure 5D), including indications for means (red lines), standard errors of the mean (red

shading), and 95% confidence intervals.

Montage effect on PLI-based MST

Given the analysis plotted for BC in Figure 5A that shows a larger difference in PLI-based BC for the different electrode montages compared to coherence-based BC, we further investigated changes in PLI-based MST BC brought about by the experimental manipulation. That is, we took time into account, for characterization of network topology modulation from baseline to stimulation. First, the 2 x 2 ANOVA run for mean PLI-based MST measures revealed a significant interaction of electrode position and time factors (p=0.0245, uncorrected) for MST BC, and a significant time effect for MST reference (p=0.0002, uncorrected). The ANOVA did not reveal significant results for global coherence-based MST topology metrics. Supplementary Tables 1 and 2 show the ANOVA results for PLI- and coherence-based MST metrics, respectively.

To find the nodes responsible for changes in the mean MST BC, a similar 2 x 2 ANOVA was conducted for the PLI-based MST BC of each node in the network. The nodes that were significantly different for the two-factor interaction results (i.e. montage-by-time) are shown in Figure 6, and included left Rolandic operculum (p=0.031), left postcentral gyrus (p=0.027), left precuneus (p=0.04), left anterior cingulate gyrus (p=0.033), right frontal superior gyrus (p=0.023), right precuneus (p=0.015), and right Heschl's gyrus (p=0.044).

As a follow-up to the node-wise 2 x 2 ANOVA of PLI-based BC finding significant differences due to electrode montage, appropriate pairwise post-hoc tests were conducted in BrainWave (i.e., pre- versus during stimulation within electrode montage) to find the direction of change in BC. Comparisons for Cz-Oz tACS versus baseline show an increase in BC for left superior frontal gyrus (p=0.026), left postcentral gyrus (p=0.037), and right precuneus (p=0.004), and a decrease in BC for left superior temporal pole (p=0.043), right superior frontal gyrus (p=0.035), and right fusiform gyrus (p=0.036). The same comparison for P5-P6 tACS shows increased BC for left inferior orbital frontal gyrus (p=0.017) and right inferior parietal lobe (p=0.043), and decreased BC in the left superior occipital gyrus (p=0.028). For each electrode montage, the left side of Figure 7 (Figure 7A: Cz-Oz, Figure 7C: P5-P6) shows the MST constructed from the absolute difference of group-averaged pre-stimulation and stimulation PLI adjacency matrices. Nodes with significantly increased BC are

highlighted in red, those with significantly decreased BC are colored blue, and their size indicates PLI BC during stimulation. As a reference for qualitative evaluation of the network topology results relative to the predicted electric field induced by stimulation with each electrode montage, finite element method model simulations from a representative subject are displayed for Cz-Oz (Figure 7B) and P5-P6 (Figure 7D).

Discussion

In this study, we addressed the question of whether phase lag index or coherence as a functional connectivity measure of BOLD fMRI time series better captures the changes in brain network topology induced by two different tACS electrode montages. To characterize network topology in an unbiased fashion, minimum spanning trees were constructed from PLI and coherence adjacency matrices, and their global and nodal topology features were compared. We found that PLI-based betweenness centrality can detect differences between stimulation with the two electrode montages more than any other measure compared. Also, group average MSTs for coherence and PLI exhibit cross-hemisphere and anterior-posterior connectivity backbones, respectively.

Functional connectivity measures of MST topography

The reference minimum spanning tree shown in Figure 4 for each functional connectivity measure gives an opportunity to first evaluate the feasibility of using either PLI or coherence as a basis for assessing network organization. Of interest, the PLI-based MST shows mostly anterior-posterior connectivity, while the coherence-based MST shows predominantly cross-hemisphere connectivity, often between functionally homologous regions. The PLI-based MST has highly-connected posterior regions, such as the medially-situated precuneus cortex and the lateral parietal cortices, that functionally project to more anterior brain regions. The tree resembles resting-state fMRI maps of the default mode network, which has increased activity in the absence of a particular task (Raichle et al., 2001). The cross-hemisphere-linked coherence-based MST reflects the high degree of interhemispheric correlation arising from homotopic regions that is well known from electrophysiology as well as rs-fMRI studies (Duffy et al., 1996; Stark et al., 2008). These differences reflect the fact that each functional connectivity measure captures a *different aspect of synchrony* between two signals, that is, delayed phase relationships versus those without delays in the frequency domain. As

such, we would consider that the two trees do not dispute each other, but rather offer complementary information, and conclude that evaluating MST topology based on both PLI and coherence appears plausible.

The ANOVA comparing FC measures across electrode position showed MST overlap to be significantly different between PLI and coherence measures, though neither measure could quantitatively capture the difference between stimulation conditions. This further illustrates the point that PLI and coherence capture different aspects of functional connectivity in the network. However, the result offers no suggestion as to which FC measure to use to compare tACS changes in the fMRI signal. The singular data points plotted in Figure 5D show that PLI-based MST topology has a high variability relative to coherence, perhaps implying more sensitivity to noise for PLI-based MST measures. On the other hand, MST betweenness centrality showed a significant difference for electrode positions. Plotting the mean values of the stimulation fraction of BC (Figure 5A) shows the PLI-based measure to better show the difference between Cz-Oz and P5-P6 tACS modulation of the network, in spite of measurement variability.

Another argument in support for considering PLI as a functional connectivity measure relates to its introduction for use in EEG to diminish the influence of blurring produced by volume conduction. The problem with volume conduction arises from the fact that EEG sensors measure the current sources from some distance, and the spatial resolution is not high enough to eliminate signal coming from neighboring sources when considering a source of interest. As such, blurring occurs, which could be considered a spurious third party signal contributing to correlation. Ignoring zero and mod pi-phase contributions allows to disregard the common source that is not of interest, and measure only delayed synchrony. Increased local correlations arise from common nonbiological sources due to unavoidable fMRI data preprocessing steps including slice timing correction and normalization. Perhaps it is conceivable that the common third party sources that we are not interested in are appropriately diminished through quantifying phase synchrony while ignoring spurious zero-lag contributions using PLI (Stam et al., 2007). Partial coherence is another example of a measure that similarly disregards zero lag synchrony, and has been proposed as a solution to both volume conduction in EEG, as well as blurring and third party source removal in fMRI (Behzadi et al., 2007; Sun et al., 2004).

PLI-based network topology changes

Following an ANOVA conducted on PLI-based MST features confirming betweenness centrality as a feature that captures electrode position by time interaction in the experiment, significant changes in PLI BC were localized to nodes of the network, as displayed in Figure 6. The right and left precuneus and the left postcentral gyrus are all regions particularly targeted by stimulation with Cz-Oz tACS, which can be seen in the representative electric field simulation in Figure 7B. The remaining anterior nodes include regions known to be highly functionally connected to the posterior nodes. For example, anterior cingulate gyrus connected to precuneus in the default mode network, and postcentral gyrus to lateral temporal regions in the somatomotor network. These results can be considered qualitatively alongside electric field simulations in conjunction with our assessment of time-based post-hoc tests conducted within electrode montage conditions, displayed in Figure 7.

Further comparisons of the PLI-based network topology measures provide some insight into the potential for PLI-based FC measures to capture differences in resting-state fMRI data. For each node, we conducted post-hoc pairwise tests of pre-stimulation versus stimulation MST BC conducted within electrode position. These comparisons allow for localizing changes to nodes responsible for overall network reorganization resulting from tACS with a specific electrode montage. The left side of Figure 7 shows significantly different nodes colored red or blue for the increased or decreased BC during stimulation relative to pre-stimulation for both electrode positions. For more insight into the results displayed, it is interesting to refer to the finite-element method model simulations of the predicted electric field for each electrode montage used in this experiment, shown to the right of Figure 7.

For Cz-Oz, the regions of the brain that have increased electric field relative to the rest of the brain in the simulation can be seen mostly in light blue. The field is highest directly below the electrodes, that is, postcentral gyrus and occipital gyrus, but there is a clear current pathway through the medial posterior cortex. BC increased for left postcentral gyrus and right precuneus, nodes which are predicted to have increased electric field during stimulation with Cz-Oz. It seems that increased current flow induced by tACS could facilitate a node's signal transmission in the network. Additionally, the results indicate P5-P6 stimulation to increase BC in the right inferior parietal lobe and decrease BC in left superior occipital gyrus, both regions where the

electric field is predicted to increase with stimulation. Regarding the contrast in direction of change in the two nodes, perhaps it is conceivable that they are both affected by the stimulation, but that the anti-phase relationship of the two current sources works against synchrony in the network. Thus, increased current would not necessarily facilitate information transmission, but work against it. Also, neural networks have a heterogeneous degree dsitribution, and brain stimulation is well known to be state dependent, so perhaps the node's place in the hierarchy of the network before stimulation determines how its stimulation affects the whole network (Ruhnau et al., 2016).

In both results, the anterior nodes with significantly changed BC in either stimulation condition could show adjustments to the network resulting from forced modulation of the dynamics in the posterior nodes. As the follow up tests were exploratory in nature, findings are not robust enough to draw specific conclusions regarding tACS stimulation with either electrode montage, however, it is encouraging to see that network dynamics appear to show regionally-specific shifts resulting from stimulation with different electrode positions. This warrants further experiments and analysis using the graph techniques applied here.

Limitations

The post-hoc tests with PLI, together with the main comparison of FC measures, show that graph analysis offers more insight into network modulations induced by tACS. We showed that functional connectivity based on PLI is not only feasible, but captures experimentally-manipulated differences in the fMRI time series better than coherence. MST reference overlap captured the temporal variance of the network, but not differences in stimulation conditions. One consideration for improved detection of MST overlap differences could be to choose a different reference MST that more closely matches the mean of the particular condition. It is possible that BC was most significantly different across MST features because of the nature of the experiment. The low current stimulation may not be enough to significantly shift degree distribution or overall organization of the network's backbone, though an incremental increase in the electric field of a certain node could subtly increase the amount of information passing through that node to others in the network. These results partially confirm our experimental hypothesis that regions directly underneath the electrodes would change

their network dynamics, increasing centrality where current should flow. However, regarding the possibility to characterize the changes as disruptive would require a well-characterized healthy PLI-based FC brain network, or an accompanying diminished behavioral measure. Changes detected in network topology were not bilaterally symmetrical, which may speak to the anti-phase relationship of the current values in the two electrodes at any given moment. Without proper control experiments, no direct conclusions about tACS phase stimulation can be made regarding the nature of P5-P6 stimulating across hemispheres.

Overall, even PLI-based measures of effects were often not significant enough to pass corrections for multiple comparisons, so more robust experimental manipulation and increased numbers of experimental measurements might strengthen findings when this analysis is applied in the future. Also, it could be the case that the choice of parcellation method to create nodes loses experimentally and functionally relevant information in averaging, as was specifically shown when using the AAL atlas by Power and colleagues (Power et al., 2011). To increase sensitivity to PLI measures, it would be worthwhile to consider other methods of parcellation in future analyses. However, our overall analysis yields plausible results using the AAL atlas. As such, it should be noted that Power et al employed thresholding in their analyses, which we circumvented through use of the MST, and maybe their AAL-based graphs lost sensitivity to subgraphs through arbitrary thresholding.

Conclusion

In this study, we asked if electrode position-dependent tACS modulation of functional brain networks measured with fMRI data is best detected and characterized using MST topology properties based on PLI or coherence as a functional connectivity measure. The affirmative findings for detection of PLI-based FC changes in MST topology, combined with the number of outstanding questions specific to tACS modulation motivates further application of these analysis techniques to this dataset, as well as other resting-state fMRI studies.

Chapter 5

General Discussion

In this study, we employed simultaneous tACS-fMRI to evaluate the causal effects of tACS on intrinsic oscillations during and after stimulation. We varied stimulation parameters and covered all combinations across six experimental sessions with each of 20 healthy volunteer subjects, imaging resting activity before, during, and after stimulation with one of two electrode montages (Cz-Oz or P5-P6) and one of three stimulation frequencies (10, 16, or 40 Hz). We simulated electric field spread in subject-specific cortical models to predict the brain regions most affected by tACS for each electrode montage. We used regions based on those simulations as seeds for resting-state functional connectivity analysis. Additionally, we examined the stimulation effects on the basis of resting-state networks.

According to these analyses, a few trends emerged. In brain regions where frequency-dependent effects of tACS were detected, 10 Hz (alpha) and 40 Hz (gamma) stimulation generally exhibited opposite effects, which maybe as a consequence of cross-frequency coupling interactions between the two frequency bands. Many significant tACS-induced effects in resting-state networks involved the left fronto-parietal control network, thus, it appears that this particular RSN could be especially vulnerable to external manipulations such as tACS. In general, most tACS effects were observed as modulation of functional connectivity between, as opposed to within, resting-state networks. Evaluating effects of tACS as predicted by the electric field simulations of the electrode montages makes several implications for future imaging and behavioral studies. That is, as some of the strongest effects in the brain were in regions functionally connected to but distant from the putative maximally stimulated regions, it can be said that tACS effects are influenced by network interactions. This insight should be considered when interpreting behavioral effects of tACS. Specifically, behavioral consequences of tACS should be interpreted based on the role of the directly stimulated regions as well as their participation in whole brain functional networks. On the aspect of statistical analysis for evaluating tACS-induced effects, many considerations can be taken.

Accounting for variance factors attributable to individual differences in subject-level and group-level analyses can give more informed results for scientific studies when a sufficient number of measurements have been acquired. These considerations prove especially important when assessing the effectiveness of a new application, such as tACS, with differences in modulation attributable to a list of factors.

Another methods consideration that proves insightful for detecting tACS-induced changes in brain activity is employing graph theory analysis. We showed that differences in network organization due to different tACS setups are detectable using the graph network characteristic betweenness centrality as computed from phase lag index functional connectivity measures. We could consider that depending on the mechanism of the induced change, some graph characteristics may be more sensitive than others at detecting experimental modulations (i.e., BC measures information flow, which could experience a critical dynamic change induced by current injection). We also used graph theory techniques to show that evaluating MST topology based on both PLI and coherence functional connectivity measures is feasible and that, together, the two offer complementary information about brain network organization.

Limitations

Throughout the chapters of this thesis, themes for the strongest limitations arise that could be considered universal for tACS experiments. Unfortunately, due to technical problems, this data set does not contain a sham condition within frequencies. Without such a control, no conclusive statements can be made about the effects of stimulation with a single frequency. The second limitation that this study suffers is the lack of a second readout for tACS-induced modulation. Possible second readouts include behavioral and physiological measures. Our study would have benefited from a resting-state EEG measure immediately before and after stimulation or imaging sessions, for example. Comparing tACS modulation of two independent readouts allows for narrowing the gap between brain oscillations and function. To close the gap, behavioral readouts accompanying the neural changes measured would reveal neural correlates of action. However, the challenge then is to choose to measure actions or behavior correctly associated with neural changes imposed during rest. Finally, given the insight about alternative group-level and subject-level analysis techniques employed in Chapters 3 and 4, respectively, perhaps reevaluating this data with additional subjects

would still allow strong, specific statements about tACS-induced effects in the brain.

Resting-state and tACS: current state of the field

An important facet of this study is that it evaluates the effects of tACS in the context of functional connectivity, illustrating the need to consider that local modulations in activity affect connected regions as well as the whole brain network. An increasing number of neuroimaging studies use functional connectivity measures and graph analysis to inform about the effects of noninvasive brain stimulation on the network level (Bächinger et al., 2017; Luft et al., 2014; Onoda et al., 2017; Weinrich et al., 2017). Using seed-based correlation to determine the spatial distribution of the motor resting-state network, Fischer and colleagues employed a clever multifocal electrode tDCS setup to exert coherent stimulation over multiple regions within the network or or use mismatched electrode polarities across the hemispheres of the network (Fischer et al., 2017). Measurement of motor evoked potentials revealed that network stimulation increased cortical excitability in the target (left M1) and its homologous contralateral region (right M1), whereas traditional two-electrode stimulation increased excitability only in the target, and mismatched network stimulation decreased cortical excitability in both hemispheres. This study exemplifies the potential to use functional connectivity to stimulate regions more readily accessible to transcranial current that share a common network with the target for modulation, or to efficiently boost a whole network based on pre-experiment subject measurement and design. Another study, which seems especially pertinent to the experiment in this thesis because of some matching stimulation parameters, employed simultaneous tACS-MEG, source reconstruction, and graph analysis to show that 10 Hz stimulation at Cz-Oz differently modulates alpha in the posterior cingulate, with greater alpha power increases occurring when the subject's eyes are closed compared to open (Fuscà et al., 2017). In addition to tACS-induced network modulation, this study gives evidence of state-dependent characteristics of tACS effects. Together, the two studies described also highlight the challenges of developing efficient stimulation protocols that arise from multiple factors influencing the effect and extent of stimulation, such as state-dependence and complex network dynamics.

Aside from recent studies employing functional connectivity analyses to elucidate stimulation effects, several other recent studies employing tACS have used similar

stimulation parameters, and their results may inform the findings of this thesis regarding frequency-specifc effects. Namely, the antagonistic relationship between alpha and gamma oscillations in brain function reappears as a driving topic in tACS studies. Through combining tACS in multiple frequency bands with behavioral tasks known to be associated with different power contributions in those bands, some research groups have made steps in linking brain oscillations and behavior. Rather than showing any evidence about cross-frequency coupling, these experiments showed that alpha and gamma tACS evoke different effects on task performance, thus making frequency-specific and sometimes anatomy-specific (based on electrode placement) associations with particular behaviors. Hopfinger and colleagues used 10 Hz and 40 Hz stimulation protocols during two attention tasks, each incorporating endogenous and exogenous cues (Hopfinger et al., 2017). Alpha stimulation was shown to increase exogenous cuing effects, with no effect on endogenous attention, while gamma stimulation improved disengagement from targets with invalid cues in the endogenous attention task. Grabner and colleagues used 10 Hz and 40 Hz stimulation during verbal creativity and verbal intelligence testing (Grabner et al., 2017). They showed that alpha tACS improved ideational fluency, but didn't change originality, and that gamma tACS elicited no performance change in the creativity measures. Driven by theories defining a relationship between alpha and attention or alpha and creativity, these studies help to make deductions about frequency-specific contributions to cognition. Notably, both studies also showed individual differences to influence the stimulation-induced performance changes.

Improving stimulation techniques: building a framework

There is still controversy regarding whether or not transcranial stimulation effectively and reliably modulates brain activity (Brignani et al., 2013; Horvath et al., 2015; Lafon et al., 2017; Rjosk et al., 2016). There are several potential reasons for lack of evidence or conflicting results starting, from the level of single experiments and accumulating into systematic reviews. From the single experiment perspective, technical issues, statistical analysis, and experimental design all can critically influence the outcome of a study. One technical problem is that the artifact induced by stimulation in electrophysiological recordings is not contained to the stimulation frequency (Noury et

al., 2016). Additionally, as discussed more extensively in Chapter 3, a list of inter- and intra-individual differences influences stimulation effects. With improved methodological practices that standardize applications across laboratories and variance factors like individual differences, we can better pinpoint actual effects of tACS (Jamil et al., 2017). Naturally, with such variance in results and quite some variation in choice of stimulation and other experimental parameters across studies, effect sizes can sum up to be negligent in systematic reviews. One tremendous boost toward discovering robust practices is pooling scientific efforts by engaging in the important practice of sharing negative findings (https://www.frontiersin.org/research-topics/5535/non-invasive-brain-stimulation-effects-on-cognition-and-brain-activity-positive-lessons-from-negativ).
Countless variations on similar experiments have likely been performed across labs that resulted in no “real” results to report and hours of “wasted” experiments. On the other side of the same coin, perhaps numerous labs systematically attempt to replicate experimental results without success, and fail to report a protocol that could inform about lack of stimulation effects. Rather than detracting from supporting evidence of tACS effects, reporting failure offers candidates for the processes of elimination regarding parameters for frequency- , function- or brain region-specific stimulation protocols, allowing for optimization of stimulation techniques for robust and reliable effects (Veniero et al., 2015).

Another important aspect of tACS effects to consider is timing from the perspective of online versus offline modulation. That is, modulation that occurs during stimulation versus aftereffects of tACS. In the conversation surrounding mechanisms of action of tACS, two main theories are proposed: entrainment and plasticity. More than likely, tACS influences both mechanisms (Veniero et al., 2015). It is possible that online entrainment of a relevant network frequency occurs, which in turn interacts with brain circuitry – perhaps through spike-timing dependent plasticity - leading to lasting changes. Proper consideration and discussion was not dedicated to aftereffects in this study, however there are notable studies employing phase-specific timing or Arnold tongue parameters to systematically test for entrainment (Herrmann and Strüber, 2017; Vossen et al., 2015). Additionally, behavioral changes may reflect plasticity-dependent modulation(Veniero et al., 2015). We have left a complete discussion of aftereffects of tACS outside the scope of this thesis, however it is important to mention because timing or mechanism of effects represent specific experimental targets. Depending on the

desired effects, whether online entrainment or offline circuitry reinforcing, for example, these pose as different targets for stimulation design. Thus, looking over the entire scope of tACS targets, a list emerges on several levels and with several mechanisms, though through a systematic approach, each can likely be specifically modulated as desired. Proper classification of parameters, effects, variability sources, measurements, and analyses will lead to robust and effective stimulation protocols that are target specific.

Several proposals for standardized frameworks surrounding target effects have been proposed for transcranial electrical stimulation protocols (Thut et al., 2017; Yavari et al., 2017). These proposals consider tACS effects from cellular (e.g., local excitability changes) to systems level (e.g., connectivity and network modulations), they incorporate measures ranging from electrophysiological to behavioral to neurochemical, and their scope ranges from individualized applications designed from measured baseline factors to group-level effects across these measures (Yavari et al., 2017). Establishing a unified framework would allow for systematic comparison of studies across laboratories, leading to faster progress in elucidating the effects of tACS on human brain function as well as the relationship between oscillations and behavior. Thus, collaboration, data sharing, and reporting negative results in the context of a framework better understanding of tACS effects as well as the relationship between brains, behavior, and oscillations (Bikson et al., 2018).

Promise for tACS: clinical applications, neuroenhancement, more?

In terms of clinical applications, few studies have employed tACS explicitly, but sinusoidal electrical current stimulation has been applied in several clinical populations using deep brain stimulation, slow oscillating tDCS, and trans-retinal techniques. Prelimiary results show potential for applications in “oscillopathies” including Parkinson's disease, schizophrenia, ADHD, bipolar disorder, Alzheimer's disease, dyslexia, and autism (Anna Fertonani and Carlo Miniussi, 2017; Uhlhaas and Singer, 2006). A recent study associating gamma frequency entrainment with amyloid load in Alzheimer's disease through entrainment with flashing light points to neurochemical benefits that come from multiple rhythmic stimulation sessions (Iaccarino et al., 2016). Beyond the clinic, additional applications for tACS include possibilities for neuroenhancement, which is gaining much attention in science and the media (Brem et

al., 2014; Schutter and Wischnewski, 2016). One question regarding how effective these applications can be pertains to whether or not there is some ceiling effect in the brain, such that there is a limit to the improvement possible to one node or network at the cost of others in the same or different network (Brem et al., 2014). Moving the concept of synchronization beyond brain regions, one study employed tACS in two subjects to explore possibilities of manipulation of inter-brain synchrony (Szymanski et al., 2017).

Conclusion

There are many open questions regarding mechanisms of online and offline stimulation effects, however evidence strongly suggests there remains much promise for future tACS applications. It is important to evaluate effects of tACS on all levels possible when measuring intrinsic brain activity: local, connectivity, and network organization. Also, it may be worth considering alternative measures of functional connectivity. To best understand the changes induced by tACS It is important to understand the underlying intrinsic oscillatory activity, as it likely underlies everything that follows. Given knowledge of the influence of tACS on intrinsic activity, one step closer is made toward successfully influencing specific targets with tACS.

Figures

Chapter 3 Figures

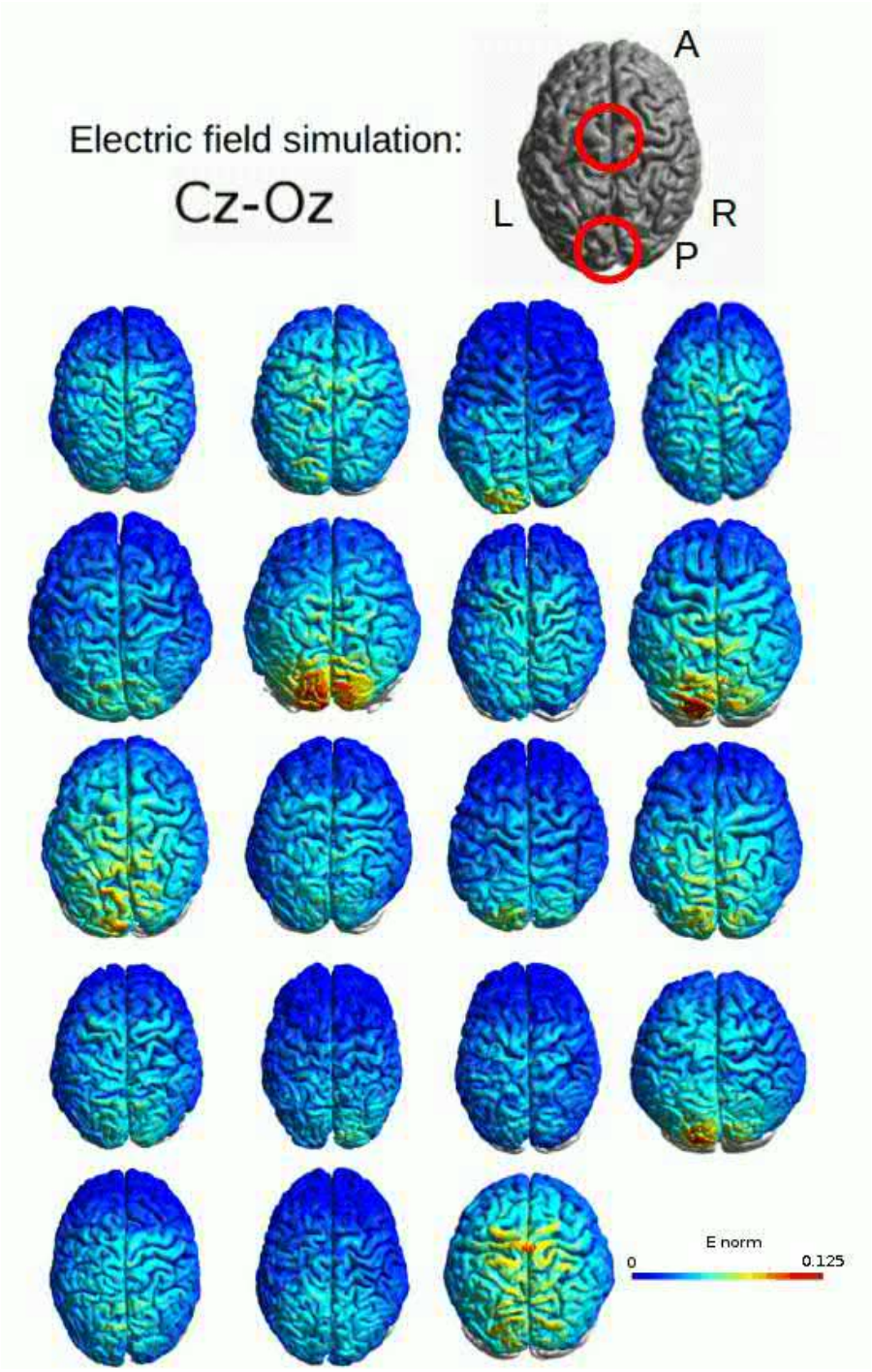

Figure 1: Subject electric field simulations for Cz-Oz stimulation based on SIMNIBS FEM models. The red circles indicate electrode locations. Values displayed are the electric field norm.

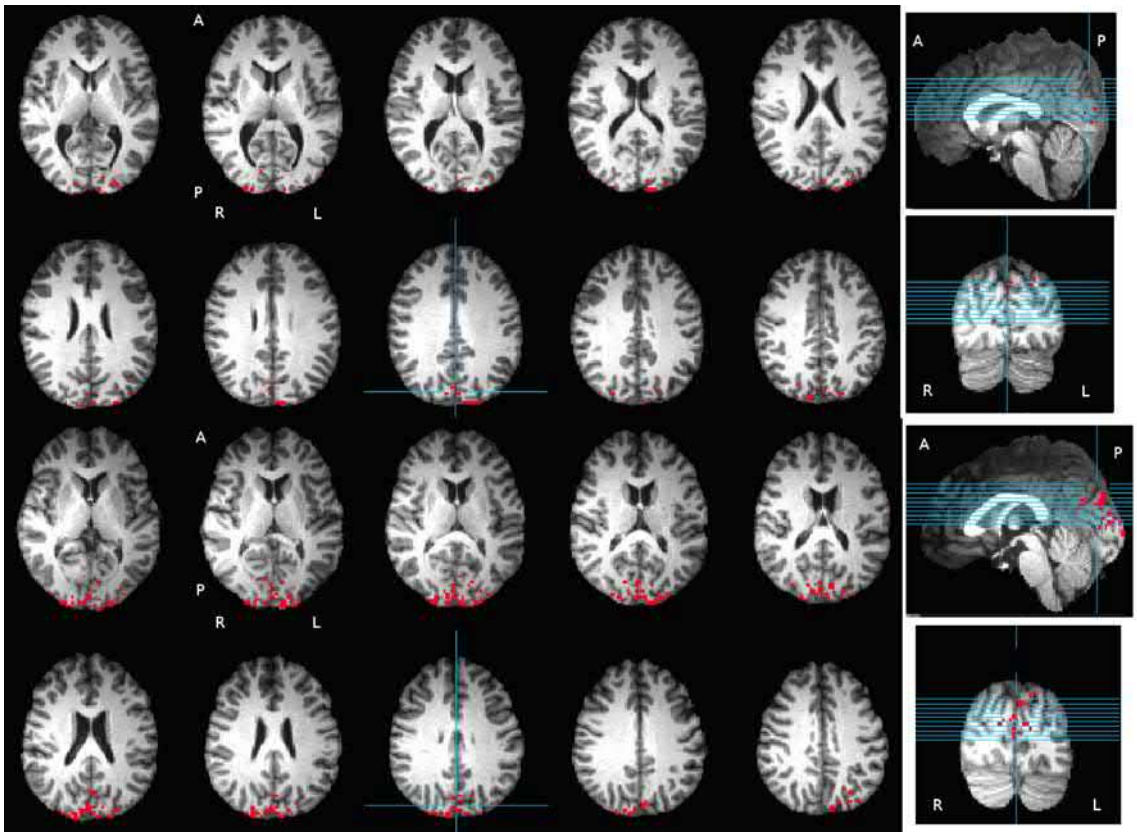

Figure 2: Oz seed used for correlation analysis from two representative subjects.

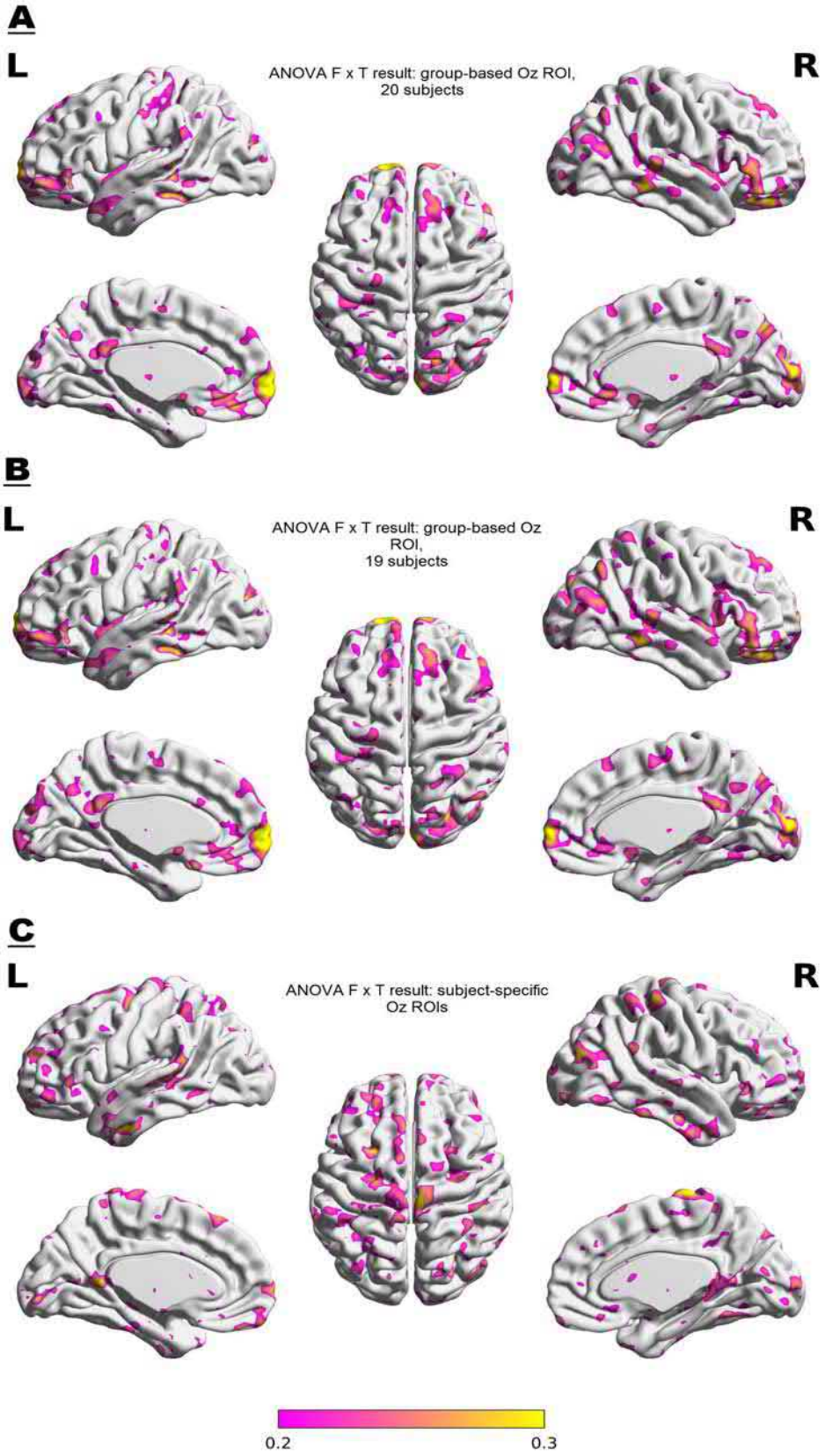

Figure 3: Statistical maps of group ANOVAs conducted using group-based Oz FC maps of 20 subjects (A), 19 subjects (B), and subject-based Oz FC maps of 19 subjects (C).

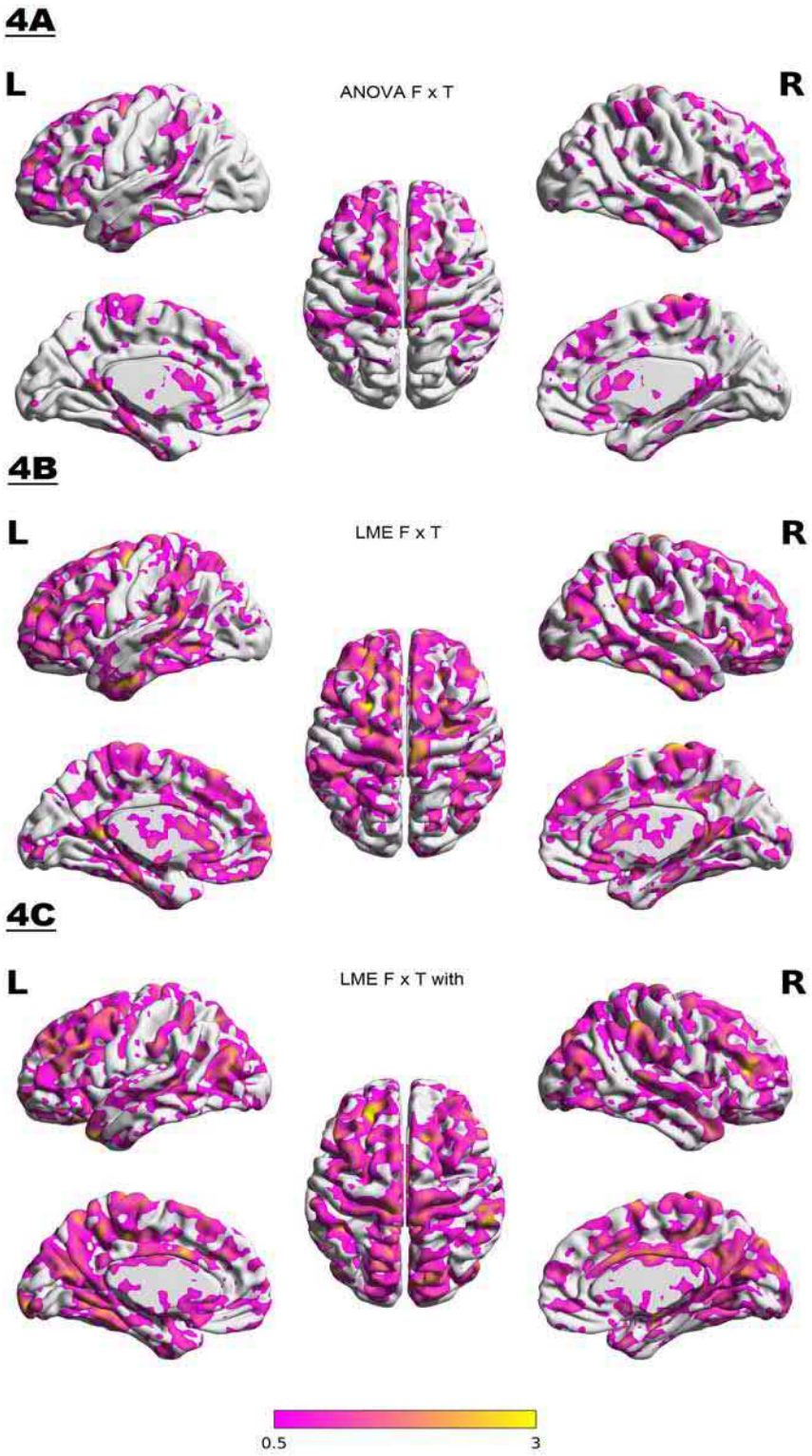

Figure 4: Figure 4A shows the results of the traditional 3 x 2 ANOVA. Figure 4B shows results of the LME model including ROI size in number of voxels as quantitative random variables to be regressed out, as its interaction with results is not specifically of interest but should be controlled for differences across subjects. Figure 4C displays results of the LME when including electric field norm means

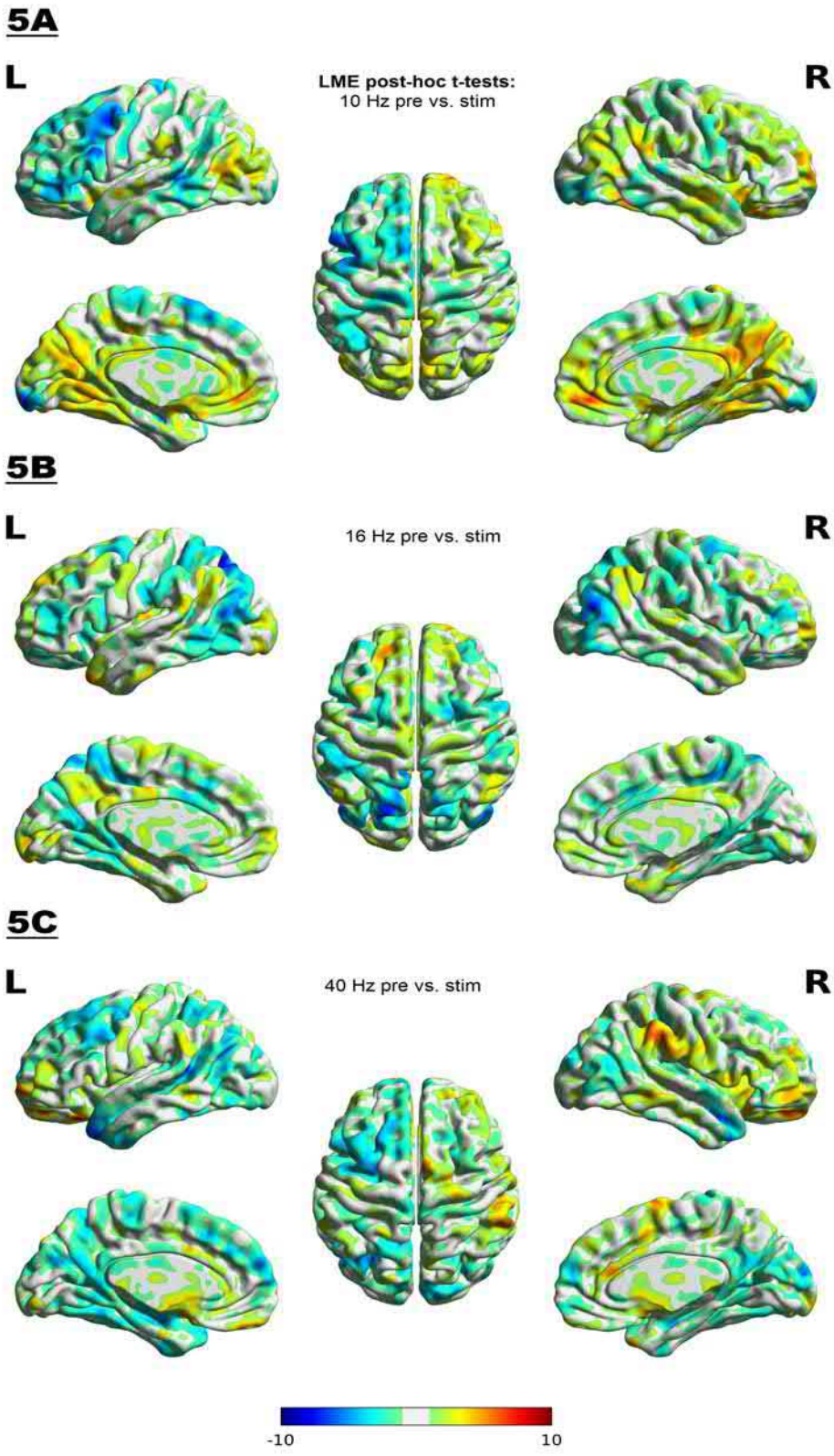

Figure 5: Panels 5A, 5B, and 5C respectively display whole-brain group level t-tests between pre- and stimulation runs within 10 Hz, 16 Hz and 40 Hz frequency stimulation conditions. The statistical t-maps show directional changes in connectivity relative to stimulation (stimulation minus pre-stimulation), such that blue indicates decreases in FC while red indicates increases in FC.

Chapter 4 Figures

A

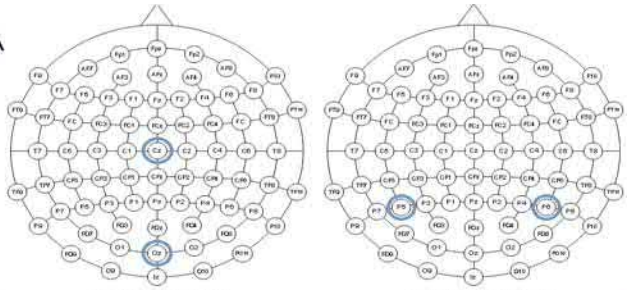

B

	Frequency 1: 10 Hz	Frequency 2: 16 Hz	Frequency 3: 40 Hz
Electrode montage 1: Cz-Oz	Condition 1: 10 Hz Cz-Oz	Condition 2: 16 Hz Cz-Oz	Condition 3: 40 Hz Cz-Oz
Electrode montage 2: P5-P6	Condition 4: 10 HzP5-P6	Condition 5: 16 Hz P5-P6	Condition 6: 40 Hz P5-P6

C

Condition order was randomized across scanning days	Run 1 pre-sham	Run 2 sham	Run 3 post-sham	anatomical (~ 8 mins)	Run 4 pre-stim	Run 5 stim	Run 6 post-stim
Condition 1					8 mins rs-fMRI	8 mins stim + rs-fMRI	
Condition 2							
Condition 3							
Condition 4							
Condition 5							
Condition 6							

Figure 1: Depiction of experimental details. Electrode montages Cz-Oz (left) and P5-P6 (right) used for stimulation displayed on the 10-20 EEG system electrode layout (A). The table describes each of the six conditions used randomly across six separate scanning days for each subject, as shown in the session flow table (C). Each scanning session consisted of six 8-minute rs-fMRI (eyes open, central cross fixation) runs separated by an 8-minute anatomical scan. The first three runs were always sham-associated, followed by real stimulation (pre-, during, and post-stimulation). The red shading indicates runs for which the data could not be used (systematic tSNR difference). The yellow borders highlight the pre-stimulation and stimulation runs used for this analysis.

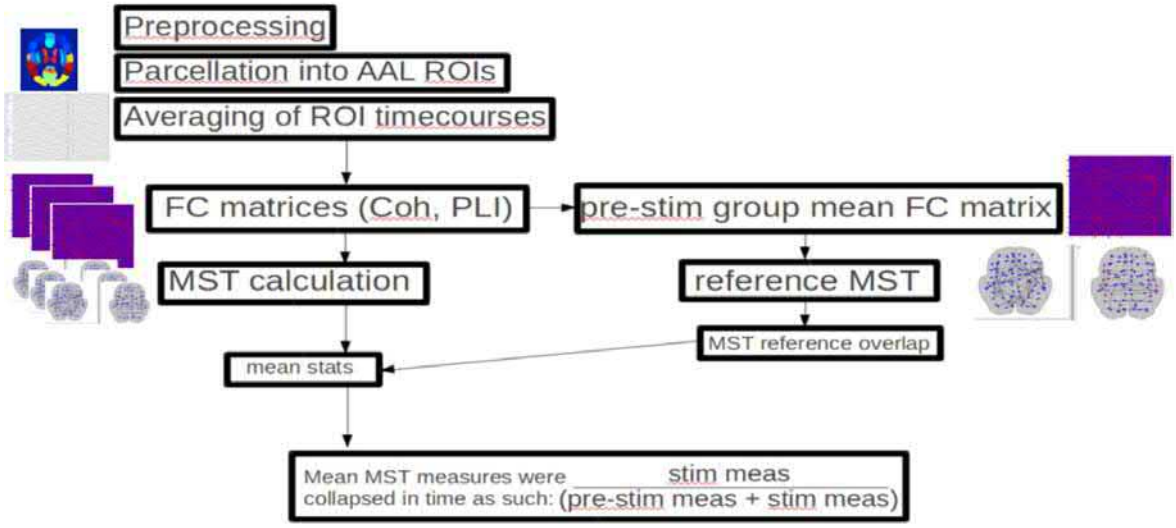

Figure 2: Processing pipeline for MST analysis of fMRI data

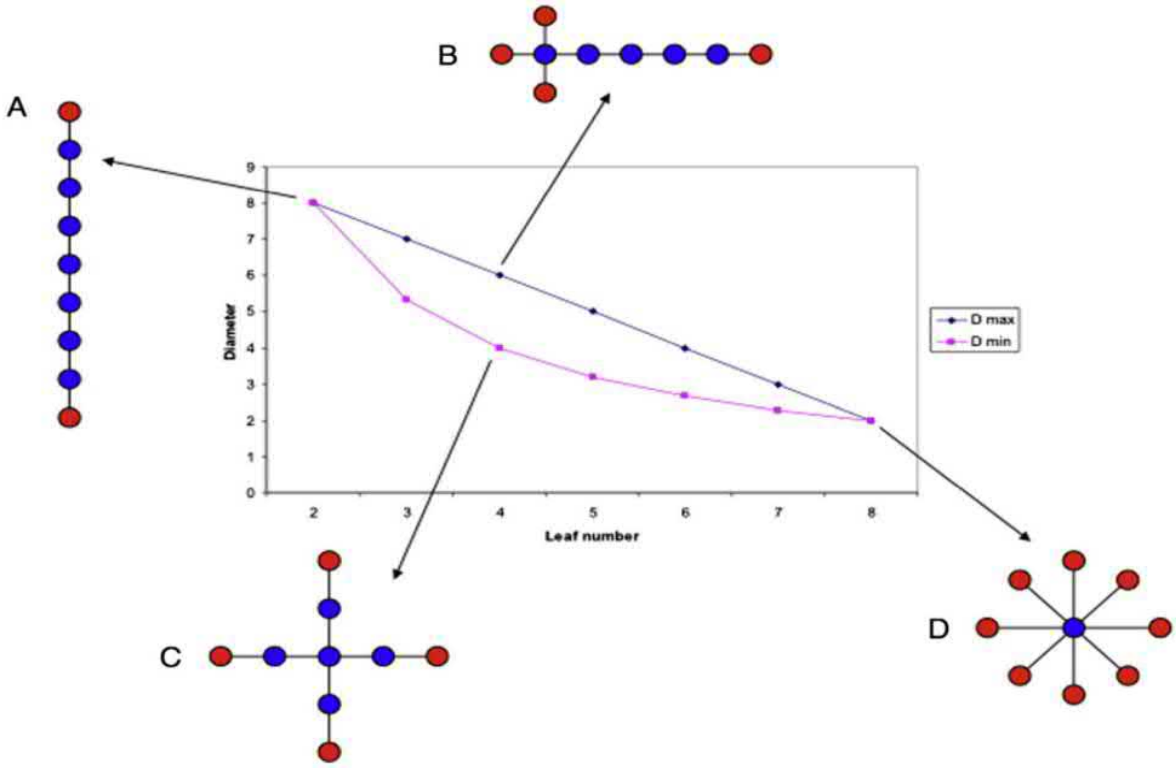

Figure 3: Schematic illustration of trees and tree measures. Different configurations of a tree consisting of N-9 nodes and m-8 edges. The plot in the middle show the diameter (maximum distance between any two edges of the tree) as a function of the leaf number (number of nodes with only one edge). Leaf nodes are shown in red. All other nodes are blue. Dmax represents the highest possible diameter for a tree with a given leaf number L. Dmax = N-L+1. Dmin represents the lowest possible diameter for a tree with a given leaf number L: Dmin = 2(N-1)/L (A) Tree with L=2 and Dmax = Dmin = 8. This type of tree is called a path. (B) Tree with the longest possible diameter (6) for a leaf number of 4. (C) Tree with the lowest possible diameter (4) for a leaf number of 4. (D) Tree with diameter of 2 and leaf number of 8. This type of tree is called a star. The path and tree represent two extreme configurations of a tree. The area between the lines corresponding to Dmax and Dmin represent a space of different possible tree configurations, bounded by maximum and minimum possible diameter for each leaf number. This figure and caption reprinted with permission from Stam et al, 2014.

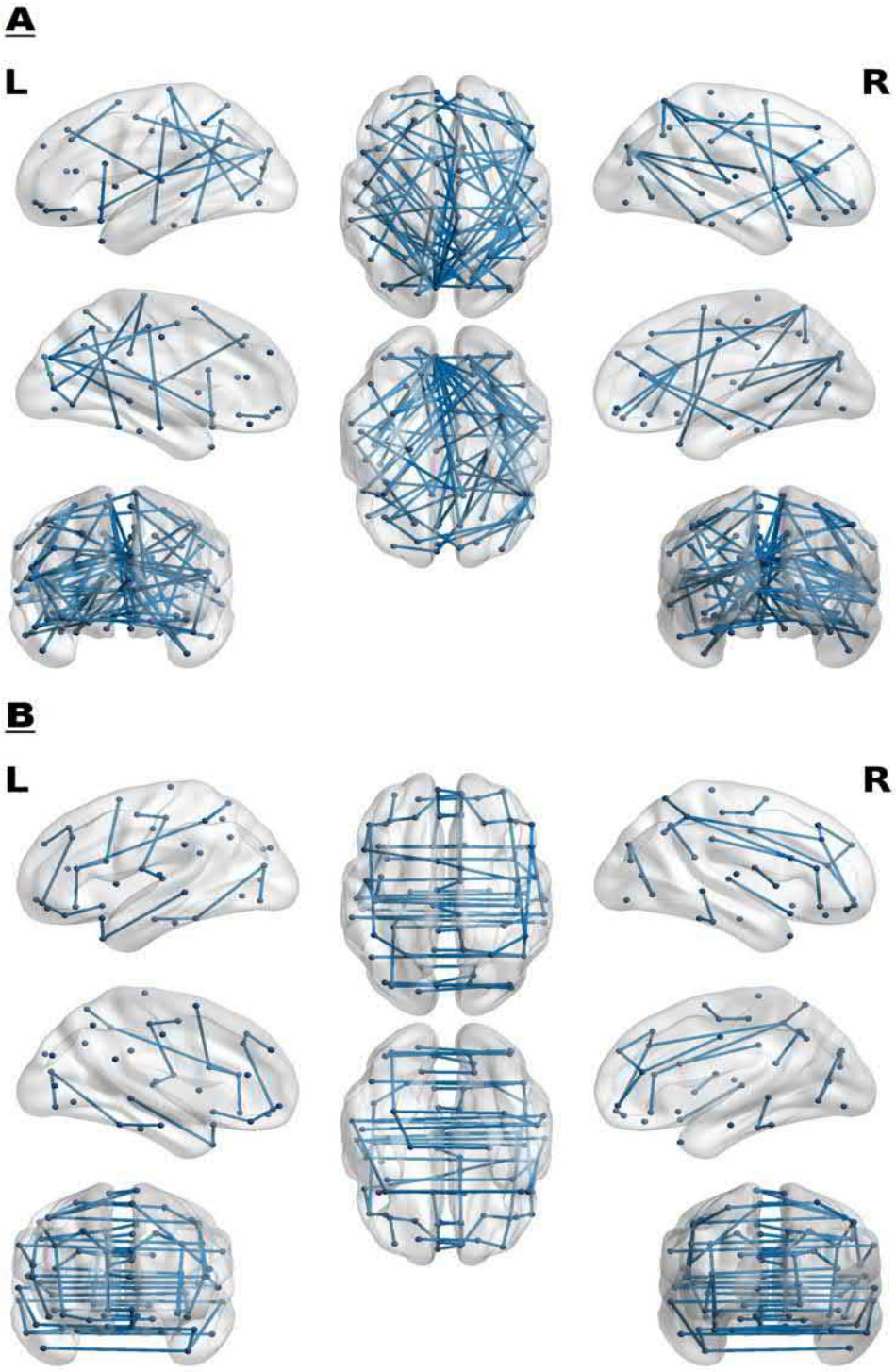

Figure 4: Group mean MSTs from the pre-stimulation data (run 4) of all conditions based on PLI (A) and coherence (B). These mean MSTs were used as a reference for overlap statistics.

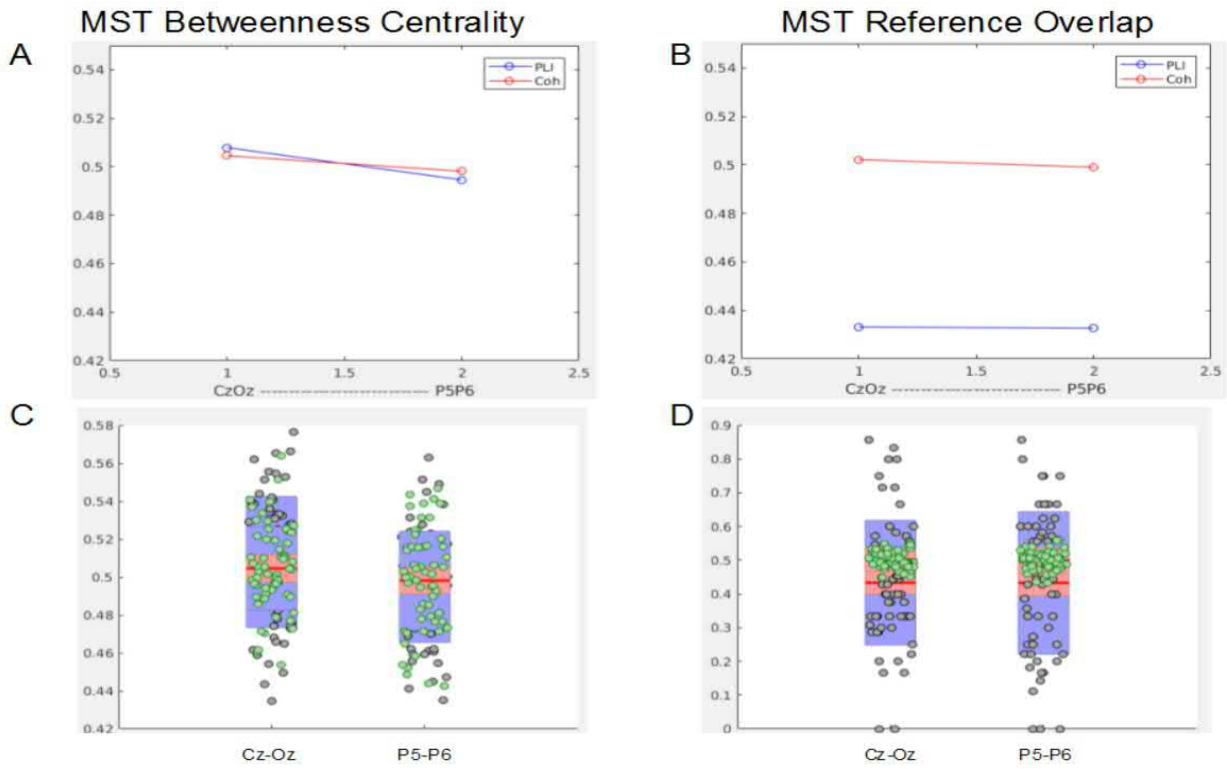

Figure 5: Post-hoc plots for 2-way ANOVA results of the MST BC (A) and MST reference overlap (B), plotted for PLI-based measures (blue) and coherence-based measures (red) across electrode position. MST BC was significantly different for electrode position ($p=0.0074$). MST reference overlap was significantly different for FC measure ($p=0.0003$). Values plotted are group means of the time-collapsed "stimulation fraction" measure. Below, each stimulation fraction data value for PLI- (gray) and coherence- (green) based MST BC (C) and MST-Ref (D) is plotted across electrode position. Blue shading indicates 95% confidence interval, red shading indicates standard error of the mean, and the red lines are mean values.

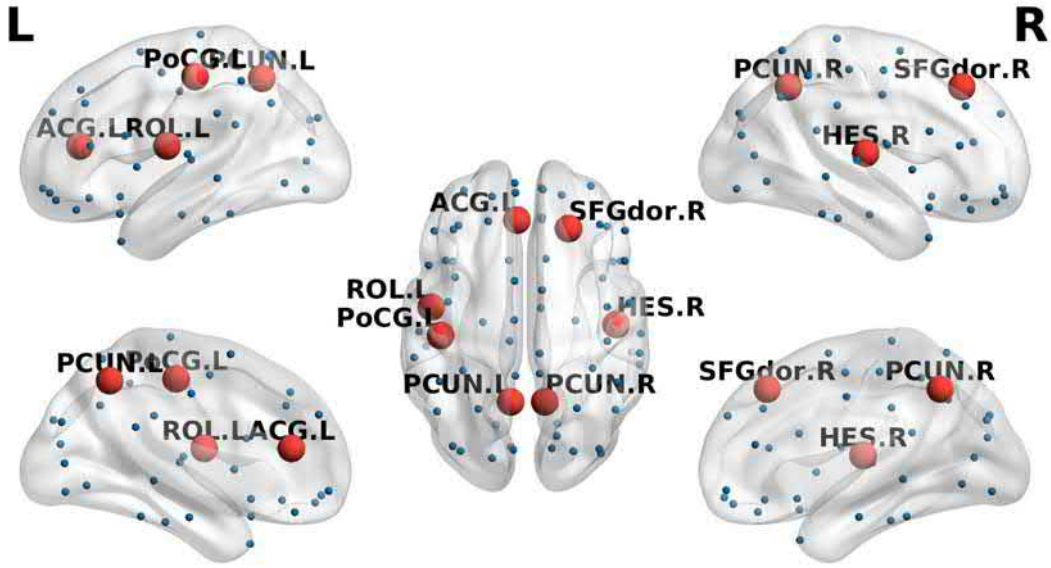

Figure 6: PLI-based betweenness centrality post-hoc ANOVA results. Red (and larger) nodes were significantly different ($p < 0.05$, uncorrected) in the post-hoc 2 x 2 (electrode position x time) ANOVA applied to PLI-based BC of each node.

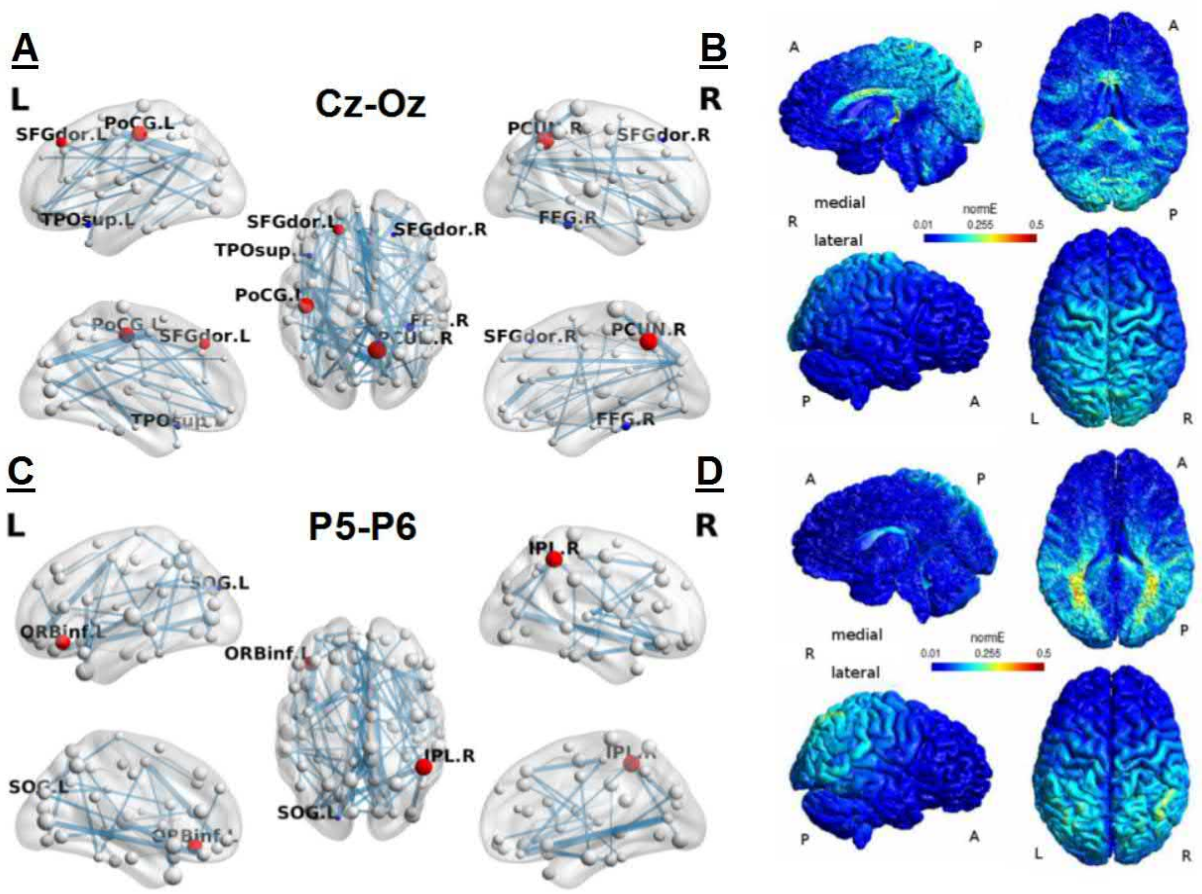

Figure 7: Post-hoc pairwise comparison (BrainWave permutation) results following 2 x 2 ANOVA on PLI BC. On the left, panels show the MST constructed from the absolute difference matrix resulting from subtracting the group and electrode position mean PLI adjacency matrix of the pre-stimulation runs from that of the stimulation runs for Cz-Oz (A) and P5-P6 (C). Node size indicates stimulation BC value, red and blue nodes indicate significant ($p<0.05$) BC increases and decreases, respectively, during stimulation. On the right, a representative subject's FEM model electrical field simulation of Cz-Oz (B) and P5-P6 (D) electrical stimulation with current and electrode parameters matching this experiment.

Tables

Chapter 4

MST topology feature	Symbol	explanation	formula
Node	N	Number of Nodes	
Link	M	Number of links (edges). Maximum leaf number	$k_i = \sum_{j \in N} a_{ij}$
Degree	k	Number of links for a given node	
Eccentricity		Longest shortest path from a reference node to any other node in the MST. The exxentricity of the whole MST is the difference between the eccentricity values of the nodes with the largest and smallest	$BC_i = \frac{1}{(n-1)(n-2)} \sum_{\substack{h,j \in N \\ h \neq j, h \neq i, \neq i}} \frac{\rho_{hj}^{(i)}}{\rho_{hj}}$ pih is the number of shortest paths between h and j that pass through i.
Betweenness centrality	BC	Fraction of all shortest paths that pass through a particular node	
Leaf fraction	Lf	Fraction of leaf nodes (L) in the MST, where a leaf node is deined as a node with degree one	$L_f = L/M$
Dieameter	D	Longest shortest path d of an MST. The diameter is also related to the leaf number. The upper limit of the diameter is defined as d_max=m-L+2, wich implies that the value of the largest possible diameter decreases when the leaf number increases.	$D = d/M$
Overlap		The fraction of links that two MSTs (MST_x and MST_y) have in common. This value can range between 0 and 1.	$\text{Overlap} = \frac{MST\_x \cap MSY\_y}{M}$

Table 1: Explanation of MST topology terminology and features evaluated in this study. Modified from Tewarie et al, 2015

MST measure	Electrode position	FC measure	Interaction
MST Ref overlap	0.92032	0.0002616 (0.002)	0.94359
Degree	0.38111	0.69908	0.67728
Eccentricity	0.10821	0.16085	0.28568
Betweenness centrality	0.0073701 (0.0516)	0.9791	0.34516
Diameter	0.12209	0.12202	0.24347
Leaf fraction	0.73462	0.81481	0.27444
FC mean	0.28545	0.061756	0.96502

Table 2: MST measures and their corresponding ANOVA results. P values listed in parentheses are shown Bonferroni corrected for multiple comparisons. All other p values reported are uncorrected. Red font indicates significance.

PLI-based FC: 2 x 2 (electrode position x time) ANOVA results

MST measure	Electrode position p	Time p	Interaction p
MST Ref overlap	0.3587	0.0002	0.1804
Degree	0.6589	0.7911	0.6589
Eccentricity	0.4333	0.5621	0.0896
Betweenness centrality	0.2281	0.7240	0.0245
Diameter	0.6204	0.5889	0.0966
Leaf fraction	0.7750	0.2580	0.3013
FC mean	0.1804	0.4785	0.5915

Supplementary Table 1: MST measures and their corresponding ANOVA results for coherence-based FC. All p values reported are uncorrected.

Coherence-based FC: 2 x 2 (electrode position x time) ANOVA results

MST measure	Electrode position	time	Interaction
MST Ref overlap	0.5027	0.0571	0.5322
Degree	1.0000	0.8534	0.2682
Eccentricity	0.8037	0.0884	0.6043
Betweenness centrality	0.3630	0.5676	0.1457
Diameter	0.7960	0.0606	0.6846
Leaf fraction	0.3571	0.6783	0.6783
FC mean	0.7408	0.9335	0.1836

Supplementary Table 2: MST measures and their corresponding ANOVA results for coherence-based FC. All p values reported are uncorrected.

References

Chapter 1

Alekseichuk, I., Turi, Z., Amador de Lara, G., Antal, A., and Paulus, W. (2016). Spatial Working Memory in Humans Depends on Theta and High Gamma Synchronization in the Prefrontal Cortex. Curr. Biol. *26*, 1513–1521.

Ali, M.M., Sellers, K.K., and Fröhlich, F. (2013). Transcranial Alternating Current Stimulation Modulates Large-Scale Cortical Network Activity by Network Resonance. J. Neurosci. *33*, 11262–11275.

Anna Fertonani, and Carlo Miniussi (2017). Transcranial Electrical Stimulation: What We Know and Do Not Know About Mechanisms. The Neuroscientist *23*, 109–123.

Antal, A., and Paulus, W. (2013). Transcranial alternating current stimulation (tACS). Front. Hum. Neurosci. *7*.

Antal, A., Boros, K., Poreisz, C., Chaieb, L., Terney, D., and Paulus, W. (2008). Comparatively weak after-effects of transcranial alternating current stimulation (tACS) on cortical excitability in humans. Brain Stimulat. *1*, 97–105.

Antal, A., Bikson, M., Datta, A., Lafon, B., Dechent, P., Parra, L.C., and Paulus, W. (2014). Imaging artifacts induced by electrical stimulation during conventional fMRI of the brain. NeuroImage *85*, 1040–1047.

Antal, A., Keeser, D., Priori, A., Padberg, F., and Nitsche, M.A. (2015). Conceptual and Procedural Shortcomings of the Systematic Review “Evidence That Transcranial Direct Current Stimulation (tDCS) Generates Little-to-no Reliable Neurophysiologic Effect Beyond MEP Amplitude Modulation in Healthy Human Subjects: A Systematic Review” by Horvath and Co-workers. Brain Stimul. Basic Transl. Clin. Res. Neuromodulation *8*, 846–849.

Beckmann, C.F., DeLuca, M., Devlin, J.T., and Smith, S.M. (2005). Investigations into resting-state connectivity using independent component analysis. Philos. Trans. R. Soc. B Biol. Sci. *360*, 1001–1013.

Berger, H. (1929). Über das Elektrenkephalogramm des Menschen. Arch. Für Psychiatr. Nervenkrankh. *87*, 527–570.

Biswal, B., Zerrin Yetkin, F., Haughton, V.M., and Hyde, J.S. (1995). Functional connectivity in the motor cortex of resting human brain using echo-planar mri. Magn. Reson. Med. *34*, 537–541.

Brookes, M.J., Hale, J.R., Zumer, J.M., Stevenson, C.M., Francis, S.T., Barnes, G.R., Owen, J.P., Morris, P.G., and Nagarajan, S.S. (2011). Measuring functional connectivity using MEG: Methodology and comparison with fcMRI. NeuroImage *56*, 1082–1104.

Buzsáki, G., and Draguhn, A. (2004). Neuronal Oscillations in Cortical Networks. Science *304*, 1926–1929.

Cabral, J., Hugues, E., Sporns, O., and Deco, G. (2011). Role of local network oscillations in resting-state functional connectivity. NeuroImage *57*, 130–139.

Cabral-Calderin, Y., Anne Weinrich, C., Schmidt-Samoa, C., Poland, E., Dechent, P., Bähr, M., and Wilke, M. (2016). Transcranial alternating current stimulation affects the BOLD signal in a frequency and task-dependent manner. Hum. Brain Mapp. *37*, 94–121.

Chang, C., Liu, Z., Chen, M.C., Liu, X., and Duyn, J.H. (2013). EEG correlates of time-varying BOLD functional connectivity. NeuroImage *72*, 227–236.

Chew, T., Ho, K.-A., and Loo, C.K. (2015). Inter- and Intra-individual Variability in Response to Transcranial Direct Current Stimulation (tDCS) at Varying Current Intensities. Brain Stimulat. *8*, 1130–1137.

Cordes, D., Haughton, V.M., Arfanakis, K., Wendt, G.J., Turski, P.A., Moritz, C.H., Quigley, M.A., and Meyerand, M.E. (2000). Mapping Functionally Related Regions of Brain with Functional Connectivity MR Imaging. Am. J. Neuroradiol. *21*, 1636–1644.

Damoiseaux, J.S., Rombouts, S. a. R.B., Barkhof, F., Scheltens, P., Stam, C.J., Smith, S.M., and Beckmann, C.F. (2006). Consistent resting-state networks across healthy subjects. Proc. Natl. Acad. Sci. *103*, 13848–13853.

De Luca, M., Beckmann, C.F., De Stefano, N., Matthews, P.M., and Smith, S.M. (2006). fMRI resting state networks define distinct modes of long-distance interactions in the human brain. NeuroImage *29*, 1359–1367.

Deligianni, F., Centeno, M., Carmichael, D.W., and Clayden, J.D. (2014). Relating resting-state fMRI and EEG whole-brain connectomes across frequency bands., Relating resting-state fMRI and EEG whole-brain connectomes across frequency bands. Front. Neurosci. Front. Neurosci.

8, *8*, 258–258.

DiFrancesco, M.W., Holland, S.K., and Szaflarski, J.P. (2008). Simultaneous EEG/Functional Magnetic Resonance Imaging at 4 Tesla: Correlates of Brain Activity to Spontaneous Alpha Rhythm During Relaxation. J. Clin. Neurophysiol. Off. Publ. Am. Electroencephalogr. Soc. *25*, 255–264.

Dowsett, J., and Herrmann, C.S. (2016). Transcranial Alternating Current Stimulation with Sawtooth Waves: Simultaneous Stimulation and EEG Recording. Front. Hum. Neurosci. *10*.

Engel, A.K., and Fries, P. (2010). Beta-band oscillations—signalling the status quo? Curr. Opin. Neurobiol. *20*, 156–165.

Farzan, F., Barr, M.S., Sun, Y., Fitzgerald, P.B., and Daskalakis, Z.J. (2012). Transcranial magnetic stimulation on the modulation of gamma oscillations in schizophrenia. Ann. N. Y. Acad. Sci. *1265*, 25–35.

Feurra, M., Paulus, W., Walsh, V., and Kanai, R. (2011). Frequency Specific Modulation of Human Somatosensory Cortex. Front. Psychol. *2*.

Foster, B.L., He, B.J., Honey, C.J., Jerbi, K., Maier, A., and Saalmann, Y.B. (2016). Spontaneous Neural Dynamics and Multi-scale Network Organization. Front. Syst. Neurosci. *10*.

Fries, P. (2005). A mechanism for cognitive dynamics: neuronal communication through neuronal coherence. Trends Cogn. Sci. *9*, 474–480.

Fröhlich, F., and McCormick, D.A. (2010). Endogenous Electric Fields May Guide Neocortical Network Activity. Neuron *67*, 129–143.

Gharabaghi, A., Kraus, D., Leão, M.T., Spüler, M., Walter, A., Bogdan, M., Rosenstiel, W., Naros, G., and Ziemann, U. (2014). Coupling brain-machine interfaces with cortical stimulation for brain-state dependent stimulation: enhancing motor cortex excitability for neurorehabilitation. Front. Hum. Neurosci. *8*.

Goldman, R.I., Stern, J.M., Engel, J., and Cohen, M.S. (2002). Simultaneous EEG and fMRI of the alpha rhythm. Neuroreport *13*, 2487–2492.

Gusnard, D.A., and Raichle, M.E. (2001). Searching for a baseline: Functional imaging and the resting human brain. Nat. Rev. Neurosci. *2*, 685.

Hacker, C.D., Snyder, A.Z., Pahwa, M., Corbetta, M., and Leuthardt, E.C. (2017). Frequency-

specific electrophysiologic correlates of resting state fMRI networks. NeuroImage *149*, 446–457.

Hanslmayr, S., Matuschek, J., and Fellner, M.-C. (2014). Entrainment of Prefrontal Beta Oscillations Induces an Endogenous Echo and Impairs Memory Formation. Curr. Biol. *24*, 904–909.

Helfrich, R.F., Knepper, H., Nolte, G., Strüber, D., Rach, S., Herrmann, C.S., Schneider, T.R., and Engel, A.K. (2014a). Selective Modulation of Interhemispheric Functional Connectivity by HD-tACS Shapes Perception. PLoS Biol. *12*.

Helfrich, R.F., Schneider, T.R., Rach, S., Trautmann-Lengsfeld, S.A., Engel, A.K., and Herrmann, C.S. (2014b). Entrainment of Brain Oscillations by Transcranial Alternating Current Stimulation. Curr. Biol. *24*, 333–339.

Herrmann, C.S., and Strüber, D. (2017). What Can Transcranial Alternating Current Stimulation Tell Us About Brain Oscillations? Curr. Behav. Neurosci. Rep. *4*, 128–137.

van den Heuvel, M.P., and Hulshoff Pol, H.E. (2010). Exploring the brain network: A review on resting-state fMRI functional connectivity. Eur. Neuropsychopharmacol. *20*, 519–534.

van den Heuvel, M.P., Mandl, R.C.W., Kahn, R.S., and Hulshoff Pol, H.E. (2009). Functionally linked resting-state networks reflect the underlying structural connectivity architecture of the human brain. Hum. Brain Mapp. *30*, 3127–3141.

Honey, C.J., Sporns, O., Cammoun, L., Gigandet, X., Thiran, J.P., Meuli, R., and Hagmann, P. (2009). Predicting human resting-state functional connectivity from structural connectivity. Proc. Natl. Acad. Sci. *106*, 2035–2040.

Horvath, J.C., Forte, J.D., and Carter, O. (2015). Quantitative Review Finds No Evidence of Cognitive Effects in Healthy Populations From Single-session Transcranial Direct Current Stimulation (tDCS). Brain Stimulat. *8*, 535–550.

Hughes, S.W., Lörincz, M., Cope, D.W., Blethyn, K.L., Kékesi, K.A., Parri, H.R., Juhász, G., and Crunelli, V. (2004). Synchronized Oscillations at α and θ Frequencies in the Lateral Geniculate Nucleus. Neuron *42*, 253–268.

Jaegle, A., and Ro, T. (2013). Direct Control of Visual Perception with Phase-specific Modulation of Posterior Parietal Cortex. J. Cogn. Neurosci. *26*, 422–432.

Jann, K., Dierks, T., Boesch, C., Kottlow, M., Strik, W., and Koenig, T. (2009). BOLD correlates of EEG alpha phase-locking and the fMRI default mode network. NeuroImage *45*, 903–916.

Jensen, O., and Colgin, L.L. (2007). Cross-frequency coupling between neuronal oscillations. Trends Cogn. Sci. *11*, 267–269.

Jensen, O., and Mazaheri, A. (2010). Shaping Functional Architecture by Oscillatory Alpha Activity: Gating by Inhibition. Front. Hum. Neurosci. *4*.

K. J. Friston, C. D. Frith, P. F. Liddle, and R. S. J. Frackowiak (1993). Functional Connectivity: The Principal-Component Analysis of Large (PET) Data Sets. J. Cereb. Blood Flow Metab. *13*, 5–14.

Kanai, R., Chaieb, L., Antal, A., Walsh, V., and Paulus, W. (2008). Frequency-Dependent Electrical Stimulation of the Visual Cortex. Curr. Biol. *18*, 1839–1843.

Klimesch, W., Sauseng, P., and Gerloff, C. (2003). Enhancing cognitive performance with repetitive transcranial magnetic stimulation at human individual alpha frequency. Eur. J. Neurosci. *17*, 1129–1133.

Kopell, N., Ermentrout, G.B., Whittington, M.A., and Traub, R.D. (2000). Gamma rhythms and beta rhythms have different synchronization properties. Proc. Natl. Acad. Sci. *97*, 1867–1872.

Laufs, H., Kleinschmidt, A., Beyerle, A., Eger, E., Salek-Haddadi, A., Preibisch, C., and Krakow, K. (2003). EEG-correlated fMRI of human alpha activity. NeuroImage *19*, 1463–1476.

Liu, Y., Wang, K., Yu, C., He, Y., Zhou, Y., Liang, M., Wang, L., and Jiang, T. (2008). Regional homogeneity, functional connectivity and imaging markers of Alzheimer's disease: A review of resting-state fMRI studies. Neuropsychologia *46*, 1648–1656.

Logothetis, N.K. (2003). The Underpinnings of the BOLD Functional Magnetic Resonance Imaging Signal. J. Neurosci. *23*, 3963–3971.

Logothetis, N.K., Pauls, J., Augath, M., Trinath, T., and Oeltermann, A. (2001). Neurophysiological investigation of the basis of the fMRI signal. Nature *412*, 150.

Lörincz, M.L., Crunelli, V., and Hughes, S.W. (2008). Cellular Dynamics of Cholinergically Induced α (8–13 Hz) Rhythms in Sensory Thalamic Nuclei In Vitro. J. Neurosci. *28*, 660–671.

Lowe, M.J., Mock, B.J., and Sorenson, J.A. (1998). Functional Connectivity in Single and Multislice Echoplanar Imaging Using Resting-State Fluctuations. NeuroImage *7*, 119–132.

Magri, C., Schridde, U., Murayama, Y., Panzeri, S., and Logothetis, N.K. (2012). The Amplitude and Timing of the BOLD Signal Reflects the Relationship between Local Field Potential Power at Different Frequencies. J. Neurosci. *32*, 1395–1407.

Makeig, S., Westerfield, M., Jung, T.-P., Enghoff, S., Townsend, J., Courchesne, E., and Sejnowski, T.J. (2002). Dynamic Brain Sources of Visual Evoked Responses. Science *295*, 690–694.

Mantini, D., Perrucci, M.G., Gratta, C.D., Romani, G.L., and Corbetta, M. (2007). Electrophysiological signatures of resting state networks in the human brain. Proc. Natl. Acad. Sci. *104*, 13170–13175.

Matsumoto, H., and Ugawa, Y. (2017). Adverse events of tDCS and tACS: A review. Clin. Neurophysiol. Pract. *2*, 19–25.

Miltner, W.H.R., Braun, C., Arnold, M., Witte, H., and Taub, E. (1999). Coherence of gamma-band EEG activity as a basis for associative learning. Nature *397*, 434.

de Munck, J.C., Gonçalves, S.I., Huijboom, L., Kuijer, J.P.A., Pouwels, P.J.W., Heethaar, R.M., and Lopes da Silva, F.H. (2007). The hemodynamic response of the alpha rhythm: An EEG/fMRI study. NeuroImage *35*, 1142–1151.

Muthukumaraswamy, S. d., and Johnson, B. w. (2004). Changes in rolandic mu rhythm during observation of a precision grip. Psychophysiology *41*, 152–156.

Nasseri, P., Nitsche, M.A., and Ekhtiari, H. (2015). A framework for categorizing electrode montages in transcranial direct current stimulation. Front. Hum. Neurosci. *9*.

Neuling, T., Wagner, S., Wolters, C.H., Zaehle, T., and Herrmann, C.S. (2012). Finite-Element Model Predicts Current Density Distribution for Clinical Applications of tDCS and tACS. Front. Psychiatry *3*.

Neuling, T., Ruhnau, P., Fuscà, M., Demarchi, G., Herrmann, C.S., and Weisz, N. (2015). Friends, not foes: Magnetoencephalography as a tool to uncover brain dynamics during transcranial alternating current stimulation. NeuroImage *118*, 406–413.

Neuling, T., Ruhnau, P., Weisz, N., Herrmann, C.S., and Demarchi, G. (2017). Faith and oscillations recovered: On analyzing EEG/MEG signals during tACS. NeuroImage *147*, 960–963.

Nir, Y., Fisch, L., Mukamel, R., Gelbard-Sagiv, H., Arieli, A., Fried, I., and Malach, R. (2007). Coupling between Neuronal Firing Rate, Gamma LFP, and BOLD fMRI Is Related to

Interneuronal Correlations. Curr. Biol. *17*, 1275–1285.

Notbohm, A., and Herrmann, C.S. (2016). Flicker Regularity Is Crucial for Entrainment of Alpha Oscillations. Front. Hum. Neurosci. *10*.

Notbohm, A., Kurths, J., and Herrmann, C.S. (2016). Modification of Brain Oscillations via Rhythmic Light Stimulation Provides Evidence for Entrainment but Not for Superposition of Event-Related Responses. Front. Hum. Neurosci. *10*.

ten Oever, S., de Graaf, T.A., Bonnemayer, C., Ronner, J., Sack, A.T., and Riecke, L. (2016). Stimulus Presentation at Specific Neuronal Oscillatory Phases Experimentally Controlled with tACS: Implementation and Applications. Front. Cell. Neurosci. *10*.

Ogawa, S., Lee, T.M., Kay, A.R., and Tank, D.W. (1990). Brain magnetic resonance imaging with contrast dependent on blood oxygenation. Proc. Natl. Acad. Sci. *87*, 9868–9872.

Opitz, A., Legon, W., Rowlands, A., Bickel, W.K., Paulus, W., and Tyler, W.J. (2013). Physiological observations validate finite element models for estimating subject-specific electric field distributions induced by transcranial magnetic stimulation of the human motor cortex. NeuroImage *81*, 253–264.

Opitz, A., Paulus, W., Will, S., Antunes, A., and Thielscher, A. (2015). Determinants of the electric field during transcranial direct current stimulation. NeuroImage *109*, 140–150.

Opitz, A., Falchier, A., Yan, C.-G., Yeagle, E.M., Linn, G.S., Megevand, P., Thielscher, A., A, R.D., Milham, M.P., Mehta, A.D., et al. (2016). Spatiotemporal structure of intracranial electric fields induced by transcranial electric stimulation in humans and nonhuman primates. Sci. Rep. *6*, 31236.

Ozen, S., Sirota, A., Belluscio, M.A., Anastassiou, C.A., Stark, E., Koch, C., and Buzsáki, G. (2010). Transcranial electric stimulation entrains cortical neuronal populations in rats. J. Neurosci. Off. J. Soc. Neurosci. *30*, 11476–11485.

Park, H.-J., and Friston, K. (2013). Structural and Functional Brain Networks: From Connections to Cognition. Science *342*, 1238411.

Pasquale, F. de, Penna, S.D., Snyder, A.Z., Lewis, C., Mantini, D., Marzetti, L., Belardinelli, P., Ciancetta, L., Pizzella, V., Romani, G.L., et al. (2010). Temporal dynamics of spontaneous MEG activity in brain networks. Proc. Natl. Acad. Sci. *107*, 6040–6045.

Pfurtscheller, G., and Aranibar, A. (1979). Evaluation of event-related desynchronization (ERD) preceding and following voluntary self-paced movement. Electroencephalogr. Clin. Neurophysiol. *46*, 138–146.

Pogosyan, A., Gaynor, L.D., Eusebio, A., and Brown, P. (2009). Boosting Cortical Activity at Beta-Band Frequencies Slows Movement in Humans. Curr. Biol. *19*, 1637–1641.

Polanía, R., Nitsche, M.A., Korman, C., Batsikadze, G., and Paulus, W. (2012). The importance of timing in segregated theta phase-coupling for cognitive performance. Curr. Biol. CB *22*, 1314–1318.

Raichle, M.E., MacLeod, A.M., Snyder, A.Z., Powers, W.J., Gusnard, D.A., and Shulman, G.L. (2001). A default mode of brain function. Proc. Natl. Acad. Sci. *98*, 676–682.

Rodriguez, E., George, N., Lachaux, J.-P., Martinerie, J., Renault, B., and Varela, F.J. (1999). Perception's shadow: long-distance synchronization of human brain activity. Nature *397*, 430.

Romei, V., Thut, G., and Silvanto, J. (2016). Information-Based Approaches of Noninvasive Transcranial Brain Stimulation. Trends Neurosci. *39*, 782–795.

Ruffini, G., Fox, M.D., Ripolles, O., Miranda, P.C., and Pascual-Leone, A. (2014). Optimization of multifocal transcranial current stimulation for weighted cortical pattern targeting from realistic modeling of electric fields. NeuroImage *89*, 216–225.

Ruhnau, P., Neuling, T., Fuscá, M., Herrmann, C.S., Demarchi, G., and Weisz, N. (2016). Eyes wide shut: Transcranial alternating current stimulation drives alpha rhythm in a state dependent manner. Sci. Rep. *6*, srep27138.

Santarnecchi, E., Polizzotto, N.R., Godone, M., Giovannelli, F., Feurra, M., Matzen, L., Rossi, A., and Rossi, S. (2013). Frequency-Dependent Enhancement of Fluid Intelligence Induced by Transcranial Oscillatory Potentials. Curr. Biol. *23*, 1449–1453.

Sanz-Arigita, E.J., Schoonheim, M.M., Damoiseaux, J.S., Rombouts, S.A.R.B., Maris, E., Barkhof, F., Scheltens, P., and Stam, C.J. (2010). Loss of 'Small-World' Networks in Alzheimer's Disease: Graph Analysis of fMRI Resting-State Functional Connectivity. PLOS ONE *5*, e13788.

Sauseng, P., Klimesch, W., Gruber, W.R., Hanslmayr, S., Freunberger, R., and Doppelmayr, M. (2007). Are event-related potential components generated by phase resetting of brain

oscillations? A critical discussion. Neuroscience *146*, 1435–1444.

Scheeringa, R., Petersson, K.M., Kleinschmidt, A., Jensen, O., and Bastiaansen, M.C.M. (2012). EEG Alpha Power Modulation of fMRI Resting-State Connectivity. Brain Connect. *2*, 254–264.

Schnitzler, A., and Gross, J. (2005). Normal and pathological oscillatory communication in the brain. Nat. Rev. Neurosci. *6*, nrn1650.

Schutter, D.J.L.G., and Wischnewski, M. (2016). A meta-analytic study of exogenous oscillatory electric potentials in neuroenhancement. Neuropsychologia *86*, 110–118.

Schwiedrzik, C.M. (2009). Retina or Visual Cortex? The Site of Phosphene Induction by Transcranial Alternating Current Stimulation. Front. Integr. Neurosci. *3*.

Sela, T., Kilim, A., and Lavidor, M. (2012). Transcranial Alternating Current Stimulation Increases Risk-Taking Behavior in the Balloon Analog Risk Task. Front. Neurosci. *6*.

Sporns, O. (2013). Structure and function of complex brain networks. Dialogues Clin. Neurosci. *15*, 247–262.

Sporns, O., Chialvo, D.R., Kaiser, M., and Hilgetag, C.C. (2004). Organization, development and function of complex brain networks. Trends Cogn. Sci. *8*, 418–425.

Stam, C.J. (2014). Modern network science of neurological disorders. Nat. Rev. Neurosci. *15*, 683–695.

Stam, C.J., Nolte, G., and Daffertshofer, A. (2007). Phase lag index: Assessment of functional connectivity from multi channel EEG and MEG with diminished bias from common sources. Hum. Brain Mapp. *28*, 1178–1193.

Stein, A. von, Chiang, C., and König, P. (2000). Top-down processing mediated by interareal synchronization. Proc. Natl. Acad. Sci. *97*, 14748–14753.

von Stein, A., and Sarnthein, J. (2000). Different frequencies for different scales of cortical integration: from local gamma to long range alpha/theta synchronization. Int. J. Psychophysiol. *38*, 301–313.

Strüber, D., Rach, S., Trautmann-Lengsfeld, S.A., Engel, A.K., and Herrmann, C.S. (2014). Antiphasic 40 Hz Oscillatory Current Stimulation Affects Bistable Motion Perception. Brain Topogr. *27*, 158–171.

Tagliazucchi, E., von Wegner, F., Morzelewski, A., Brodbeck, V., and Laufs, H. (2012). Dynamic

BOLD functional connectivity in humans and its electrophysiological correlates. Front. Hum. Neurosci. *6*.

Tallon-Baudry, C., and Bertrand, O. (1999). Oscillatory gamma activity in humans and its role in object representation. Trends Cogn. Sci. *3*, 151–162.

Tewarie, P., Bright, M.G., Hillebrand, A., Robson, S.E., Gascoyne, L.E., Morris, P.G., Meier, J., Van Mieghem, P., and Brookes, M.J. (2016). Predicting haemodynamic networks using electrophysiology: The role of non-linear and cross-frequency interactions. NeuroImage *130*, 273–292.

Thielscher, A., Antunes, A., and Saturnino, G.B. (2015). Field modeling for transcranial magnetic stimulation: A useful tool to understand the physiological effects of TMS? In 2015 37th Annual International Conference of the IEEE Engineering in Medicine and Biology Society (EMBC), pp. 222–225.

Thut, G., Miniussi, C., and Gross, J. (2012). The Functional Importance of Rhythmic Activity in the Brain. Curr. Biol. *22*, R658–R663.

Thut, G., Bergmann, T.O., Fröhlich, F., Soekadar, S.R., Brittain, J.-S., Valero-Cabré, A., Sack, A.T., Miniussi, C., Antal, A., Siebner, H.R., et al. (2017). Guiding transcranial brain stimulation by EEG/MEG to interact with ongoing brain activity and associated functions: A position paper. Clin. Neurophysiol. *128*, 843–857.

Turi, Z., Ambrus, G.G., Janacsek, K., Emmert, K., Hahn, L., Paulus, W., and Antal, A. (2013). Both the cutaneous sensation and phosphene perception are modulated in a frequency-specific manner during transcranial alternating current stimulation. Restor. Neurol. Neurosci. *31*, 275–285.

Uhlhaas, P.J., Haenschel, C., Nikolić, D., and Singer, W. (2008). The Role of Oscillations and Synchrony in Cortical Networks and Their Putative Relevance for the Pathophysiology of Schizophrenia. Schizophr. Bull. *34*, 927–943.

Veniero, D., Vossen, A., Gross, J., and Thut, G. (2015). Lasting EEG/MEG Aftereffects of Rhythmic Transcranial Brain Stimulation: Level of Control Over Oscillatory Network Activity. Front. Cell. Neurosci. *9*.

Violante, I.R., Li, L.M., Carmichael, D.W., Lorenz, R., Leech, R., Hampshire, A., Rothwell, J.C.,

and Sharp, D.J. Externally induced frontoparietal synchronization modulates network dynamics and enhances working memory performance. ELife *6*.

Chapter 3

Cabral-Calderin, Y., Williams, K.A., Opitz, A., Dechent, P., and Wilke, M. (2016). Transcranial alternating current stimulation modulates spontaneous low frequency fluctuations as measured with fMRI. NeuroImage *141*, 88–107.

Chen, B., Xu, T., Zhou, C., Wang, L., Yang, N., Wang, Z., Dong, H.-M., Yang, Z., Zang, Y.-F., Zuo, X.-N., et al. (2015). Individual Variability and Test-Retest Reliability Revealed by Ten Repeated Resting-State Brain Scans over One Month. PLOS ONE *10*, e0144963.

Chen, G., Saad, Z.S., Britton, J.C., Pine, D.S., and Cox, R.W. (2013). Linear mixed-effects modeling approach to FMRI group analysis. NeuroImage *73*, 176–190.

Cox, R.W. (1996). AFNI: Software for Analysis and Visualization of Functional Magnetic Resonance Neuroimages. Comput. Biomed. Res. *29*, 162–173.

Fox, M.D., Buckner, R.L., Liu, H., Chakravarty, M.M., Lozano, A.M., and Pascual-Leone, A. (2014). Resting-state networks link invasive and noninvasive brain stimulation across diverse psychiatric and neurological diseases. Proc. Natl. Acad. Sci. *111*, E4367–E4375.

Horvath, J.C., Forte, J.D., and Carter, O. (2015). Quantitative Review Finds No Evidence of Cognitive Effects in Healthy Populations From Single-session Transcranial Direct Current Stimulation (tDCS). Brain Stimulat. *8*, 535–550.

Jann, K., Dierks, T., Boesch, C., Kottlow, M., Strik, W., and Koenig, T. (2009). BOLD correlates of EEG alpha phase-locking and the fMRI default mode network. NeuroImage *45*, 903–916.

Li, L.M., Uehara, K., and Hanakawa, T. (2015). The contribution of interindividual factors to variability of response in transcranial direct current stimulation studies. Front. Cell. Neurosci. *9*.

Opitz, A., Paulus, W., Will, S., Antunes, A., and Thielscher, A. (2015). Determinants of the electric field during transcranial direct current stimulation. NeuroImage *109*, 140–150.

Ruffini, G., Fox, M.D., Ripolles, O., Miranda, P.C., and Pascual-Leone, A. (2014). Optimization of multifocal transcranial current stimulation for weighted cortical pattern targeting from realistic modeling of electric fields. NeuroImage *89*, 216–225.

Saiote, C., Turi, Z., Paulus, W., and Antal, A. (2013). Combining functional magnetic resonance imaging with transcranial electrical stimulation. Front. Hum. Neurosci. *7*.

von Stein, A., and Sarnthein, J. (2000). Different frequencies for different scales of cortical integration: from local gamma to long range alpha/theta synchronization. Int. J. Psychophysiol. *38*, 301–313.

Tavakoli, A.V., and Yun, K. (2017). Transcranial Alternating Current Stimulation (tACS) Mechanisms and Protocols. Front. Cell. Neurosci. *11*.

Thielscher, A., Antunes, A., and Saturnino, G.B. (2015). Field modeling for transcranial magnetic stimulation: A useful tool to understand the physiological effects of TMS? In 2015 37th Annual International Conference of the IEEE Engineering in Medicine and Biology Society (EMBC), pp. 222–225.

Uhlhaas, P.J., Haenschel, C., Nikolić, D., and Singer, W. (2008). The Role of Oscillations and Synchrony in Cortical Networks and Their Putative Relevance for the Pathophysiology of Schizophrenia. Schizophr. Bull. *34*, 927–943.

Windhoff, M., Opitz, A., and Thielscher, A. (2013). Electric field calculations in brain stimulation based on finite elements: An optimized processing pipeline for the generation and usage of accurate individual head models. Hum. Brain Mapp. *34*, 923–935.

Xia, M., Wang, J., and He, Y. (2013). BrainNet Viewer: A Network Visualization Tool for Human Brain Connectomics. PLOS ONE *8*, e68910.

Yavari, F., Nitsche, M.A., and Ekhtiari, H. (2017). Transcranial Electric Stimulation for Precision Medicine: A Spatiomechanistic Framework. Front. Hum. Neurosci. *11*.

Ziemann, U., and Siebner, H.R. (2015). Inter-subject and Inter-session Variability of Plasticity Induction by Non-invasive Brain Stimulation: Boon or Bane? Brain Stimulat. *8*, 662–663.

Chapter 4

Alekseichuk, I., Turi, Z., Amador de Lara, G., Antal, A., and Paulus, W. (2016). Spatial Working Memory in Humans Depends on Theta and High Gamma Synchronization in the Prefrontal Cortex. Curr. Biol. *26*, 1513–1521.

Andellini, M., Cannatà, V., Gazzellini, S., Bernardi, B., and Napolitano, A. (2015). Test-retest reliability of graph metrics of resting state MRI functional brain networks: A review. J. Neurosci. Methods *253*, 183–192.

Antal, A., Boros, K., Poreisz, C., Chaieb, L., Terney, D., and Paulus, W. (2008). Comparatively weak after-effects of transcranial alternating current stimulation (tACS) on cortical excitability in humans. Brain Stimulat. *1*, 97–105.

Antal, A., Bikson, M., Datta, A., Lafon, B., Dechent, P., Parra, L.C., and Paulus, W. (2014). Imaging artifacts induced by electrical stimulation during conventional fMRI of the brain. NeuroImage *85*, 1040–1047.

Baumgartner, R., Somorjai, R., Summers, R., and Richter, W. (2001). Ranking fMRI Time Courses by Minimum Spanning Trees: Assessing Coactivation in fMRI. NeuroImage *13*, 734–742.

Behzadi, Y., Restom, K., Liau, J., and Liu, T.T. (2007). A Component Based Noise Correction Method (CompCor) for BOLD and Perfusion Based fMRI. NeuroImage *37*, 90–101.

Braun, U., Plichta, M.M., Esslinger, C., Sauer, C., Haddad, L., Grimm, O., Mier, D., Mohnke, S., Heinz, A., Erk, S., et al. (2012). Test–retest reliability of resting-state connectivity network characteristics using fMRI and graph theoretical measures. NeuroImage *59*, 1404–1412.

Brignani, D., Ruzzoli, M., Mauri, P., and Miniussi, C. (2013). Is Transcranial Alternating Current Stimulation Effective in Modulating Brain Oscillations? PLOS ONE *8*, e56589.

Cabral-Calderin, Y., Schmidt-Samoa, C., and Wilke, M. (2015). Rhythmic Gamma Stimulation Affects Bistable Perception. J. Cogn. Neurosci. *27*, 1298–1307.

Cabral-Calderin, Y., Williams, K.A., Opitz, A., Dechent, P., and Wilke, M. (2016). Transcranial alternating current stimulation modulates spontaneous low frequency fluctuations as measured with fMRI. NeuroImage *141*, 88–107.

Çiftçi, K. (2011). Minimum Spanning Tree Reflects the Alterations of the Default Mode Network During Alzheimer's Disease. Ann. Biomed. Eng. *39*, 1493–1504.

Dayan, E., Censor, N., Buch, E.R., Sandrini, M., and Cohen, L.G. (2013). Noninvasive brain stimulation: from physiology to network dynamics and back. Nat. Neurosci. *16*, 838–844.

van Dellen, E., Bohlken, M.M., Draaisma, L., Tewarie, P.K., van Lutterveld, R., Mandl, R., Stam, C.J., and Sommer, I.E. (2016). Structural Brain Network Disturbances in the Psychosis Spectrum. Schizophr. Bull. *42*, 782–789.

van Diessen, E., Numan, T., van Dellen, E., van der Kooi, A.W., Boersma, M., Hofman, D., van Lutterveld, R., van Dijk, B.W., van Straaten, E.C.W., Hillebrand, A., et al. (2015). Opportunities and methodological challenges in EEG and MEG resting state functional brain network research. Clin. Neurophysiol. *126*, 1468–1481.

Duffy, F.H., Mcanulty, G.B., and Albert, M.S. (1996). Effects of age upon interhemispheric EEG coherence in normal adults. Neurobiol. Aging *17*, 587–599.

Fiecas, M., Ombao, H., van Lunen, D., Baumgartner, R., Coimbra, A., and Feng, D. (2013). Quantifying temporal correlations: A test–retest evaluation of functional connectivity in resting-

state fMRI. NeuroImage *65*, 231–241.

Guevara, M.A., and Corsi-Cabrera, M. (1996). EEG coherence or EEG correlation? Int. J. Psychophysiol. Off. J. Int. Organ. Psychophysiol. *23*, 145–153.

He, Y., Wang, J., Wang, L., Chen, Z.J., Yan, C., Yang, H., Tang, H., Zhu, C., Gong, Q., Zang, Y., et al. (2009). Uncovering Intrinsic Modular Organization of Spontaneous Brain Activity in Humans. PLOS ONE *4*, e5226.

Herrmann, C.S., Rach, S., Neuling, T., and Strüber, D. (2013). Transcranial alternating current stimulation: a review of the underlying mechanisms and modulation of cognitive processes. Front. Hum. Neurosci. *7*.

Iaccarino, H.F., Singer, A.C., Martorell, A.J., Rudenko, A., Gao, F., Gillingham, T.Z., Mathys, H., Seo, J., Kritskiy, O., Abdurrob, F., et al. (2016). Gamma frequency entrainment attenuates amyloid load and modifies microglia. Nature *540*, 230–235.

Kanai, R., Chaieb, L., Antal, A., Walsh, V., and Paulus, W. (2008). Frequency-Dependent Electrical Stimulation of the Visual Cortex. Curr. Biol. *18*, 1839–1843.

Kim, D.-H., Noh, J.D., and Jeong, H. (2004). Scale-free trees: The skeletons of complex networks. Phys. Rev. E *70*, 046126.

Lee, H., Mashour, G.A., Noh, G.-J., Kim, S., and Lee, U. (2013). Reconfiguration of Network Hub Structure after Propofol-induced Unconsciousness. Anesthesiol. J. Am. Soc. Anesthesiol. *119*, 1347–1359.

Neuling, T., Wagner, S., Wolters, C.H., Zaehle, T., and Herrmann, C.S. (2012). Finite-Element Model Predicts Current Density Distribution for Clinical Applications of tDCS and tACS. Front. Psychiatry *3*.

Reijneveld, J.C., Ponten, S.C., Berendse, H.W., and Stam, C.J. (2007). The application of graph theoretical analysis to complex networks in the brain. Clin. Neurophysiol. *118*, 2317–2331.

Romei, V., Thut, G., and Silvanto, J. (2016). Information-Based Approaches of Noninvasive Transcranial Brain Stimulation. Trends Neurosci. *39*, 782–795.

Sanz-Arigita, E.J., Schoonheim, M.M., Damoiseaux, J.S., Rombouts, S.A.R.B., Maris, E., Barkhof, F., Scheltens, P., and Stam, C.J. (2010). Loss of ‘Small-World’ Networks in Alzheimer’s Disease: Graph Analysis of fMRI Resting-State Functional Connectivity. PLOS ONE *5*,

e13788.

Shafi, M.M., Westover, M.B., Fox, M.D., and Pascual-Leone, A. (2012). Exploration and modulation of brain network interactions with noninvasive brain stimulation in combination with neuroimaging. Eur. J. Neurosci. *35*, 805–825.

Sporns, O., and Betzel, R.F. (2016). Modular Brain Networks. Annu. Rev. Psychol. *67*, 613–640.

Sporns, O., Chialvo, D.R., Kaiser, M., and Hilgetag, C.C. (2004). Organization, development and function of complex brain networks. Trends Cogn. Sci. *8*, 418–425.

Stam, C.J. (2014). Modern network science of neurological disorders. Nat. Rev. Neurosci. *15*, 683–695.

Stam, C.J., and de Bruin, E.A. (2004). Scale-free dynamics of global functional connectivity in the human brain. Hum. Brain Mapp. *22*, 97–109.

Stam, C.J., Nolte, G., and Daffertshofer, A. (2007). Phase lag index: Assessment of functional connectivity from multi channel EEG and MEG with diminished bias from common sources. Hum. Brain Mapp. *28*, 1178–1193.

Stam, C.J., Tewarie, P., Van Dellen, E., van Straaten, E.C.W., Hillebrand, A., and Van Mieghem, P. (2014). The trees and the forest: Characterization of complex brain networks with minimum spanning trees. Int. J. Psychophysiol. *92*, 129–138.

Stark, D.E., Margulies, D.S., Shehzad, Z.E., Reiss, P., Kelly, A.M.C., Uddin, L.Q., Gee, D.G., Roy, A.K., Banich, M.T., Castellanos, F.X., et al. (2008). Regional Variation in Interhemispheric Coordination of Intrinsic Hemodynamic Fluctuations. J. Neurosci. *28*, 13754–13764.

Tewarie, P., van Dellen, E., Hillebrand, A., and Stam, C.J. (2015). The minimum spanning tree: An unbiased method for brain network analysis. NeuroImage *104*, 177–188.

Thut, G., Schyns, P.G., and Gross, J. (2011). Entrainment of Perceptually Relevant Brain Oscillations by Non-Invasive Rhythmic Stimulation of the Human Brain. Front. Psychol. *2*.

Veniero, D., Benwell, C.S.Y., Ahrens, M.M., and Thut, G. (2017). Inconsistent Effects of Parietal α-tACS on Pseudoneglect across Two Experiments: A Failed Internal Replication. Front. Psychol. *8*.

Violante, I.R., Li, L.M., Carmichael, D.W., Lorenz, R., Leech, R., Hampshire, A., Rothwell, J.C., and Sharp, D.J. Externally induced frontoparietal synchronization modulates network dynamics

and enhances working memory performance. ELife *6*.

Vossen, A., Gross, J., and Thut, G. (2015). Alpha Power Increase After Transcranial Alternating Current Stimulation at Alpha Frequency (α-tACS) Reflects Plastic Changes Rather Than Entrainment. Brain Stimulat. *8*, 499–508.

Vosskuhl, J., Huster, R.J., and Herrmann, C.S. (2016). BOLD signal effects of transcranial alternating current stimulation (tACS) in the alpha range: A concurrent tACS–fMRI study. NeuroImage *140*, 118–125.

Watts, D.J., and Strogatz, S.H. (1998). Collective dynamics of 'small-world' networks. Nature *393*, 440–442.

Witkowski, M., Garcia-Cossio, E., Chander, B.S., Braun, C., Birbaumer, N., Robinson, S.E., and Soekadar, S.R. (2016). Mapping entrained brain oscillations during transcranial alternating current stimulation (tACS). NeuroImage *140*, 89–98.

Yavari, F., Nitsche, M.A., and Ekhtiari, H. (2017). Transcranial Electric Stimulation for Precision Medicine: A Spatiomechanistic Framework. Front. Hum. Neurosci. *11*.

Zaehle, T., Rach, S., and Herrmann, C.S. (2010). Transcranial Alternating Current Stimulation Enhances Individual Alpha Activity in Human EEG. PLOS ONE *5*, e13766.

Zou, Q.-H., Zhu, C.-Z., Yang, Y., Zuo, X.-N., Long, X.-Y., Cao, Q.-J., Wang, Y.-F., and Zang, Y.-F. (2008). An improved approach to detection of amplitude of low-frequency fluctuation (ALFF) for resting-state fMRI: Fractional ALFF. J. Neurosci. Methods *172*, 137–141.

Chapter 5

Anna Fertonani, and Carlo Miniussi (2017). Transcranial Electrical Stimulation: What We Know and Do Not Know About Mechanisms. Neuroscientist *23*, 109–123.

Bächinger, M., Zerbi, V., Moisa, M., Polania, R., Liu, Q., Mantini, D., Ruff, C., and Wenderoth, N. (2017). Concurrent tACS-fMRI Reveals Causal Influence of Power Synchronized Neural Activity on Resting State fMRI Connectivity. J. Neurosci. *37*, 4766–4777.

Bikson, M., Brunoni, A.R., Charvet, L.E., Clark, V.P., Cohen, L.G., Deng, Z.-D., Dmochowski, J., Edwards, D.J., Frohlich, F., Kappenman, E.S., et al. (2018). Rigor and reproducibility in research with transcranial electrical stimulation: An NIMH-sponsored workshop. Brain Stimulation *11*, 465–480.

Brem, A.-K., Fried, P.J., Horvath, J.C., Robertson, E.M., and Pascual-Leone, A. (2014). Is neuroenhancement by noninvasive brain stimulation a net zero-sum proposition? NeuroImage *85*, 1058–1068.

Brignani, D., Ruzzoli, M., Mauri, P., and Miniussi, C. (2013). Is Transcranial Alternating Current Stimulation Effective in Modulating Brain Oscillations? PLOS ONE *8*, e56589.

Fischer, D.B., Fried, P.J., Ruffini, G., Ripolles, O., Salvador, R., Banus, J., Ketchabaw, W.T., Santarnecchi, E., Pascual-Leone, A., and Fox, M.D. (2017). Multifocal tDCS targeting the resting state motor network increases cortical excitability beyond traditional tDCS targeting unilateral motor cortex. Neuroimage *157*, 34–44.

Fuscà, M., Ruhnau, P., Neuling, T., and Weisz, N. (2017). Local network-level integration mediates effects of transcranial Alternating Current Stimulation. BioRxiv 216176.

Grabner, R.H., Krenn, J., Fink, A., Arendasy, M., and Benedek, M. (2017). Effects of alpha and gamma transcranial alternating current stimulation (tACS) on verbal creativity and intelligence test performance. Neuropsychologia.

Herrmann, C.S., and Strüber, D. (2017). What Can Transcranial Alternating Current Stimulation Tell Us About Brain Oscillations? Curr Behav Neurosci Rep *4*, 128–137.

Hopfinger, J.B., Parsons, J., and Fröhlich, F. (2017). Differential effects of 10-Hz and 40-Hz transcranial alternating current stimulation (tACS) on endogenous versus exogenous attention. Cognitive Neuroscience *8*, 102–111.

Horvath, J.C., Forte, J.D., and Carter, O. (2015). Quantitative Review Finds No Evidence of Cognitive Effects in Healthy Populations From Single-session Transcranial Direct Current Stimulation (tDCS). Brain Stimulation *8*, 535–550.

Iaccarino, H.F., Singer, A.C., Martorell, A.J., Rudenko, A., Gao, F., Gillingham, T.Z., Mathys, H., Seo, J., Kritskiy, O., Abdurrob, F., et al. (2016). Gamma frequency entrainment attenuates amyloid load and modifies microglia. Nature *540*, 230–235.

Jamil, A., Batsikadze, G., Kuo, H.-I., Labruna, L., Hasan, A., Paulus, W., and Nitsche, M.A. (2017). Systematic evaluation of the impact of stimulation intensity on neuroplastic after-effects induced by transcranial direct current stimulation. J Physiol *595*, 1273–1288.

Lafon, B., Henin, S., Huang, Y., Friedman, D., Melloni, L., Thesen, T., Doyle, W., Buzsáki, G.,

Devinsky, O., Parra, L.C., et al. (2017). Low frequency transcranial electrical stimulation does not entrain sleep rhythms measured by human intracranial recordings. Nature Communications *8*, 1199.

Luft, C.D.B., Pereda, E., Banissy, M.J., and Bhattacharya, J. (2014). Best of both worlds: promise of combining brain stimulation and brain connectome. Front Syst Neurosci *8*.

Noury, N., Hipp, J.F., and Siegel, M. (2016). Physiological processes non-linearly affect electrophysiological recordings during transcranial electric stimulation. NeuroImage *140*, 99–109.

Onoda, K., Kawagoe, T., Zheng, H., and Yamaguchi, S. (2017). Theta band transcranial alternating current stimulations modulates network behavior of dorsal anterior cingulate cortex. Scientific Reports *7*, 3607.

Rjosk, V., Kaminski, E., Hoff, M., Gundlach, C., Villringer, A., Sehm, B., and Ragert, P. (2016). Transcranial Alternating Current Stimulation at Beta Frequency: Lack of Immediate Effects on Excitation and Interhemispheric Inhibition of the Human Motor Cortex. Front. Hum. Neurosci. *10*.

Schutter, D.J.L.G., and Wischnewski, M. (2016). A meta-analytic study of exogenous oscillatory electric potentials in neuroenhancement. Neuropsychologia *86*, 110–118.

Szymanski, C., Müller, V., Brick, T.R., von Oertzen, T., and Lindenberger, U. (2017). Hyper-Transcranial Alternating Current Stimulation: Experimental Manipulation of Inter-Brain Synchrony. Front. Hum. Neurosci. *11*.

Thut, G., Bergmann, T.O., Fröhlich, F., Soekadar, S.R., Brittain, J.-S., Valero-Cabré, A., Sack, A.T., Miniussi, C., Antal, A., Siebner, H.R., et al. (2017). Guiding transcranial brain stimulation by EEG/MEG to interact with ongoing brain activity and associated functions: A position paper. Clinical Neurophysiology *128*, 843–857.

Uhlhaas, P.J., and Singer, W. (2006). Neural Synchrony in Brain Disorders: Relevance for Cognitive Dysfunctions and Pathophysiology. Neuron *52*, 155–168.

Veniero, D., Vossen, A., Gross, J., and Thut, G. (2015). Lasting EEG/MEG Aftereffects of Rhythmic Transcranial Brain Stimulation: Level of Control Over Oscillatory Network Activity. Front. Cell. Neurosci. *9*.

Vossen, A., Gross, J., and Thut, G. (2015). Alpha Power Increase After Transcranial Alternating Current Stimulation at Alpha Frequency (α-tACS) Reflects Plastic Changes Rather Than Entrainment. Brain Stimulation *8*, 499–508.

Weinrich, C.A., Brittain, J.-S., Nowak, M., Salimi-Khorshidi, R., Brown, P., and Stagg, C.J. (2017). Modulation of Long-Range Connectivity Patterns via Frequency-Specific Stimulation of Human Cortex. Current Biology *27*, 3061-3068.e3.

Yavari, F., Nitsche, M.A., and Ekhtiari, H. (2017). Transcranial Electric Stimulation for Precision Medicine: A Spatiomechanistic Framework. Front Hum Neurosci *11*.

Appendix A

NeuroImage 141 (2016) 88–107

Contents lists available at ScienceDirect

NeuroImage

journal homepage: www.elsevier.com/locate/ynimg

Transcranial alternating current stimulation modulates spontaneous low frequency fluctuations as measured with fMRI

Yuranny Cabral-Calderin [a,b,*,1], Kathleen A. Williams [a,1], Alexander Opitz [c,d], Peter Dechent [a], Melanie Wilke [a,b,e]

[a] Department of Cognitive Neurology, University Medical Center, Georg-August University Goettingen, Robert-Koch-Str. 40, Goettingen 37075, Germany
[b] German Primate Center, Leibniz Institute for Primate Research, Kellnerweg 4, Goettingen 37077, Germany
[c] Center for Biomedical Imaging and Neuromodulation, Nathan Kline Institute for Psychiatric Research, Orangeburg, NY 10962, USA
[d] Center for the Developing Brain, Child Mind Institute, New York, NY 10022, USA
[e] DFG Center for Nanoscale Microscopy & Molecular Physiology of the Brain (CNMPB), Germany

ARTICLE INFO

Article history:
Received 31 May 2016
Accepted 2 July 2016
Available online 5 July 2016

Keywords:
tACS
Brain stimulation
fMRI
Oscillations
Entrainment
fALFF/ALFF
Intrinsic functional connectivity
Resting state
Cross-frequency coupling

ABSTRACT

Transcranial alternating current stimulation (tACS) is a promising tool for modulating brain oscillations. Combining tACS with functional magnetic resonance imaging (fMRI), we recently showed that tACS applied over the occipital cortex did not exert its strongest effect on regions below the electrodes, but mainly on more distant fronto-parietal regions. Theoretically, this effect could be explained by tACS-induced modulation of functional connectivity between directly stimulated areas and more distant but anatomically and functionally connected regions. In the present study, we aimed to characterize the effect of tACS on low frequency fMRI signal fluctuations. We employed simultaneous fMRI-tACS in 20 subjects during resting state (eyes open with central fixation for ~8 min). Subjects received tACS at different frequencies (10, 16, 40 Hz) and with different electrode montages (Cz-Oz, P5–P6) previously used in behavioral studies. Electric field simulations showed that tACS over Cz-Oz directly stimulates occipital cortex, while tACS over P5–P6 primarily targets parietal cortices. Group-level simulation-based functional connectivity maps for Cz-Oz and P5–P6 resembled the visual and fronto-parietal control resting-state networks, respectively. The effects of tACS were frequency and partly electrode montage dependent. In regions where frequency-dependent effects of tACS were observed, 10 and 40 Hz tACS generally induced opposite effects. Most tACS effects on functional connectivity were observed between, as opposed to within, resting-state networks. The left fronto-parietal control network showed the most extensive frequency-dependent modulation in functional connectivity, mainly with occipito-parietal regions, where 10 Hz tACS increased and 40 Hz tACS decreased correlation values. Taken together, our results show that tACS modulates local spontaneous low frequency fluctuations and their correlations with more distant regions, which should be taken into account when interpreting tACS effects on brain function.

Introduction

Transcranial alternating current stimulation (tACS) is a non-invasive brain stimulation technique that has proven to be effective in modulating brain oscillations (Ali et al., 2013; Helfrich et al., 2014a; Ozen et al., 2010; Zaehle et al., 2010; Reato et al., 2013). A growing body of literature exists documenting frequency-dependent effects of tACS on different brain functions in health (Cabral-Calderin et al., 2015; Feurra et al., 2013, 2011a; Helfrich et al., 2014b; Joundi et al., 2012; Kanai et al., 2008; Kar and Krekelberg, 2014; Laczo et al., 2012; Polania et al., 2012; Santarnecchi et al., 2013; Wach et al., 2013; Wang et al., 2015) and disease (Brittain et al., 2013; Fedorov et al., 2010). For instance, effects of tACS on visual perception have been reported when tACS was applied over occipital and parietal cortices at alpha or gamma frequencies (Helfrich et al., 2014a; Cabral-Calderin et al., 2015; Laczo et al., 2012; Wang et al., 2015). Although these effects have been mainly attributed to increasing the power or synchrony of alpha/gamma oscillations in occipito-parietal areas, recent studies indicate that underlying mechanisms of tACS effects are far more complicated. With the exception of a few studies combining tACS with electroencephalographic (EEG) recordings (Helfrich et al., 2014a; Zaehle et al., 2010) or functional magnetic resonance imaging (fMRI) (Alekseichuk et al., 2015; Cabral-Calderin et al., 2016; Vosskuhl et al., 2015), most of our knowledge about tACS is derived from behavioral studies. Technical challenges inherent to concurrent measurements of brain activity when applying tACS, such as artifacts in EEG signals or the need for specialized

* Corresponding author at: Department of Cognitive Neurology, University Medical Center, Robert-Koch-Str. 40, Goettingen 37075, Germany.
E-mail address: yurany.cabral-calderin@med.uni-goettingen.de (Y. Cabral-Calderin).
[1] Shared first author.

http://dx.doi.org/10.1016/j.neuroimage.2016.07.005
1053-8119/

MRI-safe equipment, leave only several published studies of combined brain imaging and tACS, making it difficult to interpret the behavioral results in terms of the underlying brain activity (Zaehle et al., 2010; Helfrich et al., 2014b; Alekseichuk et al., 2015; Cabral-Calderin et al., 2016; Vosskuhl et al., 2015; Witkowski et al., 2015; Neuling et al., 2015).

In a recent study combining tACS with fMRI (Cabral-Calderin et al., 2016) we showed that the effect of tACS on brain activity, as inferred from the blood-oxygenation-level-dependent (BOLD) signal, is rather complex and cannot entirely be predicted based on electrode positions alone. In general, the effects of tACS over Cz-Oz were frequency-, region-, and task-dependent. Specifically, BOLD activity changes were stronger with lower tACS frequencies; that is, alpha (10 Hz) and beta (16 Hz) frequencies were more effective than gamma (60, 80 Hz). Additionally, effects were mainly observed in regions not activated by the task and that were distant from the electrodes (i.e., fronto-parietal but not occipital regions) (Cabral-Calderin et al., 2016). The fact that the above-mentioned study reported tACS effects mainly in areas distant from the electrodes (i.e., fronto-parietal) could indicate that the effects of tACS are transmitted from directly stimulated brain regions (i.e., occipital) to more distant but anatomically and functionally connected regions. In fact, it has been proposed that the effects of phase entrainment (a possible mechanism of tACS) in a given brain area may propagate through a larger network due to inter-regional phase locking (Canolty and Knight, 2010). It is thus reasonable to assume that tACS also interferes with the dynamics of brain networks. A recent study combining tACS (applied over occipito-parietal areas) with EEG has reported tACS-induced modulation of interhemispheric functional connectivity in occipito-parietal cortices in a phase-specific manner (Helfrich et al., 2014b). The authors reported that in-phase tACS in the gamma range (40 Hz) enhanced interhemispheric synchrony while anti-phase tACS impaired it, providing evidence of the possibility of modifying functional coupling between brain regions with tACS.

The dynamics of intrinsically functionally connected networks have been largely studied with resting-state fMRI (rs-fMRI), in which subjects are not engaged in an active task (e.g., awake with eyes closed or eyes open, with or without eye fixation (Van Dijk et al., 2010)). Over the last two decades many studies have documented the presence of resting-state networks (RSNs) arising from regionally distributed but temporally correlated low frequency BOLD signal fluctuations (<0.1 Hz) in the resting brain (Fox et al., 2005; Fox and Raichle, 2007; Biswal et al., 1995; Beckmann et al., 2005; Raichle, 2015). These RSNs are constrained by, but not limited to, structural connectivity (Park and Friston, 2013) and resemble several networks of functionally connected regions modulated by active tasks such as the dorsal attention network (DAN), lateralized right and left fronto-parietal control networks (r-FP and l-FP, respectively), executive network, motor network, visual network, and default mode network (DMN). It has been suggested that spontaneous BOLD signal fluctuations have neurophysiological origins (Raichle, 2010; Shmuel and Leopold, 2008; Tagliazucchi et al., 2012). Previous studies attempted to correlate the power of specific EEG rhythms with resting-state measurements and showed that RSNs are related not only to one brain rhythm, but to combinations of several. In terms of the BOLD signal amplitude in resting-state networks, global (i.e., average over all EEG channels), as well as particularly occipital, alpha (8–13 Hz) power has been positively correlated with DMN and negatively correlated with DAN, r-FP, l-FP, and visual networks (Mantini et al., 2007; Mo et al., 2013; Zhan et al., 2014). Global beta (13–30 Hz) power has been positively correlated with DMN and negatively correlated with DAN, visual and motor networks (Mantini et al., 2007). Global gamma (>30 Hz) power has been positively correlated with global resting-state activity and, in particular, with regions from the executive network (e.g., medial-ventral prefrontal cortex and anterior cingulate (Mantini et al., 2007)). In terms of functional connectivity (expressed as temporal correlations), special attention has been paid to occipital alpha power, which negatively correlates with functional connectivity within visual cortices and between visual and more frontal and subcortical regions (Scheeringa et al., 2012). An inverse relationship has also been reported between central alpha and beta power spectra and changes in functional connectivity, mostly between subcortical regions and association cortices. In addition, a positive relationship has been found between gamma power and functional connectivity changes between subcortical, association and primary cortices (central and occipital gamma power) and within these regions (frontal gamma power) (Tagliazucchi et al., 2012). These links between specific EEG frequencies and RSNs motivate the possibility of probing RSNs by modulating oscillatory activity with tACS.

The aim of the present study was to evaluate whether tACS applied over occipital and parietal cortices induces changes in spontaneous activity measured with rs-fMRI. To this end, we applied tACS at three different frequencies in the alpha, beta, and gamma range (10, 16, 40 Hz, respectively), and with two different electrode montages (Cz-Oz and P5–P6). The tACS frequencies and electrode montages were chosen based on previous studies showing modulatory effects of tACS at alpha or gamma frequencies on visual perception (Helfrich et al., 2014a; Laczo et al., 2012; Wang et al., 2015; Cabral-Calderin et al., 2016).

Given that our previous fMRI study indicated strongest tACS effects in regions that were distant from the electrodes (i.e., fronto-parietal but not occipital regions) (Cabral-Calderin et al., 2016), (I) we hypothesized that tACS would change functional connectivity between directly stimulated regions and more distant areas. Based on previous EEG/fMRI and tACS/fMRI studies, (II) we expected to observe frequency-dependent modulation of RSNs with tACS. Given the previously reported negative correlations between the power of alpha/beta rhythms and functional connectivity, as well as BOLD signal amplitude in most RSNs (Tagliazucchi et al., 2012; Mantini et al., 2007; Scheeringa et al., 2012), (III) we hypothesized that tACS at alpha and beta frequencies should reduce the amplitude of spontaneous low frequency fluctuations and functional connectivity in most RSNs (e.g., DAN and visual network). An exception should be observed in the DMN, where the power of alpha and beta rhythms have been found to positively correlate with that network's BOLD signal amplitude, therefore, (IV) alpha and beta tACS should increase the amplitude of spontaneous low frequency fluctuations in the DMN (Mantini et al., 2007; Mo et al., 2013). Since gamma power has been positively associated with the amplitude of BOLD signal fluctuations and their correlations (Tagliazucchi et al., 2012; Mantini et al., 2007), (V) tACS in the gamma range should increase the amplitude of spontaneous low frequency fluctuations and functional connectivity. According to our previous study (Cabral-Calderin et al., 2016) we hypothesized that (VI) the strongest modulation of spontaneous low frequency fluctuations would be observed with alpha/beta tACS mainly in fronto-parietal networks (i.e., r-FP and l-FP). In addition, since different electrode positions induce different electric field distributions (Neuling et al., 2012; Windhoff et al., 2013), (VII) we expected to observe a difference in the low frequency fluctuation changes associated with each electrode montage. Based on a previous study that simulated the electric field distribution induced by transcranial electric stimulation (Neuling et al., 2012), (VIII) we expect tACS over Cz-Oz to stimulate mainly occipital cortex and, as a result, to modulate the amplitude of low frequency fluctuations and functional connectivity relative to the visual network. Following the same reasoning, (IX) tACS over P5–P6 should stimulate mainly parietal regions, translating into modulation of the amplitude of low frequency fluctuations in parietal cortices and functional connectivity of RSNs involving parietal regions such as r-FP, l-FP and DAN.

Methods

Transcranial alternating current stimulation (tACS)

A battery-driven Eldith DC-stimulator Plus (NeuroConn GmbH, Ilmenau, Germany) delivered tACS through a pair of conductive rubber electrodes attached with electrode paste (Weaver and Company,

Aurora, CO). Two different electrode montages were used in the experiment: (1) electrodes placed over Cz-Oz, (2) electrodes placed over P5–P6, as determined by the International 10–20 EEG system (Fig. 1A). Each montage was comprised of two round electrodes with each electrode covering an area of 16 cm^2. The stimulation sites were chosen to induce oscillations bilaterally in occipital and parietal cortices (Neuling et al., 2012; Windhoff et al., 2013). For both montages, tACS was applied at 10, 16, and 40 Hz for 8 min. The waveform of the stimulation was sinusoidal without DC offset. The current was fixed to 1 mA (peak-to-peak), resulting in a mean current density of 0.063 mA/cm^2 (peak-to-peak) under each electrode. The current was ramped up and down over 1 s in order to make the protocol more comparable to our previous study (Cabral-Calderin et al., 2016). Impedance was kept below 20 kΩ (impedances below 10 kΩ, as commonly used in tACS studies, cannot be accomplished because our MR-compatible stimulation setup has a minimum possible impedance of 11.8 kΩ (Cabral-Calderin et al., 2016)). Previous studies using similar tACS equipment have reported no significant artifacts induced by tACS on the BOLD signal (Cabral-Calderin et al., 2016; Antal et al., 2014). However, possible artifacts induced by electrical stimulation might be specific to imaging and stimulation parameters. In order to evaluate possible tACS-induced artifacts, we performed additional scanning sessions with a phantom, using the same tACS parameters that were used in the main experiment. In agreement with our previous study (Cabral-Calderin et al., 2016), we observed differences in the temporal signal-to-noise ratio (tSNR) when compared between scans with (i.e., electrodes placed and connected to the tACS stimulator outside the shielded room) or without tACS setup. However, tSNR values were stable when comparing tACS-on with tACS-off, while keeping all the other conditions the same. In our study, the tACS setup was always in place and, therefore, we do not expect tACS-induced artifacts to influence our results. Each subject participated in a total of six sessions, in each of which tACS was applied with a single tACS frequency-electrode montage combination in a randomized order. Each session was conducted on a different day, separated by at least 48 h (average time between experimental sessions across subjects: 208 h, SD: 117 h).

Magnetic resonance imaging (MRI)

Experimental setup and design

Twenty subjects (10 females, mean age 25.1 ± 3.1 years) with normal or corrected-to-normal vision and without history of neurological or psychiatric disease took part in the study. All subjects gave written informed consent. All procedures were performed according to the declaration of Helsinki and approved by the local Ethics Committee of the University Medical Center Göttingen. All subjects were naive to the purpose of the experiments and were paid for their participation.

In each of the six sessions, a total of six resting-state scans were collected. Each resting-state scan lasted ~8 min, during which subjects were asked to remain still with eyes open while fixating on a central cross. Eye position was monitored using an MR-compatible eye tracking system (Arrington Research, Inc., Scottsdale, AZ) to verify that subjects remained awake and fixating on the central cross throughout the resting-state scan. The first three resting-state scans of each session referred to pre-sham, sham, and post-sham conditions. During the sham condition, tACS was applied with the same parameters as the active stimulation but with a total duration of 10 s. In each session, the last three resting-state scans referred to pre-stimulation, stimulation, and post-stimulation conditions. During the stimulation condition, tACS was applied with a total duration of 8 min. The sham and active stimulation blocks were separated by at least 8 min (in which anatomical data were collected). In each session, the sham stimulation block preceded the active stimulation block to prevent after-effects of long stimulation from contaminating sham conditions. After each run, the subjects rated the strength of perceived phosphenes, cutaneous sensation, and fatigue intensities on a scale ranging from 1 to 10. Due to technical problems in the first functional run of each session (lower tSNR with respect to the other runs within the session), this run (pre-sham) was not used for analysis. Therefore, the sham condition for each of the different frequencies was not included in the final analyses. The post-sham run was used for defining RSNs (see Methods) and, for simplicity, will be referred to as "baseline" throughout the manuscript. The session flow is depicted in Fig. 1B.

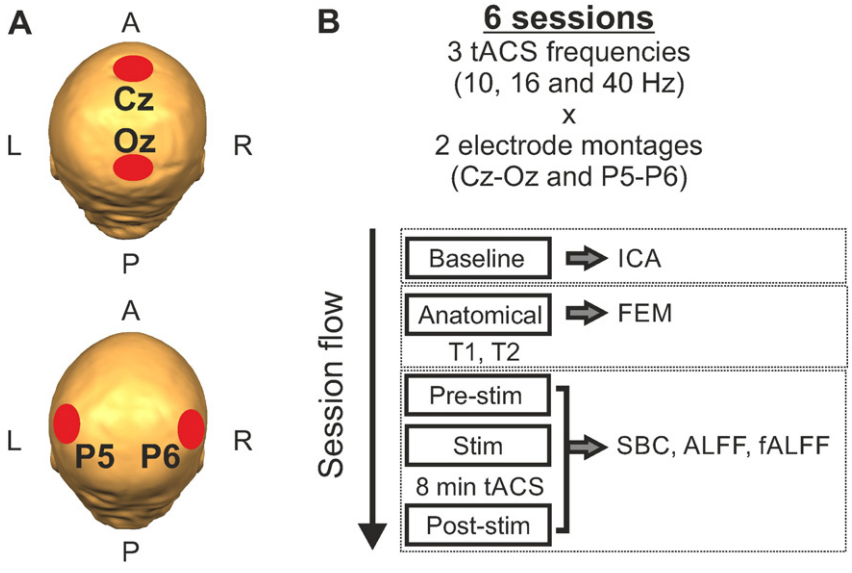

Fig. 1. Experimental design. A) The two electrode montages used in our experiment are illustrated with colored circles on top of a 3D reconstruction of one example participant. L: left, R: right, A: anterior, P: posterior. B) Session flow. Each session included a baseline and three stimulation runs (pre-stimulation, stimulation and post-stimulation) separated by one anatomical measurement (T1-weighted/T2-weighted with/without fat saturation). The session flow was kept constant across sessions but the tACS condition (frequency x electrode montage combination) and the type of anatomical measurement collected in each session were pseudorandomized across participants. Dashed boxes on the right of the panel contain depictions of the analysis implemented with the dataset collected in the specific run. ICA: independent component analysis for defining the resting-state networks, FEM: finite element method simulations, SBC: seed-based functional connectivity analysis, and ALFF: amplitude of low frequency fluctuations and its fraction (fALFF).

Data acquisition

All images were acquired using a 3 Tesla Magnetom TIM Trio scanner (Siemens Healthcare, Erlangen, Germany) with a 32-channel phased-array head coil. First, a high-resolution T1-weighted anatomical scan (three-dimensional (3D) turbo fast low angle shot; repetition time (TR): 2250 ms, inversion time (TI): 900 ms, echo time (TE): 3.26 ms, flip angle 9°, isotropic resolution of $1 \times 1 \times 1$ mm^3) was obtained. All functional data were acquired using the 2D multiband gradient-echo echo-planar imaging sequence from the Center for Magnetic Resonance Research, University of Minnesota (Xu et al., 2013; Moeller et al., 2010; Setsompop et al., 2012) with T2*-weighting (TR: 900 ms, TE: 30 ms, flip angle 50°, 39 slices of 3-mm thickness, gap between slices of 10%, in-plane resolution of 3×3 mm^2, multiband acceleration factor 3). A total of 544 whole-brain volumes were acquired in each functional run. In the stimulation run, tACS was initiated after 10 volumes were acquired. Six additional anatomical datasets were collected, one in each session, between sham and active stimulation blocks. Four of these datasets were used for creating individualized finite element method (FEM) head models for the electric field simulations (see section below, (Windhoff et al., 2013; Thielscher et al., 2015)). These four anatomical datasets consisted of two T1-weighted anatomical scans with the parameters described above, with and without fat suppression, and two T2-weighted anatomical scans (3D turbo spin echo; TR: 3500 ms, TE: 282 ms, variable flip angle, with integrated parallel acquisition technique: factor 2, isotropic resolution of $1 \times 1 \times 1$ mm^3), with and without fat suppression. The other two anatomical datasets were not used for any further analyses but were collected in order to have the same time interval between the sham and active stimulation blocks in all the six sessions.

Electric field simulations

The FEM models simulating the electric field induced by tACS were calculated using SimNibs (Windhoff et al., 2013; Thielscher et al., 2015). One participant was excluded from the electric field simulations due to a mesh generation error with one of the anatomical datasets. For the remaining 19 subjects, each subject's set of T1- and T2-weighted images (with and without fat suppression) was used to create an individualized FEM mesh for modeling the electric field for the electrode montages used in this experiment. Inconsistencies in head meshes due to electrode deformations were corrected manually. Electrode position coordinates were determined using a virtual 10–20 cap placed on the mesh based on each subject's anatomy using customized Matlab scripts (Matlab R2011b, www.mathworks.com, Natick, MA). Electric field simulations were generated in SimNibs for Cz-Oz and P5–P6 electrode placements for each subject using standard tissue conductivities of $\sigma_{skin} = 0.465$ S/m, $\sigma_{skull} = 0.010$ S/m, $\sigma_{CSF} = 1.654$ S/m, $\sigma_{GM} = 0.275$ S/m, $\sigma_{WM} = 0.126$ S/m, for skin, skull, cerebral spinal fluid (CSF), gray matter and white matter (WM), respectively (Thielscher et al., 2011). To generate regions of interest (ROI) for seed-based functional connectivity analysis, the electric field strength (norm E) for each simulation was transformed to corresponding subject gray matter masks segmented from original MR volume space. The resulting MR-space electric field simulation data were Talairach transformed, thresholded at 50% of the maximum electric field of each map (Opitz et al., 2015a), and binarized. Binarized electric field masks were overlaid for all subjects for a given electrode montage and then thresholded such that any voxel in which four or more subjects had 50% or greater electric field strength for the given montage was included. The resulting thresholded group mask was used as a seed for cross-correlation analysis for each electrode position, except Cz, which left only a few voxels, as is evident from the group participation maps (Supplemental materials, Fig. S1). Seeds for P5 and P6 electrode positions were separated using a right-left hemisphere mask in Talairach space. For each subject, the mean electric field strength from the 50% thresholded map was extracted for each electrode montage and used to quantitatively characterize the single subject's electric field properties. The extracted values were used for comparing the electric field strength induced by each electrode montage at the group level using *paired t-test* as implemented in STATISTICA version 12.

Functional MRI data analysis

Preprocessing

All data preprocessing was performed in AFNI (Cox, 1996). The first 10 volumes were discarded to align stimulation start time to the functional data. Preprocessing steps included: despiking, slice timing correction, deobliquing, motion correction, resampling to $3 \times 3 \times 3$ mm, transformation to Talairach space using each session's T1-to-MNI152 standard template transformation (MNI template was transformed to Talairach space using AFNI's 3dWarp in order to ensure compatibility between software used for individual processing and group statistical analyses), and 6 mm full-width-at-half-maximum-kernel Gaussian smoothing. With the exception of data used for creating the RSN seeds, the following preprocessing steps were also implemented: 4th-order polynomial regression (equivalent to demeaning, linear trend removal, and high-pass filtering), regression of motion parameters and the first derivative of the motion parameters, bandpass filtering between 0.01 and 0.1 Hz, and nuisance regression of WM and CSF signals extracted from masks segmented from individual anatomical data.

Amplitude of low frequency fluctuations (ALFF) and fractional ALFF (fALFF) analysis

The ALFF and fALFF were computed for all runs using AFNI (Zang et al., 2007; Zou et al., 2008). Both ALFF and fALFF measure the power of low frequency fluctuations, which gives an indication of local metabolic changes associated with the BOLD signal. The algorithm was run on the preprocessed data before bandpass filtering. Briefly, on a voxel-by-voxel basis, the time course was converted into the frequency domain using a Fast Fourier Transform, the square root of the power spectrum was computed, and the average of the amplitudes in the range of 0.01–0.1 Hz were then calculated to obtain the ALFF (Zang et al., 2007; Zou et al., 2008). Dividing each voxel's ALFF value by the amplitudes of the entire detectable frequency range (0–0.55 Hz) yields that voxel's fALFF (Zou et al., 2008) (Supplemental materials, Fig. S2A). Both ALFF maps and fALFF maps were standardized with Z transformation (subtract global mean and divide by standard deviation) prior to statistical analyses. While the ALFF reports the absolute power of low frequency fluctuations, it can be sensitive to high frequency pulsatile changes such as heart rate, an artifact that can be mitigated by considering the fALFF, which has reduced sensitivity to such noise sources but lower test-retest reliability (Zuo et al., 2010). Thus, it is important to consider both measures. In our dataset, ALFF results closely resembled fALFF results and therefore are not shown or described.

Seed-based functional connectivity analysis

Cross-correlation analyses were carried out in AFNI. Two different sets of ROI seeds were defined for these analyses. The first set was defined to represent commonly used RSNs using independent component analysis (ICA), and the second set consisted of seeds derived from the electric field simulation, as described in the previous section ('*Electric field simulations*').

In order to define group-level, subject-based RSNs for analysis of effects of tACS on intrinsic functional connectivity, temporal concatenation group ICA was performed on the baseline run from every session of every subject using FSL's MELODIC toolbox (Jenkinson et al., 2012). Using the baseline run from every imaging session allows for group-level definition of independent components without the use of the experimental data (pre-stimulation, stimulation, and post-stimulation runs), which is subsequently used for evaluating tACS-effects. In addition, including runs from all sessions can account for day-to-day subject

variability in the RSNs. The algorithm was run on preprocessed data before any nuisance regression or bandpass filtering and was fixed to extract 30 components. Choosing 30 independent components allowed reliable extraction of the seven RSNs that we chose to focus on; that is, the DAN, DMN, executive, visual, motor, l-FP, and r-FP networks. We chose these networks because we were interested in tACS effects in well-known RSNs (Fox et al., 2005; Beckmann et al., 2005). The resulting group components were then used to create ROI masks for seed-based functional connectivity analysis by binarizing 50% of the maximum positive signal from each of the chosen components. The ICA components chosen for the purpose of our analysis, as well as the corresponding seeds derived for calculating functional connectivity, are depicted in Fig. 2. A graphical representation of the procedure can be found in Supplemental materials Fig. S2 B. Since the 50% mask of the DAN seed did not include the bilateral parietal regions (Fox et al., 2005), we chose the mask threshold (70%) that included left and right intraparietal sulci.

Network-to-network functional connectivity. As a strategy of data reduction, a network-to-network functional connectivity approach was conducted in order to evaluate first the gross impact of tACS on intrinsic functional connectivity between RSNs. For each condition of an individual subject, the average time course extracted for each RSN was correlated with that of every other network using Pearson's correlation. The correlation values were transformed with the Fisher's r-to-z procedure in order to be able to conduct statistical analyses on correlation values. The resulting z-transformed correlations are summarized in a 7×7 inter-network functional connectivity matrix in Supplemental materials (Fig. S2 B).

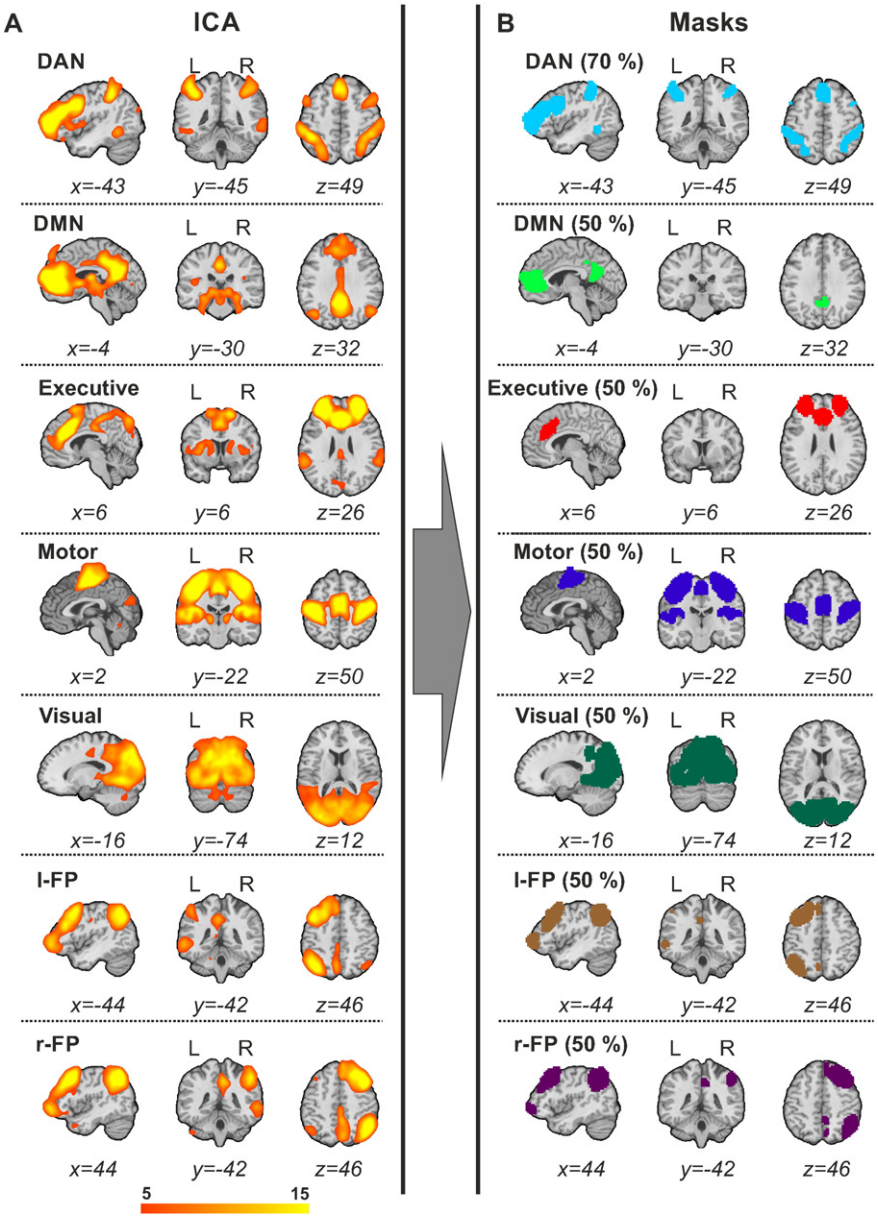

Fig. 2. ICA results. A) Selected components representing the seven resting-state networks selected for further analysis (from top: dorsal attention network (DAN), default mode network (DMN), executive network, motor network, visual network, left fronto-parietal control network (l-FP) and right fronto-parietal control network (r-FP). B) Masks created from each component (thresholded at 50% or 70%) representing each network to be used in the SBC.

Whole-brain functional connectivity. For each stimulation run (pre-stimulation, stimulation, and post-stimulation) of each subject, whole-brain functional connectivity was computed for all aforementioned seeds. Each seed was resampled into functional data resolution ($3 \times 3 \times 3$ mm^3) and used as a mask to extract the average time course from the ROI. For a given seed, the resulting time course was then correlated with that of every other voxel in the brain using Pearson's correlation. The resulting coefficient indexes how temporally similar any voxel in the brain is to the network or region in question; thus, as measured with BOLD contrast, seed-based functional connectivity is always an indication of the functional state of the brain relative to the seed of interest. Supplemental materials (Fig. S2 B, C) illustrate the general scheme for obtaining whole-brain correlations on the basis of RSN and electric field simulation-based seeds, respectively. Finally, for a total of ten seeds (7 RSNs, 3 electric field simulation-based ROIs), six sessions and three (pre-stimulation, stimulation, post-stimulation) runs, 180 whole-brain correlation maps were computed for each subject. Correlation maps were Fisher r-to-z transformed prior to statistical analyses.

Statistical analysis

All statistical comparisons were performed between the different tACS frequencies and electrode montages for the active stimulation (pre-stimulation, stimulation, and post-stimulation), combinations of which were applied in a pseudorandomized manner across subjects and sessions. This way, each frequency and electrode montage combination works as an implicit control condition for the others, controlling for placebo effects, which should be universal across conditions. For this reason, we focus on tACS frequency- and electrode montage-dependent effects but not on non-specific tACS effects.

Network-to-network functional connectivity

Statistical analyses were implemented in STATISTICA. To obtain a general overview for evaluating the impact of tACS on the functional connectivity between networks, we analyzed the 7×7 inter-network functional connectivity matrices. A four-factor repeated measures analysis of variance (rANOVA) was conducted for each network with the within factors tACS frequency (3 levels: 10, 16, and 40 Hz), electrode montage (2 levels: Cz-Oz and P5–P6), time (3 levels: pre-stimulation, stimulation, and post-stimulation) and network combination (6 levels: e.g., for DAN the network combinations were DAN-DMN, DAN-executive, DAN-motor, DAN-visual, DAN-l-FP, and DAN-r-FP). Accordingly, seven different four-factor rANOVAs were conducted. In cases that the rANOVA showed significant interaction effects (e.g., interaction tACS frequency $\times$ electrode montage $\times$ time $\times$ network), a three-factor rANOVA was conducted for each level of the network combination factor while keeping the remaining factors as in the original four-factor rANOVA. In cases of significant interactions, post-hoc analyses were performed using *paired t-tests* to further explore the differences.

Whole-brain functional connectivity and fALFF

All group-level volume statistics were conducted using BrainVoyager QX Software version 2.8 (Brain Innovation, Maastricht, The Netherlands), and the Neuroelf 0.9c toolbox for Matlab (retrieved from http://neuroelf.net/). For fALFF and network-to-whole-brain functional connectivity, statistical analyses were done using a three-factor rANOVA with the within factors tACS frequency (3 levels: 10, 16, and 40 Hz), electrode montage (2 levels: Cz-Oz and P5–P6), and time (3 levels: pre-stimulation, stimulation, and post-stimulation). For correlation maps resulting from P5, P6, and Oz seeds, two-factor rANOVAs were applied using only conditions where tACS was applied with the respective electrode montage. For Oz seed-based maps, a two-factor rANOVA with the within factors tACS frequency (3 levels: 10, 16, and 40 Hz) and time (3 levels: pre-stimulation, stimulation, and post-stimulation) was conducted for Cz-Oz stimulation conditions. For P5 and P6 seed-based maps, similar two-factor rANOVAs were conducted for P5–P6 stimulation conditions. For all whole-brain analyses, in cases of statistical significance in the rANOVAs, the standardized fALFF or Fisher's z-transformed correlation values were extracted from each significant cluster and post-hoc analyses were conducted using *paired t-tests* as implemented in STATISTICA.

For all statistical maps, multiple comparisons correction was performed at the cluster level. Maps were thresholded at an initial cluster-forming threshold of $p < 0.005$. The sizes of the resulting clusters were assessed for significance using Monte Carlo simulations as implemented in BrainVoyager's cluster-level statistical threshold estimator plugin. Reported clusters are significant at a level of $p < 0.05$. For labeling the significant regions, the peak activation voxel from each cluster was entered into the Talairach client tool (Research Imaging Institute, http://www.talairach.org/client.html), a 5 mm range cube was defined around the peak voxel and the cluster was labeled according to the region to which most of the defined voxels belong. The statistical volume maps in the figures are overlaid on the Colin brain template.

Phosphene perception, cutaneous sensation and fatigue ratings

Statistical analyses for phosphene perception, cutaneous sensation, and fatigue ratings were performed using a three-factor rANOVA with the within factors tACS frequency (3 levels: 10, 16, and 40 Hz), electrode montage (2 levels: Cz-Oz and P5–P6) and time (3 levels: pre-stimulation, stimulation, and post-stimulation). In cases of statistical significance, post-hoc analyses were conducted by using *paired t-tests* as implemented in STATISTICA. Additional analyses were performed correlating phosphene perception and cutaneous sensation ratings with the fALFF values extracted from ROIs located in the corresponding primary sensory cortices. The detailed procedure is described in Supplemental materials.

Results

Electric field simulations

Using a finite element method, the electric field for each montage was simulated for every participant in order to predict the regions being directly stimulated by tACS. According to the simulation, the electric field induced by tACS over Cz-Oz is more centered on the occipital cortex while the electric field induced by tACS over P5–P6 is more centered over parietal areas in both hemispheres, as can be viewed in a representative subject shown in Fig. 3. Although the region of maximum stimulation is different for each electrode montage, some areas receiving lower electric fields are shared in both montage setups, primarily in medial occipito-parietal areas. Visual inspection of the electric field simulations showed that the electric field is stronger and more widespread for tACS over P5–P6 than for tACS over Cz-Oz. This might be due to the proximity of the electrodes to the brain and CSF in each montage as well as the composition of the skull in the regions directly underneath the electrodes (Opitz et al., 2015b). For instance, CSF is one of the most conductive materials in the head, and therefore, it constitutes a less resistive path for the applied electric currents (Opitz et al., 2015b). With Cz-Oz, the electrodes are directly above a larger volume of CSF than P5–P6 electrodes, thus possibly shunting the highest electric field to regions of the brain not directly underneath the electrodes. On the contrary, with the P5–P6 montage, generally only a thin layer of CSF sits between the skull and the brain, thus possibly less current is carried away before entering the gray matter regions underneath the electrodes. In fact, it has been previously reported that gray matter regions that have a thin overlying CSF layer exhibit higher electric fields than those overlaid with a thick CSF layer (Opitz et al., 2015b). In addition, individuals' electric fields are the strongest in subjects with the thinnest layer of CSF (Laakso et al., 2015). The group participation maps for each electrode montage, in which the single-subject electric field maps transformed to MRI space and thresholded at 50% are overlaid

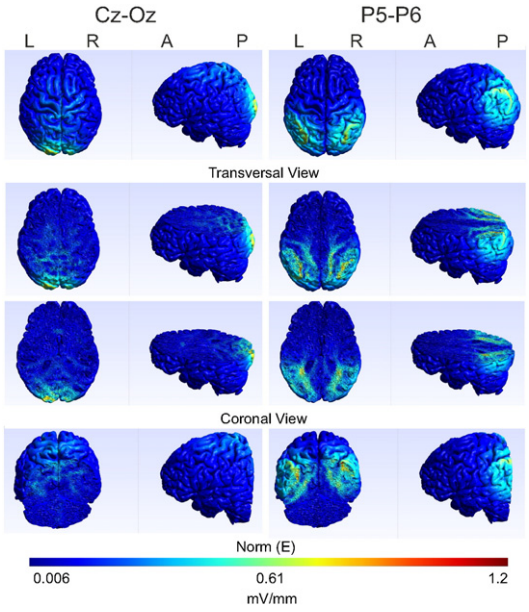

Fig. 3. Electric field distributions obtained from the finite element method simulations for each electrode montage for a representative subject. L: left hemisphere, R: right hemisphere, A: anterior, and P: posterior.

on a representative brain, are shown in Fig. S1. As expected from visual inspection of the maps, a *paired t-test* analysis on the mean electric field strength extracted from each subject's 50% thresholded map showed that the mean electric field induced by P5–P6 was stronger than that induced by Cz-Oz ($t(18) = 5.05, p < 0.001$). Overall, the mean strength of the electric field maps (within the 50% thresholded maps) did not show high variability across subjects. Nonetheless, inter-subject variability was higher for Cz-Oz than for P5–P6 (Cz-Oz: *mean* = 0.40 mV/mm, *SD* = 0.09, *range* = 0.31; P5–P6: *mean* = 0.51 mV/mm, *SD* = 0.08, *range* = 0.27).

Taken together, individual electric field simulations as well as the group participation maps suggest that direct effect of tACS with our electrode montages is expected over occipital (Cz-Oz) and parietal (P5–P6) areas.

Effect of tACS on fALFF

We investigated tACS-induced changes in the fALFF, which represents the intensity of spontaneous regional brain activity (Methods, Supplemental materials, Fig. S2A). With this approach, we evaluated local changes in resting-state activity independent of functional connectivity measures, which require interpretations relative to particular regions of interest (Zang et al., 2007; Zou et al., 2008). The three-factor rANOVA, evaluating the main effect of tACS frequency, electrode montage, time, and their interactions, showed a significant main effect of time ($F(2, 38) > 6.11, p < 0.005$) mainly in frontal and occipital regions, which in most cases was observed as a decrease in fALFF over time. However, since the order of the different levels (pre-stimulation, stimulation and post-stimulation) in the time factor is fixed, the effect of time cannot exclusively be attributed to tACS effects. Time effects could also manifest through cognitive state or scanner-related factors that systematically fluctuate over time (Chang and Glover, 2010; Murphy et al., 2013). Therefore, for this and the remainder of the statistical analyses, we do not report main effects of time, but focus our attention on the interactions: tACS frequency × time, electrode montage × time, and tACS frequency × electrode montage × time. With this approach, we control for time and placebo effects, which should be universal across conditions. These interactions could be understood as follows: the tACS frequency × time interaction shows the effect of time that is dependent on the tACS frequency (frequency-dependent effects), regardless of the electrode montage (the effect of frequency can be similar across electrode montages); the electrode montage × time interaction shows the effect of time that is dependent on the electrode montage (montage-dependent effects), regardless of the frequency (the effect of electrode montage can be similar across frequencies); and the tACS frequency × electrode montage × time interaction shows significant interaction between the frequency- and montage-dependent effects (frequency-dependent effects are different between electrode montages). Significant tACS frequency × time interaction ($F(4, 76) > 4.05, p < 0.005$) was found in a few clusters, including the precuneus (PCu) and the right middle occipital gyrus (MOG) (Fig. 4A). Post-hoc analyses on these clusters showed that, in general, tACS effects on fALFF were almost exclusively found in the post-stimulation period with opposite effects induced by 10 and 40 Hz tACS. In some regions, the effect of tACS at 16 Hz followed the effect of 10 Hz tACS (PCu) and in other regions, it followed that of 40 Hz tACS (MOG). Significant electrode montage × time interaction ($F(2, 38) > 6.11, p < 0.005$) was observed in a few clusters, including the cuneus (Cu) and the right medial frontal gyrus (MedialFG) (Fig. 4B). Post-hoc analyses on these clusters showed opposite effects induced by each electrode montage during and after the stimulation period. In general, the observed trend was that, in the most posterior regions (e.g., Cu), tACS over Cz-Oz increased the fALFF during the stimulation, which decreased or returned to pre-stimulation levels in the post-stimulation period, while tACS over P5–P6 decreased fALFF mainly in the stimulation period. The tACS frequency × electrode montage × time interaction was significant ($F(4,76) > 4.05, p < 0.005$) for a few clusters, including bilateral postcentral gyrus (PoC) close to primary motor/somatosensory cortices, and the inferior parietal lobule (IPL) (Fig. 4C). Post-hoc analyses showed that for PoC, tACS at 10 Hz increased fALFF during the stimulation period when it was applied over Cz-Oz while it decreased fALFF during and after the stimulation when it was applied over P5–P6. A different pattern was observed for IPL, where 10 Hz decreased fALFF when it was applied over Cz-Oz and it increased fALFF when applied over P5–P6, both effects observed during the stimulation but not after. The effects of 16 and 40 Hz tACS were observed in PoC where 16 Hz P5–P6 and 40 Hz Cz-Oz decreased fALFF, both effects observed only in post-stimulation. A detailed description of the three-factor rANOVA results – including statistical values for each cluster that showed a significant interaction effect as well as the post-hoc test performed on the fALFF values extracted from the specific cluster – is provided in Supplemental materials, Table 1.

In a complementary analysis, it was observed that for some tACS conditions, the mean strength of the electric field induced by tACS predicted the stimulation effects mainly in posterior regions. For instance, subjects exhibiting higher mean electric field strengths with the Cz-Oz montage showed higher decreases in fALFF values in posterior regions, such as PCu and the left fusiform gyrus (both during stimulation), due to 10 Hz tACS over Cz-Oz ($r < -0.62, p < 0.005$). A detailed description of these results is provided in Supplemental materials (Results, Fig. S3, Table 2).

Taken together, fALFF analysis indicates that tACS affected the regional metabolic activity in a frequency- and electrode montage-dependent manner during and after the stimulation period, with 10 and 40 Hz tACS inducing opposite effects. Electrode montage-dependent effects were observed in a few regions close to the electrodes (i.e., PoC and IPL), but specific regional effects were not exclusive to their correspondingly expected montage. For example, based on simulations, we would expect IPL modulation only with tACS over P5–P6, however, both montages showed significant effects, albeit in opposite directions. The significant correlations observed between the electric field strength and the effect of tACS on fALFF suggests that incorporating individual predictions based on electric field simulations could be a valuable approach for evaluating tACS effects in both, neural and behavioral studies.

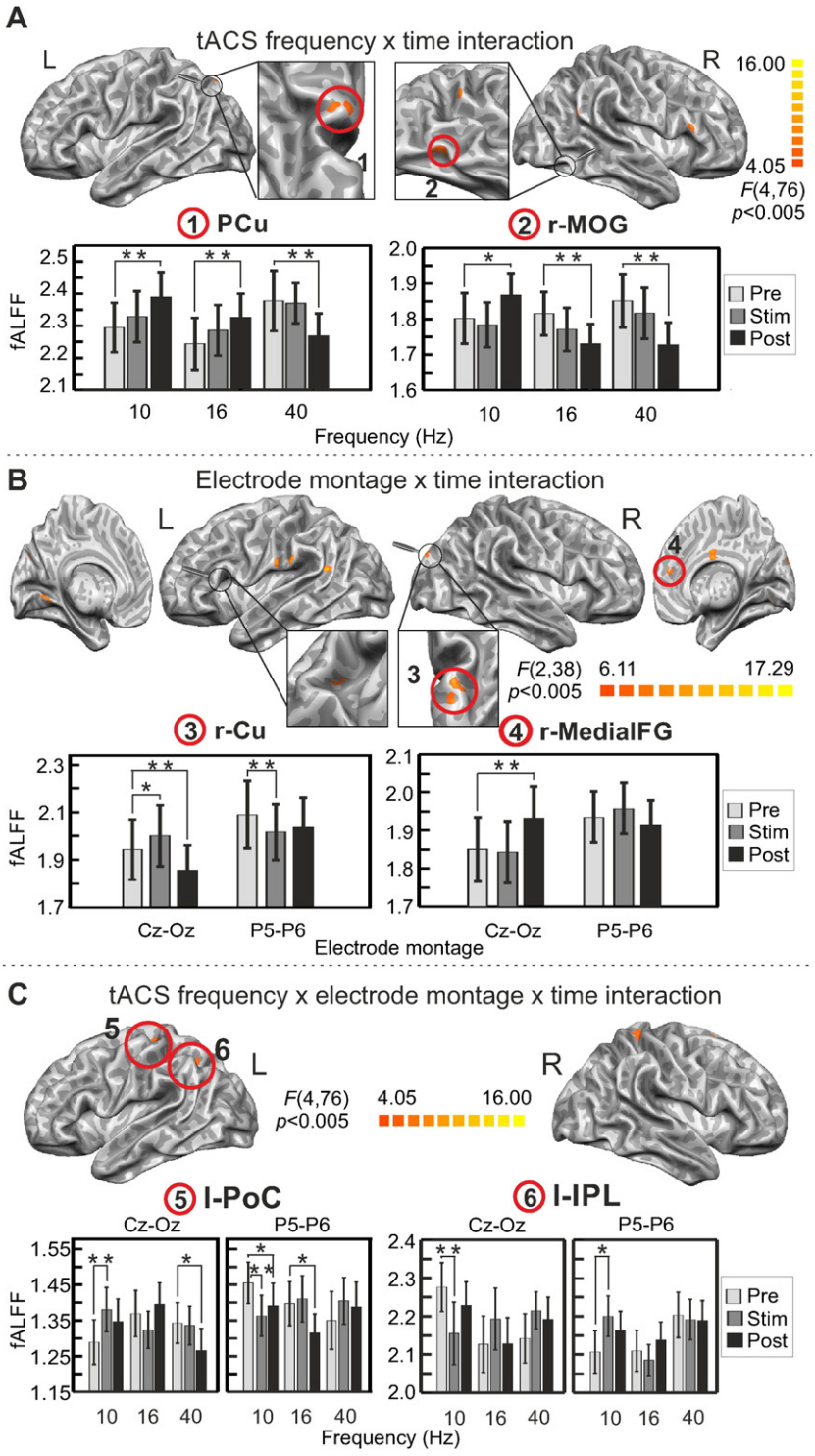

Fig. 4. Effect of tACS on fALFF. Significant interactions in the three-factor rANOVA performed on the fALFF overlaid on the surface-rendered Colin brain template. A) tACS frequency × time interaction, B) Electrode montage × time interaction, and C) tACS frequency × electrode montage × time interaction. Maps were thresholded using clusters determined by $p < 0.005$ and a corrected cluster significance threshold of $p < 0.05$. The resulting cluster size threshold was 6 functional voxels (162 mm) for A and 7 functional voxels (189 mm) for B and C. Bar graphs show post-hoc results for representative clusters for each interaction effect. Error bars denote standard error of the mean. L: left hemisphere, R: right hemisphere. MOG: middle occipital gyrus, PCu: precuneus, Cu: cuneus, MedialFG: medial frontal gyrus, PoC: postcentral gyrus, and IPL: inferior parietal lobe. $^{*}p < 0.05$, $^{**}p < 0.01$.

Effect of tACS on resting-state network functional connectivity (seed-based functional connectivity analysis)

Network-to-network functional connectivity changes

After evaluating tACS-induced changes in fALFF as a measure of intensity of spontaneous regional brain activity, we next focused on evaluating tACS-induced changes on functional connectivity expressed by temporal correlations. Seven well-known resting-state networks (Fox et al., 2005; Beckmann et al., 2005) were defined from the baseline scans using temporal concatenation group ICA (Methods, Fig. 2A). The main components resulting from the ICA matched the previously reported RSNs (Fox et al., 2005; Biswal et al., 1995; Beckmann et al.,

2005; Corbetta and Shulman, 2002; Gao and Lin, 2012; Raichle et al., 2001; Amadi et al., 2013; Lowe et al., 1998; Spreng et al., 2013; Vincent et al., 2008). The selected component representing the DAN included regions located bilaterally along the intraparietal sulci (IPS), frontal eye fields (FEF), human visual motion complex (V5/hMT+), and part of the MedialFG (Fox et al., 2005; Corbetta and Shulman, 2002; Gao and Lin, 2012). The DMN component included bilateral angular gyri and, most strongly, anterior and posterior cingulate cortices (ACC/PCC) (Fox et al., 2005; Gao and Lin, 2012; Raichle et al., 2001). The executive network component included cingulate gyrus (CG) and bilateral middle frontal gyrus (MFG)/superior frontal gyri (SFG) (Beckmann et al., 2005; Amadi et al., 2013). The motor network component included bilateral pre-central gyrus (PrC) and PoC, insula and supplementary motor area (SMA) (Biswal et al., 1995). The visual network component included mainly occipital cortex (Lowe et al., 1998). The components representing the r-FP and l-FP included regions in the MFG, inferior temporal gyrus (ITG), PCu and IPL/superior parietal lobe (SPL), located in the right and left hemispheres, respectively (Gao and Lin, 2012; Spreng et al., 2013; Vincent et al., 2008). These components were thresholded at 50% (except for DAN, which was thresholded at 70%) and used to represent RSNs (Fig. 2B) in seed-based functional connectivity analysis.

To obtain a general overview of the impact of tACS on resting-state functional connectivity, we first evaluated between-network correlation changes. To this end, seed-based functional connectivity analysis was conducted by correlating each RSN's average time course with that of every other network (Methods, Supplemental materials, Fig. S2 B). Visual inspection of the network-to-network results (Supplemental materials, Fig. S4) shows that the functional connectivity pattern between networks remained similar in all conditions (i.e., tACS frequency, electrode montage, and time). As reported in the literature of resting-state functional connectivity, there was an anticorrelation between DAN and DMN, and positive correlations between DAN and the fronto-parietal control networks (l-FP and r-LP) (Fox et al., 2005; Gao and Lin, 2012). The four-factor rANOVA evaluating the main effects and interactions between tACS frequency, electrode montage, time, and network combination was significant only for the DAN (tACS frequency × electrode montage × time × network interaction: $F\,(20, 380) = 1.66$, $p = 0.037$) and for the l-FP (tACS frequency × time × network interaction: $F\,(20, 380) = 1.71$, $p = 0.029$; tACS frequency × electrode montage × time × network interaction: $F\,(20, 380) = 1.97$, $p = 0.007$). Follow-up three-factor rANOVAs for the functional connectivity between each of these networks (DAN and l-FP) and the remaining six RSNs showed significant tACS frequency × electrode montage × time interaction for the DAN to visual network combination ($F\,(4, 76) = 2.70$, $p = 0.036$). With respect to the l-FP, a significant tACS frequency × time interaction was observed for the combination l-FP to visual network ($F\,(4, 76) = 3.16$, $p = 0.018$), and a significant tACS frequency × electrode montage × time interaction was observed for the functional connectivity of l-FP to DMN ($F\,(4, 76) = 2.64$, $p = 0.040$). It is worth noting that for the two above-mentioned significant tACS frequency × electrode montage × time interactions (DAN to visual network, l-FP to DMN), post-hoc analyses showed that tACS was effective only when applied over Cz-Oz, but not when applied over P5–P6. A more detailed description about the main effects and post-hoc analyses are shown in Supplemental materials, Fig. S5. In summary, tACS-induced modulation of the network-to-network functional connectivity was only significant for the DAN (i.e., with the visual network) and the l-FP (i.e., with the visual network and DMN), mainly with tACS over Cz-Oz.

Network-to-whole-brain functional connectivity changes

To gain further insight into network-based interactions, each RSN's average time course was correlated with that of every other voxel in the brain (Supplemental materials, Fig. S2 B). This approach offers the opportunity to evaluate functional connectivity changes within a network as well as between the network and the whole brain in a less categorical manner than the network-to-network analysis (Methods). We focus our description of the results on the networks that showed tACS-induced modulation in either the fALFF or the network-to-network analysis, i.e., DAN, l-FP, motor, and visual networks. Focus on the visual and l-FP networks was also motivated by the electric field simulation prediction that tACS at Cz-Oz and P5–P6 maximally stimulate occipital and parietal cortices, respectively. The DMN, executive network and the r-FP did not show significant tACS modulation in either fALFF or network-to-network analysis; therefore, we will not describe network-to-whole-brain analysis results for these networks.

Dorsal attention network (DAN). For the DAN (Fig. 5A), the functional connectivity maps obtained in the pre-stimulation conditions (Fig. 5B) are similar to the original DAN component obtained from the ICA (compare Fig. 5B to Fig. 2A). A significant tACS frequency × time interaction ($F\,(4, 76) > 4.05$, $p < 0.005$, Fig. 5C) was observed in a few clusters, including the right MOG and the left lentiform nucleus (LN), an anatomical region that comprises the putamen and the globus pallidus in the basal ganglia. In the case of the MOG, post-hoc analyses showed that its functional connectivity with the DAN was significantly modulated by tACS at 10 and 16 Hz, with 10 Hz decreasing functional connectivity and 16 Hz tACS increasing it. These changes were restricted to the stimulation period. For the LN, 10 and 16 Hz tACS increased functional connectivity during (10 Hz) or after (16 Hz) the stimulation period while 40 Hz decreased it both during and after the stimulation. Significant electrode montage × time interaction ($F\,(2, 38) > 6.11$, $p < 0.005$, Fig. 5D) was observed in the right MFG and most strongly in the bilateral thalamus. Post-hoc analyses showed that in both regions, tACS over Cz-Oz decreased its functional connectivity with the DAN while tACS over P5–P6 increased it, however, for the right MFG, these effects were observed only in the post-stimulation period, while for the thalamus, these effects were observed both during and after the stimulation period. A significant tACS frequency × electrode montage × time interaction ($F\,(4, 76) > 4.05$, $p < 0.005$, Fig. 5E) was observed mainly for the right superior temporal gyrus (STG) and for left IPL. Post-hoc analyses showed that for the right STG, 16 Hz tACS increased its functional connectivity with the DAN during the stimulation period when applied over Cz-Oz while 40 Hz decreased it in the post-stimulation period. For this cluster, 40 Hz tACS was the only effective frequency when tACS was applied over P5–P6, which increased the functional connectivity in the post-stimulation period. For the left IPL, 10 Hz tACS applied over Cz-Oz decreased its functional connectivity with the DAN during and after the stimulation period while it increased it in the post-stimulation period when applied over P5–P6. Stimulations with 16 and 40 Hz tACS were effective when applied over P5–P6, decreasing the left IPL-to-DAN functional connectivity during (16 and 40 Hz) and after (only 16 Hz) the stimulation period. A detailed description of the three-factor rANOVA results – including statistical values for each cluster that showed a significant interaction effect as well as the post-hoc test performed on the z-transformed correlation values extracted from the specific cluster – is provided in Supplemental materials, Table 3.

In general, tACS-induced modulation of the functional connectivity between the DAN and the whole brain was mainly observed in regions outside the network (e.g., right MOG). Within network changes were observed, for example, in the left IPL.

Left fronto-parietal control network (l-FP). For the l-FP (Fig. 6A), the correlation maps in the pre-stimulation conditions (Fig. 6B) resemble closely the original l-FP component obtained from ICA (compare Fig. 6B to Fig. 2A). The tACS frequency × time interaction was significant ($F\,(4, 76) > 4.05$, $p < 0.005$, Fig. 6C) in several regions in frontal, parietal and occipital cortices as well as in the LN. The largest clusters included one covering a broad area in the right occipito-parietal cortices and another in the LN. Post-hoc analyses showed that 10 Hz tACS increased functional connectivity between l-FP and these two clusters while

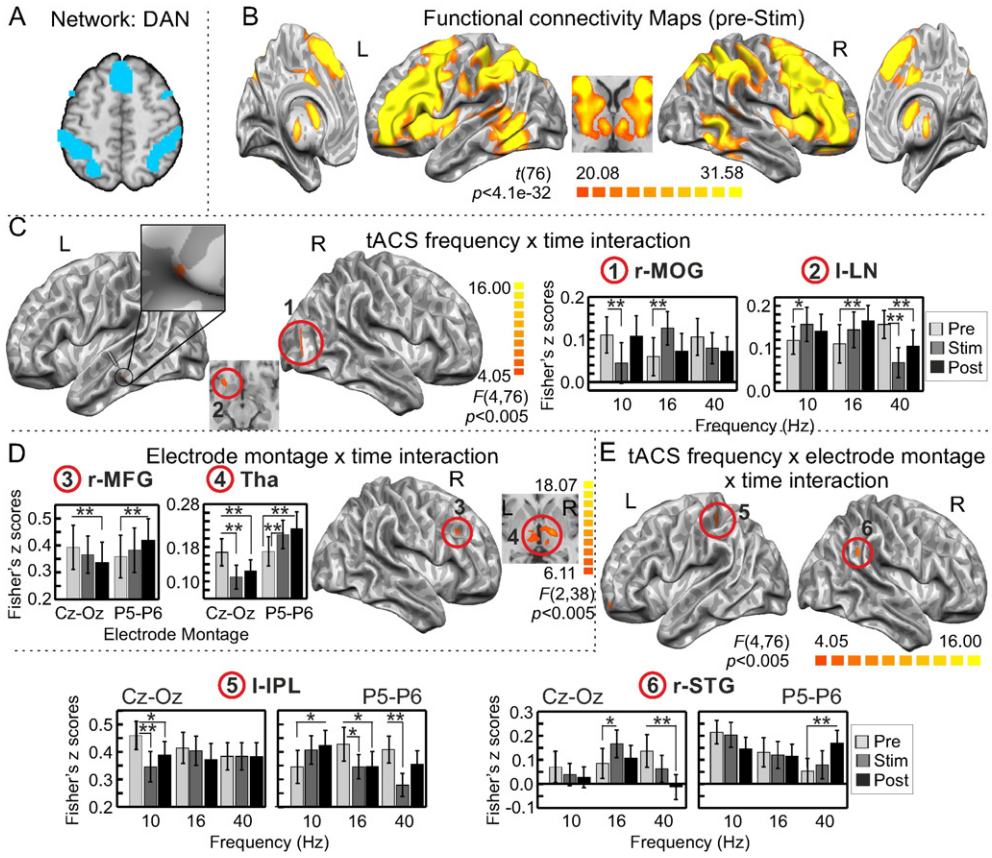

Fig. 5. Effect of tACS on functional connectivity relative to DAN. Significant interactions in the three-factor rANOVA performed on the DAN network-to-whole-brain functional connectivity analysis. A) Mask used for the DAN seed, B) Functional connectivity maps in the pre-stimulation conditions, C) tACS frequency × time interaction, D) Electrode montage × time interaction, E) tACS frequency × electrode montage × time interaction. Maps in C–E were thresholded using clusters determined by $p < 0.005$ and a corrected cluster significance threshold of $p < 0.05$. The resulting cluster size threshold was 9 functional voxels (243 mm) for C and 10 functional voxels (270 mm) for D and E. Bar graphs show post-hoc results for representative clusters for each interaction effect. Error bars denote standard error of the mean. L: left hemisphere, R: right hemisphere. MOG: middle occipital gyrus, LN: lentiform nucleus, MFG: middle frontal gyrus, Tha: thalamus, IPL: inferior parietal lobe, and STG: superior temporal gyrus. $^{*}p < 0.05$, $^{**}p < 0.01$.

40 Hz tACS decreased it both during and after the stimulation period. No significant electrode montage × time interaction was observed for this network. Significant tACS frequency × electrode montage × time interactions ($F(4, 76) > 4.05$, $p < 0.005$, Fig. 6D) were observed in a few clusters, including the right middle temporal gyrus (MTG) and CG. Post-hoc analyses showed that for the MTG, 10 Hz tACS decreased functional connectivity during and after the stimulation period when it was applied over Cz-Oz and increased functional connectivity during the stimulation period when applied over P5–P6. Stimulation with 16 Hz tACS decreased functional connectivity during the stimulation period only when it was applied over P5–P6. For the CG, 10 Hz tACS decreased functional connectivity during the stimulation over Cz-Oz. In addition, when tACS was applied over P5–P6, 16 Hz tACS increased functional connectivity after the stimulation period and 40 Hz decreased it during and post stimulation. A detailed description of the three-factor rANOVA and post-hoc results can be found in Supplemental materials, Table 4.

Similar to the DAN, tACS-induced modulation of functional connectivity between the l-FP and the whole brain was mainly observed in regions outside the network whose functional connectivity is low in the pre-stimulation periods. Spatially extensive tACS frequency × time interaction was observed between the l-FP and occipito-parietal regions, which matched our prediction of tACS modulating functional connectivity between regions close to the electrodes and more distant fronto-parietal areas.

Motor network. As for the networks described above, the correlation maps with the motor network seed (Fig. 7A) obtained in the pre-stimulation conditions (Fig. 7B) are similar to the original motor network component obtained from the ICA (compare Fig. 7B to Fig. 2A). Significant tACS frequency × time interaction ($F(4, 76) > 4.05$, $p < 0.005$, Fig. 7C) was observed in the left MFG and bilateral pulvinar nucleus in the thalamus. Post-hoc analyses showed that 10 Hz tACS increased functional connectivity between the motor network and both clusters, during the stimulation. This effect was observed in the post-stimulation period only for the pulvinar. The effect of 16 Hz tACS was observed as a decrease in functional connectivity between the motor network and the MFG during the stimulation and between the motor network and the pulvinar in the post-stimulation period. Stimulation with tACS at 40 Hz decreased functional connectivity only during the stimulation period for the MFG. Significant electrode montage × time interaction ($F(2, 38) > 6.11$, $p < 0.005$, Fig. 7D) was observed for the left SFG and the lingual gyrus (LingG). Post-hoc analyses showed that tACS decreased functional connectivity between the motor network and the left SFG only in the post-stimulation period when it was applied over Cz-Oz. For the LingG, tACS over Cz-Oz decreased functional connectivity during the stimulation period, while tACS over P5–P6 increased it both during and after the stimulation period. Significant tACS frequency × electrode montage × time interaction ($F(4, 76) > 4.05$, $p < 0.005$, Fig. 7E) was observed for several clusters, including the left insula and PoC. Interestingly, these two clusters are located within the motor network (Fig. 7B). For both clusters, and in agreement with the results obtained in the fALFF analysis, 10 Hz tACS increased functional connectivity during (PoC) and after (insula, PoC) the stimulation period when tACS was applied over Cz-Oz. Stimulation with 40 Hz tACS over Cz-Oz decreased functional connectivity during (insula) and after (insula, PoC) the stimulation period. When tACS was applied over P5–P6, 10 Hz tACS decreased functional connectivity in the post-

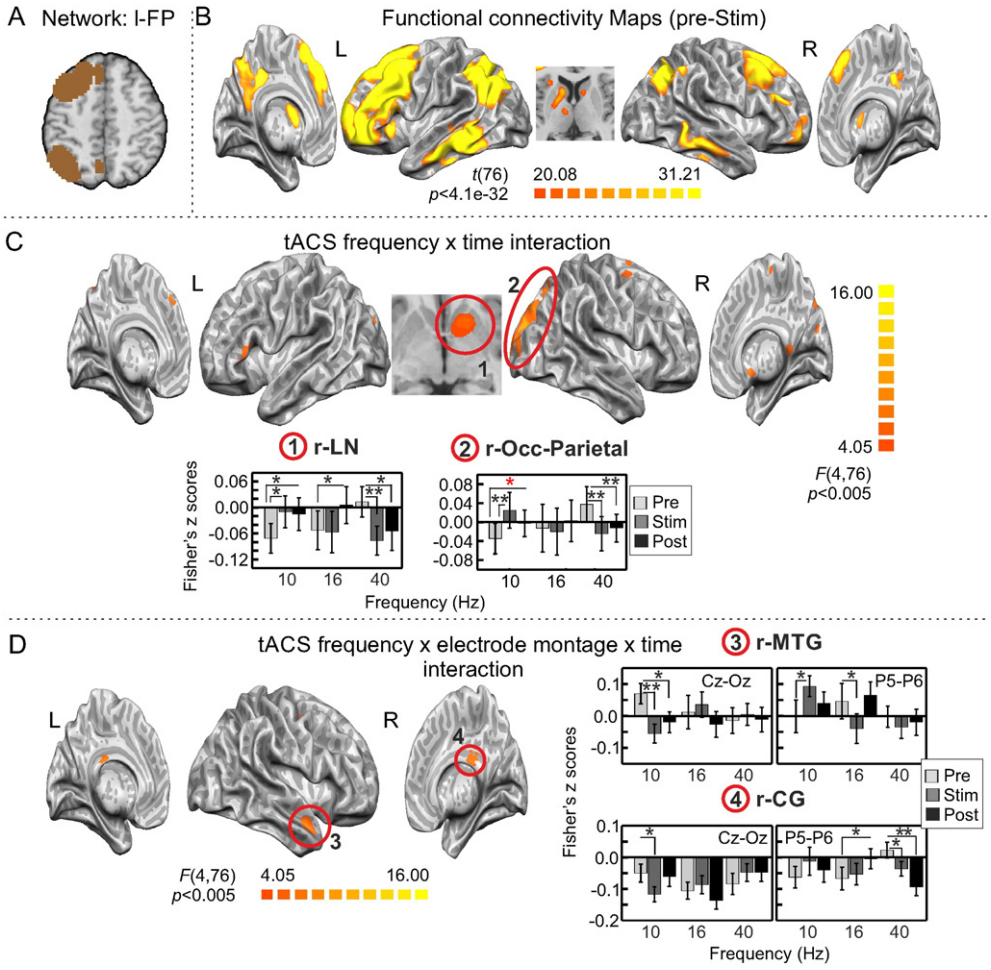

Fig. 6. Effect of tACS on functional connectivity relative to l-FP. Significant interactions in the three-factor rANOVA performed on the l-FP network-to-whole-brain functional connectivity analysis. A) Mask used for the l-FP seed, B) functional connectivity maps in the pre-stimulation conditions, C) tACS frequency × time interaction, D) tACS frequency × electrode montage × time interaction. Maps in C–D were thresholded using clusters determined by $p < 0.005$ and a corrected cluster significance threshold of $p < 0.05$. The resulting cluster size threshold was 13 functional voxels (351 mm) for C and 9 functional voxels (243 mm) for D. Bar graphs show post-hoc results for representative clusters for each interaction effect. Error bars denote standard error of the mean. L: left hemisphere, and R: right hemisphere. LN: lentiform nucleus, Occ: occipital, MTG: middle temporal gyrus, and CG: cingulate gyrus. Red* $p = 0.05$, * $p < 0.05$, ** $p < 0.01$.

stimulation period for both clusters while 16 Hz tACS decreased functional connectivity only for the PoC in the post-stimulation period. A detailed description of the three-factor rANOVA and post-hoc analyses is provided in Supplemental materials, Table 5.

In general, functional connectivity changes relative to the motor network resembled the pattern described in the previous section for the fALFF and for the other networks, with 10 and 40 Hz tACS showing opposite effects. Within-network functional connectivity changes were observed in insula and PoC.

Visual network. Correlation maps in the pre-stimulation conditions resemble closely the original component representing the visual network obtained with ICA (Figs. 8A–B, compare Fig. 8B to Fig. 2A). Significant tACS frequency × time interaction ($F(4, 76) > 4.05$, $p < 0.005$, Fig. 8C) was found for a few clusters, including the PCC and the left MOG. Post-hoc analyses showed that the visual network functional connectivity to both clusters increased with 10 Hz tACS during and after (only PCC) the stimulation period. Stimulation with tACS at 16 Hz increased functional connectivity between the visual network and the PCC after the stimulation and decreased functional connectivity between the visual network and the MOG during and after the stimulation. Stimulation with tACS at 40 Hz decreased functional connectivity between the visual network and the PCC after the stimulation period. Note that the MOG cluster belongs to the visual network, given by high correlation values between the visual network and this cluster in the pre-stimulation condition (Fig. 2A, Fig. 8B). Significant electrode montage × time interaction ($F(2, 38) > 6.11$, $p < 0.005$, Fig. 8D) was found for a few clusters, including the left insula and the right IFG. Post-hoc analyses showed that Cz-Oz stimulation increased functional connectivity between the visual network and the insula while P5–P6 decreased this relationship during stimulation. In terms of electrode montage, Cz-Oz tACS also decreased visual network correlation with IFG in the post-stimulation period. A significant tACS frequency × electrode montage × time interaction ($F(4, 76) > 4.05$, $p < 0.005$, Fig. 8E) was found for left MFG and in a cluster intersecting middle and superior frontal gyri (MFG/SFG). The visual network correlation with MFG/SFG was affected only when tACS was applied over P5–P6, with 10 Hz increasing this functional connectivity during the stimulation period, and 16 and 40 Hz decreasing it during and after (only for 40 Hz) the stimulation. The functional connectivity between the visual network and the MFG increased with 10 Hz tACS over Cz-Oz in the post-stimulation period and decreased with 40 Hz tACS over Cz-Oz during the stimulation. Stimulation with 16 Hz tACS decreased functional connectivity between the visual network and the MFG during the stimulation period, when it was applied over P5–P6. A detailed description of the three-factor rANOVA and post-hoc results is provided in Supplemental materials, Table 6.

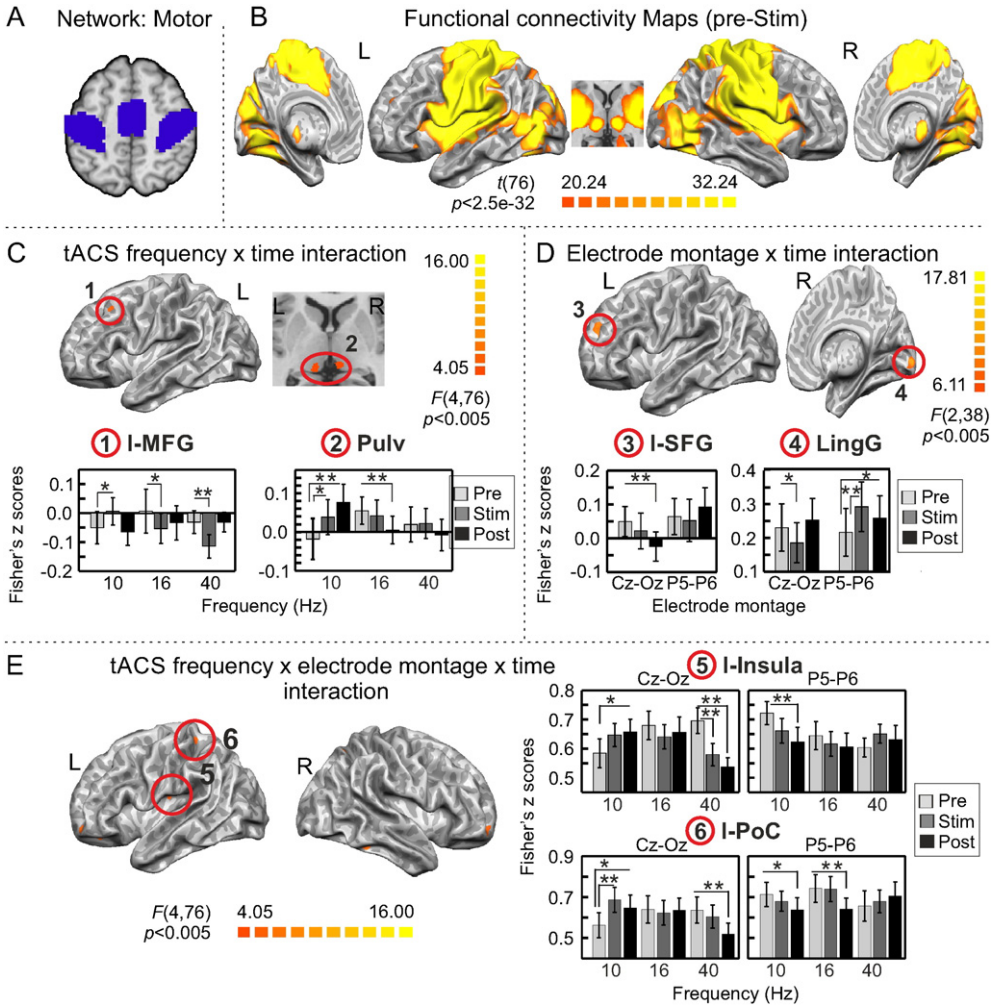

Fig. 7. Effect of tACS on functional connectivity relative to motor network. Significant interactions in the three-factor rANOVA performed on the motor network-to-whole-brain functional connectivity analysis. A) Mask used for the motor network, B) functional connectivity maps in the pre-stimulation conditions, C) tACS frequency × time interaction, D) electrode montage × time interaction, E) tACS frequency × electrode montage × time interaction. Maps in C–E were thresholded using clusters determined by $p < 0.005$ and a corrected cluster significance threshold of $p < 0.05$. The resulting cluster size threshold was 10 functional voxels (270 mm) for C and E, and 9 functional voxels (243 mm) for D. Bar graphs show post-hoc results for representative clusters for each interaction effect. Error bars denote standard error of the mean. L: left hemisphere, R: right hemisphere. MFG: middle frontal gyrus, Pulv: pulvinar, SFG: superior frontal gyrus, LingG: lingual gyrus, and PoC: postcentral gyrus. $^{*}p < 0.05$, $^{**}p < 0.01$.

In summary, functional connectivity changes relative to the visual network were mainly observed between this network and regions outside of the network, except for the MOG, and followed the previously described pattern of 10 and 40 Hz tACS showing opposite effects.

Overall, results from the seed-based functional connectivity analyses using the selected RSNs showed that tACS effects on RSN functional connectivity were frequency- and electrode montage-dependent, with 10 and 40 Hz tACS often inducing opposite sign of effects. Most of the tACS effects were observed as modulation of *inter*-network functional connectivity (as observed in network-to-network and network-to-whole-brain correlations). *Intra*-network functional connectivity changes were observed for the DAN (IPL), the motor network (insula, PoC) and the visual network (MOG). The l-FP showed the most extensive frequency-dependent modulation in functional connectivity, mainly with occipito-parietal areas.

tACS-induced changes in functional connectivity relative to maximally stimulated areas

Apart from assessing intrinsic resting-state networks, another important question is whether tACS modulates functional connectivity between directly stimulated and distant brain regions. This analysis would help explain results from our previous study showing that tACS modulated the BOLD signal in regions distant from the electrodes. To this end, three different ROIs were generated based on the regions with the highest electric field across subjects (Oz, P5, P6, see Methods) as predicted by simulations (Fig. 3, Fig. S2). These ROIs were employed as seeds for seed-based functional connectivity analyses, wherein each seed's average time course was correlated with that of every other voxel in the brain (Supplemental materials, Fig. S2 C).

For tACS over Cz-Oz, the seed (Oz) region was located within the occipital cortex (Fig. 9A, Supplemental materials, Fig. S1). The group functional connectivity map of the pre-stimulation conditions shows that this seed exhibits greatest functional connectivity with other regions within the occipital cortex (Fig. 9B), constituting a network that resembles the visual network component obtained with our ICA analysis (compare Fig. 9B to Fig. 2A). This suggests that, based on the electric field simulations, tACS over Cz-Oz maximally stimulates the visual network. To evaluate whether tACS over Cz-Oz modulates functional connectivity of the area directly stimulated (as predicted by our electric field simulations), a two-factor rANOVA evaluating tACS frequency × time interaction effects was conducted with the data collected when tACS was applied with the Cz-Oz montage. Significant tACS frequency × time interaction ($F(4, 76) > 4.05$, $p < 0.005$, Fig. 9C) was observed within the network in the left Cu, but mainly in regions outside of the visual network, including the left MedialFG and insula.

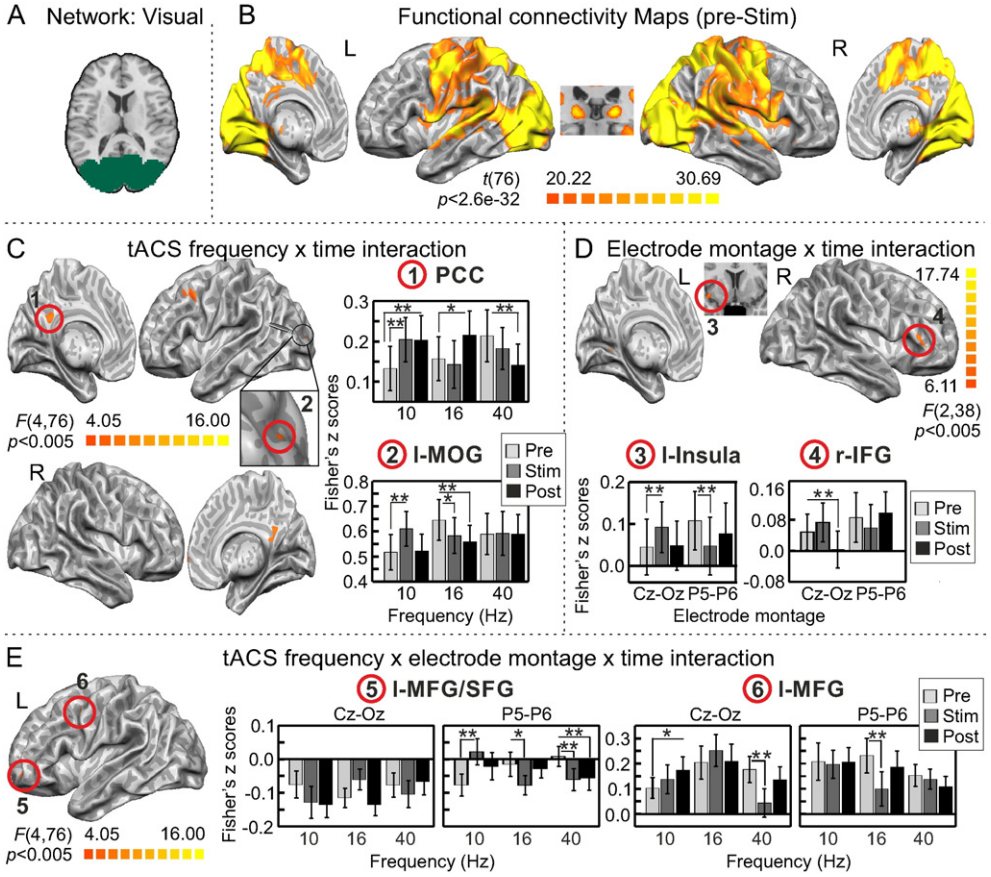

Fig. 8. Effect of tACS on functional connectivity relative to the visual network. Significant interactions in the three-factor rANOVA performed on the visual network-to-whole-brain functional connectivity analysis. A) Mask used for the visual network seed, B) functional connectivity maps in the pre-stimulation conditions, C) tACS frequency × time interaction, D) electrode montage × time interaction, E) tACS frequency x electrode montage x time interaction. Maps in C-E were thresholded using clusters determined by $p < 0.005$ and a corrected cluster significance threshold of $p < 0.05$. The resulting cluster size threshold was 11 functional voxels (297 mm) for C, 9 functional voxels (243 mm) for D, and 10 functional voxels (270 mm) for E. Bar graphs show post-hoc results for representative clusters for each interaction effect. Error bars denote standard error of the mean. L: left hemisphere, R: right hemisphere. PCC: posterior cingulate cortex, MOG: middle occipital gyrus, IFG: inferior frontal gyrus, MFG: middle frontal gyrus, and SFG: superior frontal gyrus. $^{*}p < 0.05$, $^{**}p < 0.01$.

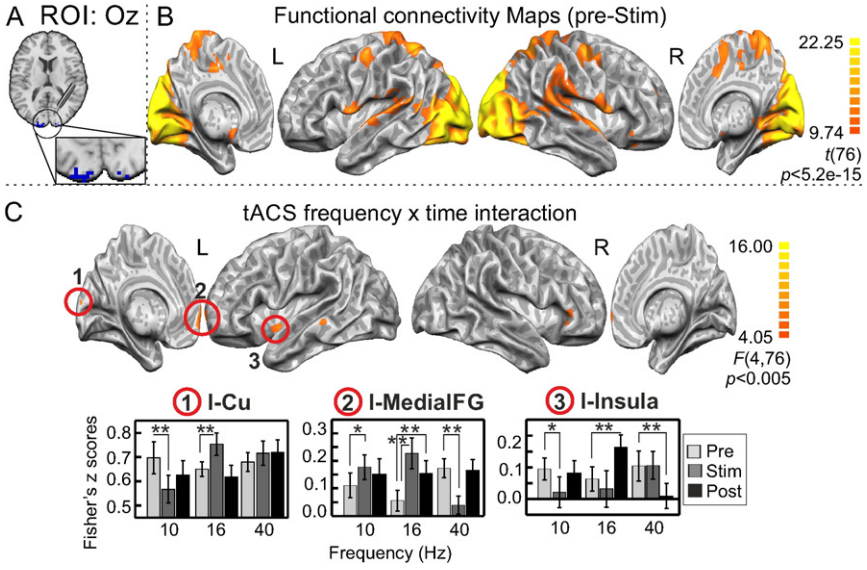

Fig. 9. Effect of tACS on functional connectivity relative to simulation-based ROI Oz. Significant interactions in the two-factor rANOVA performed on the Oz functional connectivity analysis. A) Mask used for the Oz seed, B) Functional connectivity maps in the pre-stimulation conditions, C) tACS frequency x time interaction. Maps in C were thresholded using clusters determined by $p < 0.005$ and a corrected cluster significance threshold of $p < 0.05$. The resulting cluster size threshold was 11 functional voxels (297 mm). Bar graphs show post-hoc results for representative clusters for the interaction effect. Error bars denote standard error of the mean. L: left hemisphere, R: right hemisphere. Cu: cuneus, and MedialFG: medial frontal gyrus. $^{*}p < 0.05$, $^{**}p < 0.01$.

Post-hoc analyses showed that 10 Hz tACS was most effective during the stimulation period, significantly decreasing functional connectivity between the Oz seed and the Cu as well as the insula, and increasing it with the MedialFG. Stimulation with tACS at 16 Hz increased functional connectivity between the seed and these three regions, which was observed during (Cu) or after (insula) the stimulation period, or both (MedialFG). On the other hand, 40 Hz tACS mainly decreased functional connectivity between the seed and regions outside the visual network during or after the stimulation period. For a more detailed description of the results, please refer to Supplemental materials, Table 7.

Continuing with the electric field simulation-based seeds, for tACS over P5–P6, one seed region was situated in the posterior parietal cortex in each hemisphere (P5, P6) (Supplemental materials, Fig. S1). Two-factor rANOVAs were conducted separately for the P5 and P6 seeds, including only the conditions with stimulation applied over P5–P6 in order to test whether this montage was able to induce changes in the functional connectivity of the regions being maximally stimulated. For the P5 seed (Fig. 10A), the group functional connectivity map of the pre-stimulation conditions shows greatest functional connectivity between this seed and fronto-parietal regions, which is more pronounced in the left hemisphere (Fig. 10B). This functional connectivity map resembles the l-FP component obtained with our ICA analysis (compare Fig. 10B to Fig. 2A). A significant tACS frequency × time interaction ($F(4, 76) > 4.05$, $p < 0.005$, Fig. 10C) was observed in several clusters, including right Cu and LN. Post-hoc analyses showed that in most of the clusters, as already reported for previous analyses, 10 and 40 Hz tACS induced opposite effects, with 10 Hz tACS mainly increasing functional connectivity (during and/or after the stimulation period) and 40 Hz tACS decreasing it (mainly after the stimulation period). Note that similar clusters (i.e., Cu and LN) exhibited the same functional connectivity modulation in the P5 seed analysis and l-FP network-to-whole-brain functional connectivity analysis (compare Fig. 10C to Fig. 6C). Most changes in functional connectivity relative to the P5 seed (left hemisphere) were observed in regions in the right hemisphere, suggesting tACS modulation of inter-hemispheric functional connectivity, as shown in EEG-tACS studies (Helfrich et al., 2014b). For a more detailed description of the results, please refer to Supplemental materials, Table 8.

Stimulation with tACS was less effective at modulating the functional connectivity with the P6 seed, whose functional connectivity map in the pre-stimulation condition resembles that of the r-FP (compare Supplemental materials Fig. S6 to Fig. 2A). A significant tACS frequency × time interaction ($F(4, 76) > 4.05$, $p < 0.005$) was found only for the right SFG, where 10 and 40 Hz tACS induced opposite effects in the post-stimulation period. Note that no inter-hemispheric functional connectivity changes were observed for P6.

Overall, using electric field simulation-based seed correlations, we observed that tACS over Cz-Oz and P5–P6 maximally stimulate different networks, with stimulation over Cz-Oz targeting the visual network and stimulation over P5–P6 targeting left and right fronto-parietal control networks. As expected, tACS modulated functional connectivity between directly stimulated regions and areas distant from the electrodes. However, no significant functional connectivity changes were observed between the Oz seed and fronto-parietal areas, contrary to our expectations based on the results from our previous tACS-fMRI study (Cabral-Calderin et al., 2016). The effects of tACS over P5–P6 on functional connectivity with the left seed (P5) were more pronounced than with the right seed (P6).

In the present study, we reported only frequency- or/and electrode montage-dependent effects of tACS. Additional analyses evaluating non-specific tACS effects suggested that the effects of tACS on fALFF and functional connectivity were mostly frequency dependent and that non-specific effects were minimal (see Supplemental materials, Results and Fig. S7).

Phosphene perception, cutaneous sensation and fatigue ratings

We evaluated sensory and fatigue experience ratings related to tACS at each frequency and with each electrode montage. The three-factor rANOVA showed a significant tACS frequency × time interaction on the phosphene perception ratings ($F(4, 76) > 3.78$, $p = 0.007$, Supplemental materials, Fig. S8). As already described in the literature, post-hoc analyses showed a significant increase in the phosphene ratings during 10 and 16 Hz tACS ($p = 0.01$ and $p < 0.001$, respectively, (Kanai et al., 2008; Turi et al., 2013)). Stimulation with tACS at 40 Hz did not induce phosphene perception. No significant electrode montage × time interaction or tACS frequency × electrode montage × time interaction was observed for the phosphene ratings. No significant interactions were observed for the cutaneous sensation and the fatigue ratings. Overall, these analyses showed that 10 and 16 Hz tACS induced phosphenes with a similar strength while 40 Hz tACS did not induce

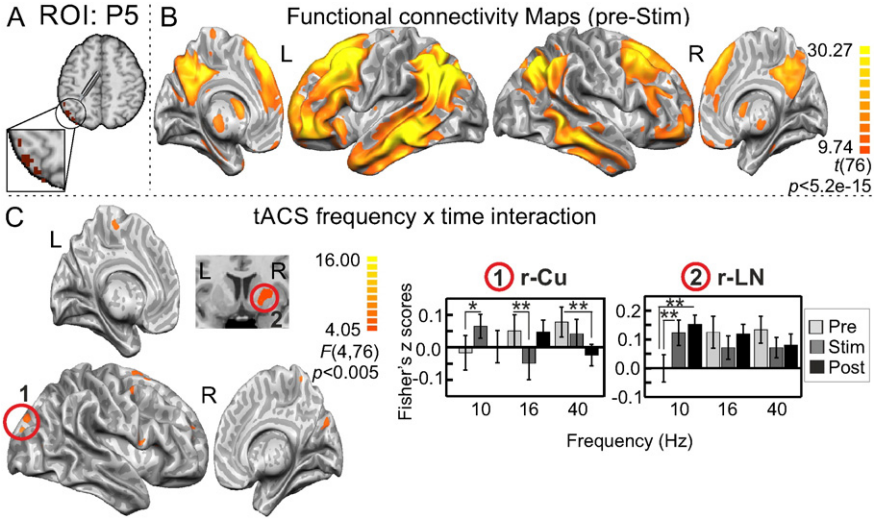

Fig. 10. Effect of tACS on functional connectivity relative to simulation-based ROI P5. Significant interactions in the two-factor rANOVA performed on the P5 functional connectivity analysis. A) Mask used for the P5 seed, B) functional connectivity maps in the pre-stimulation conditions, C) tACS frequency × time interaction. Maps in C were thresholded using clusters determined by $p < 0.005$ and a corrected cluster significance threshold of $p < 0.05$. The resulting cluster size threshold was 12 functional voxels (324 mm). Bar graphs show post-hoc results for representative clusters for the interaction effect. Error bars denote standard error of the mean. L: left hemisphere, R: right hemisphere. Cu: cuneus, and LN: lentiform nucleus. $^{*}p < 0.05$, $^{**}p < 0.01$.

significant phosphene perception. Subjects perceived the stimulation with similar discomfort across frequencies and electrode montages.

In order to evaluate the impact of tACS-induced sensory experiences on spontaneous low frequency BOLD signal fluctuations, the individual phosphene perception and cutaneous sensation ratings were correlated to the individual mean fALFF values extracted from sample ROIs located in primary visual (V1) and somatosensory (S1) cortices, respectively (Supplementary materials). Four ROIs were created by defining a 7 mm radius sphere around the center of Brodmann area 17 (for V1) and Brodmann areas 1–3 (for S1), for each hemisphere. We hypothesized that any effect of tACS-induced sensory experiences should be largest in the corresponding primary sensory cortices. No significant correlation was observed between the fALFF and either phosphene perception (mean p-value across comparisons: $p = 0.547$, *range* 0.089–0.916) or somatosensory ratings (mean p-value across comparisons: $p = 0.535$, *range* 0.122–0.974) during tACS stimulation for any ROI. Note that, overall, participants rated phosphene perception and cutaneous sensation with low intensities (mean values ranged from 1 to 2.25 (on a scale of 1–10)), probably due to the long stimulation times. Sensory experiences with higher intensities could have a different impact on fALFF values in primary cortices.

Discussion

In the present study, we investigated the effects of tACS on spontaneous low frequency BOLD signal fluctuations, a measure that allows characterization of RSNs. The practice of using resting-state functional connectivity to inform brain stimulation targets is increasingly gaining attention in the quest for effective brain stimulation methods (Opitz et al., 2015a; Fox et al., 2014; Fox et al., 2012). The focus of the discussion will be on the most significant and stable findings across the different analysis approaches rather than every specific result. The electric field simulations showed that tACS over Cz-Oz mainly stimulates the occipital cortex, while tACS over P5–P6 primarily stimulates parietal cortices. As partly predicted from previous behavioral/imaging studies (Feurra et al., 2011a; Kanai et al., 2008; Alekseichuk et al., 2015; Cabral-Calderin et al., 2016; Raco et al., 2014; Feurra et al., 2011b), tACS effects were frequency and partially electrode montage dependent. In regions where frequency-dependent effects of tACS were observed, 10 and 40 Hz tACS generally induced opposite effects. Most tACS effects were observed as modulation of inter-network functional connectivity (e.g., l-FP to visual network, l-FP to DMN). Intra-network functional connectivity changes were observed only in a few clusters within DAN (IPL), motor network (insula, PoC) and visual network (MOG). The l-FP showed the most extensive frequency-dependent modulation in functional connectivity, mainly with occipito-parietal regions. Taken together, our results show that tACS is able to modulate local spontaneous low frequency fluctuations and their correlations with distant regions, which should be taken into account when interpreting tACS effects on brain function.

Effects of tACS as predicted by the electrode montages and electric field simulations

Using electric field-based seeds predicted by FEM model simulations, we showed that tACS over Cz-Oz is most likely to maximally stimulate the visual network while over P5–P6 it targets left and right fronto-parietal control networks (Neuling et al., 2012). Further analyses showed that most electrode-dependent effects were given by opposite sign of effects induced by tACS with each electrode montage, though both montages affected similar regions, at least to some extent. It is important to note that, although the maximum electric field for each montage was located in different regions, given the spatial proximity of the two electrode montages, lower electric fields from the individual simulations that did not pass the 50% masking threshold share common brain regions, primarily in medial occipito-parietal areas. This suggests that, even though each electrode montage strongly targets a particular network, part of the applied current could still extend to regions common to both montages. More focal montages (e.g., high-density montages) might induce more specific montage-dependent effects. The opposite effects of electrode montage could arise from the fact that, with our electrode montages, tACS stimulation is antiphase (i.e., 180° phase difference between the two stimulated sites (Polania et al., 2012; Struber et al., 2014)). With tACS over Cz-Oz, posterior regions are stimulated with a 180° phase difference with respect to each electrode, however, stimulation is hemispherically symmetric along the midline. A different pattern is induced by tACS over P5–P6, where the hemispheres are stimulated with a 180° phase difference. However, the goal of the present study was not to compare inter-hemispheric functional connectivity changes, but to analyze tACS modulation in the context of resting-state networks, which are typically bilaterally defined (Fox et al., 2005; Beckmann et al., 2005). In addition, we aimed to examine changes relative to directly stimulated sites, which are also not constrained to single hemispheres in this study. Inferences about inter-hemispheric functional connectivity could perhaps be made with our electric field simulation-based seeds for tACS over P5–P6. Here, seeds were unilaterally placed over parietal areas in each hemisphere, although it is important to note that though the seeds are separated into hemispheres, the stimulation was not. Stimulation with tACS over P5–P6 might be more likely to induce changes in functional connectivity between hemispheres than Cz-Oz tACS because, as mentioned above, each hemisphere is stimulated with a 180° phase relationship to the other, in contrast to the Cz-Oz montage. In a previous tACS-EEG study, it was shown that 40 Hz tACS applied with a similar montage (~P7–P8) impaired interhemispheric functional coupling observed as a decrease in the interhemispheric EEG coherence (Helfrich et al., 2014b). Therefore, we would expect to observe decreases in functional connectivity between corresponding areas in both hemispheres. In agreement with that prediction, we observed that 40 Hz tACS decreased functional connectivity between the left parietal seed (P5) and several clusters in the right hemisphere, including the right cuneus. However, induced modulation was frequency dependent, with 10 Hz causing the opposite effect, i.e., increased functional connectivity between the P5 seed and the right cuneus. Therefore, a direct link to inter-hemispheric coupling impairments due to anti-phasic stimulation cannot be made. In their study, Helfrich et al. (2014b) evaluated tACS effects in interhemispheric EEG coherence only for tACS at 40 Hz; whether the same pattern should be observed for other tACS frequencies still needs to be established. Future studies could expand on inter- vs. intra-hemispheric changes in functional connectivity by directly comparing in-phase vs. anti-phase montages over the same regions with the same frequencies. Although the present study was not aimed at evaluating how individual differences affect tACS effects, the inclusion of the electric field strength information in the fALFF analysis suggested that incorporating individual predictions based on electric field simulations could be a valuable approach for evaluating tACS effects in both neural and behavioral studies.

Opposite effects of 10 and 40 Hz tACS

One main finding of this study was that in most of the analyzed networks, 10 Hz tACS increased functional connectivity while 40 Hz tACS decreased it, or vice versa. This is in line with the opposite effects of 10 Hz and 40 Hz stimulation on local activity as determined by fALFF analysis. The antagonism between alpha and gamma frequencies has been well documented in the literature, suggesting that alpha power is more related to idling brain state and functional inhibition of task-irrelevant regions (Jensen and Mazaheri, 2010; Spaak et al., 2012) while gamma oscillations are more related to the performance of perceptual and cognitive operations (Tagliazucchi et al., 2012; Spaak et al., 2012). Different conceptions of neural activity could be related to this antagonism of 10 and 40 Hz tACS. First, there is evidence that

during visual processing, alpha oscillations are related to feedback projections and gamma oscillations are more related to feedforward mechanisms (Tagliazucchi et al., 2012; Spaak et al., 2012; Jensen et al., 2015). Second, alpha oscillations have been related to information transmission across long-distance areas while gamma oscillations are associated with local cortical assemblies (von Stein and Sarnthein, 2000). Third, it has been shown that alpha and gamma oscillations relate to each other via cross-frequency coupling (e.g., phase-amplitude coupling or amplitude-envelope correlations) (Canolty and Knight, 2010; Helfrich et al., 2015). For example, recent studies reported no modulation of gamma power but reduced alpha power due to gamma tACS entrainment (Helfrich et al., 2014b; Helfrich et al., 2015). According to this, our results could be explained by opposite modulations of alpha power, i.e., tACS at 10 Hz increased alpha power (Helfrich et al., 2014a; Helfrich et al., 2015) while tACS at 40 Hz decreased alpha power via cross-frequency coupling (Helfrich et al., 2014b; Helfrich et al., 2015). However, given the nature of our study (low frequency measurement without concurrent electrophysiological measurements), sound conclusions about cross-frequency coupling cannot be made.

The effects of tACS were not always as predicted for the different combinations of tACS frequencies and electrode montages used in our study. For instance, for each electrode montage, tACS effects were not limited to the directly stimulated regions. In addition, the effects of a given frequency were not always as expected according to the existent literature linking brain oscillations to RSNs (Tagliazucchi et al., 2012; Mantini et al., 2007; Mo et al., 2013; Zhan et al., 2014; Scheeringa et al., 2012). A particular example is the observed effect induced by tACS at 10 Hz. Contrary to our expectations, we found that, in some brain regions, 10 Hz tACS increased functional connectivity with particular RSNs rather than decreased it. Examples of this pattern are the increase in functional connectivity of the l-FP with occipito-parietal regions and LN as well as the increase in functional connectivity of the visual network with MOG. This finding is reminiscent of findings in our previous study (Cabral-Calderin et al., 2016) where short periods (30 s) of tACS at alpha and beta frequencies mainly increased BOLD signal amplitude in fronto-parietal areas.

These results are surprising if one takes into account the vast literature suggesting that the BOLD signal at rest is mainly negatively correlated to alpha oscillations and positively linked to gamma rhythms. One important aspect to take into account is the relationship between oscillatory entrainment and the BOLD signal, which is not well understood (Muthukumaraswamy and Singh, 2009; Parkes et al., 2004). Previous EEG studies have found that alpha tACS increased alpha power in occipito-parietal areas (Helfrich et al., 2014a; Neuling et al., 2013), however, whether or not these power increases observed in the EEG are translated the same way into the BOLD signal is not clear. It might be that the online entrainment induced by tACS does not impose a change in the metabolic demand of the entrained brain area, therefore the expected change in the spontaneous activity induced by alpha or gamma tACS may not be observed during the stimulation period with fMRI. Note that the apparent discrepancy between the results from this study and our previous study, and the previously reported negative correlation between alpha power and BOLD signal relies on the assumption that 10 Hz tACS increased alpha power (Helfrich et al., 2014a; Neuling et al., 2013). However, since we did not measure concurrent electrophysiological data, we cannot be certain about the latter. A recent study showed that one second of alpha tACS did not produce after-effects in amplitude or phase of the EEG signals (Struber et al., 2015). Along those lines, it could be that short stimulation periods of 10 Hz tACS are not enough to increase alpha power, which would explain the lack of negative association between 10 Hz tACS and the BOLD signal in our previous study, where tACS was applied only for 30 s (Cabral-Calderin et al., 2016). Moreover, the effect of tACS is task-dependent and increase in alpha power seems to depend on brain state (Neuling et al., 2013). Therefore, increased alpha power resulting from 10 Hz tACS, however likely, cannot always be assumed. Further research is needed to work out the mechanisms that led to the observed effects of tACS in fALFF and functional connectivity.

Across the different analyses, we did not observe a clear pattern distinguishing between online and after-effects of tACS. The effects of tACS were observed either as changes in functional connectivity during the stimulation that outlasted stimulation or returned to non-significant levels in the post-stimulation period, or as changes in functional connectivity only in the post-stimulation period. Differences between online and after-effects of tACS might be explained by different dynamic mechanisms, i.e., online changes could reflect oscillatory entrainment while after-effects could be related to changes in plasticity (Vossen et al., 2015).

As previously mentioned in the results, one possible confound in any tACS study is that the observed changes induced by stimulation could reflect sensory experiences rather than tACS entrainment (Schutter, 2015; Kar and Krekelberg, 2012). It has been shown that tACS induces phosphene perception and cutaneous sensation in a frequency-dependent manner (Kanai et al., 2008; Turi et al., 2013). We did not find any significant difference in somatosensory ratings between the different frequencies. In addition, although gamma tACS induced less phosphene perception, ratings for tACS at alpha and beta frequencies were similar. If one assumes that tACS effects in our study are related to phosphene perception, one would expect to observe similar effects with 10 and 16 Hz tACS because they induced phosphene perception with a similar strength in our participants. However, this was not the case for most results reported here. Moreover, if tACS-induced sensory experiences affect spontaneous fMRI signal fluctuations, we expect this effect to be maximal in the corresponding primary sensory cortices. However, the during-stimulation fALFF values extracted from specific ROIs within the primary visual and somatosensory cortices did not show a significant correlation with phosphene perception or somatosensory ratings, respectively, for any tACS frequency for any electrode montage. Based on our results, we assume that sensory experiences are unlikely to account for the here reported changes in fALFF or functional connectivity. These findings are also in agreement with our previous study where no significant association between cutaneous sensation, phosphene perception ratings and tACS-induced modulation in the BOLD signal was observed during eyes-open conditions (Cabral-Calderin et al., 2016). Nonetheless, it is worth mentioning that, similar to our previous study (Cabral-Calderin et al., 2016), participants rated their subjective phosphene perception and cutaneous sensation intensities. We cannot entirely exclude that unconsciously perceived phosphenes induced secondary effects such as attention shifts (Brignani et al., 2013).

Effects of tACS as a modulation of inter-network functional connectivity

Most of the effects found in this study were changes in functional connectivity between networks or regions belonging to different RSNs. Exceptions from this rule were changes in a few clusters within the DAN, motor and visual networks. It is possible that our network-based analysis might be biased to detect functional connectivity changes between the given RSN and areas outside of the seed, and that smaller within-network node ROIs or voxel-wise analyses might be more suitable for detecting within-network changes. However, the analysis with electric field simulation-based ROIs, in which a smaller seed was used as reference for functional connectivity maps, did not show additional within-network changes. We thus believe that during resting conditions, tACS is more likely to modulate functional connectivity between than within networks. One could speculate that changes in functional connectivity due to tACS are more easily induced between areas in which reciprocal functional connectivity is weak, while a higher energy level might be required for modulating strong functional connectivity. Previous studies suggested that the lack of effect with non-invasive brain stimulation methods could be explained by a ceiling effect (Neuling et al., 2013; Salomons et al., 2014; Nettekoven et al., 2015).

In our case, "ceiling effect" could be defined in terms of either ongoing oscillations or the BOLD signal itself. In other words, it could be that the amplitude of the oscillations at the applied frequency was already at (or close to) a maximum value (Ehm et al., 2011), therefore no further enhancement is observed with tACS. Another possibility is that the metabolic demands of some functional networks were already optimally driven, and therefore these networks are not driven more by electrical stimulation (Ekstrom et al., 2008). A particular example of this could be the lack of tACS effect in the fALFF and functional connectivity analysis with the DMN. The DMN is a task-negative network that has been reported to be most active in resting conditions; therefore, we hypothesize that already strongly activated networks/regions that exhibit high functional and anatomical connectivity cannot be modulated more with tACS. This point of view would be in agreement with our previous study where we showed that the effect of tACS during motor or visual task conditions was mainly observed in regions not activated by the task (Cabral-Calderin et al., 2016). Along the same lines, a previous EEG study showed that tACS-entrainment only occurred when the intrinsic power at this frequency was present, but relatively low (Neuling et al., 2013).

Left fronto-parietal control network: a particularly vulnerable candidate?

One of the networks showing strongest modulation in its functional connectivity was the left fronto-parietal control network (l-FP), which showed tACS-induced changes in functional connectivity in the network-to-network and network-to-whole-brain functional connectivity analyses, and it was also found to be modulated when the P5 seed from the electric field simulation was analyzed. The most extensive frequency-dependent modulation in functional connectivity relative to the l-FP was observed in occipito-parietal regions, where 10 Hz tACS increased and 40 Hz tACS decreased correlation values. This result is reminiscent of our previous study showing stronger tACS-induced increases in BOLD signal in left fronto-parietal regions (Cabral-Calderin et al., 2016). One possibility is that tACS is most effective in particular cortical regions because of vulnerability brought on by metabolic energy compromises that must take place in regions that play multiple roles or act as functional hubs but have not evolved high efficiency (Tomasi et al., 2013). A study modeling the relationship between glucose metabolism, measured with fludeoxyglucose in positron emission tomography, and resting-state functional connectivity found higher metabolism associated with higher rs-fMRI signal amplitudes in the cerebellum, occipital cortex, and parietal cortices relative to the rest of the brain. However, the same study showed that glucose efficiency in cerebellum, thalamus, and other subcortical structures is higher than in the cortex. Thus, it could be postulated that functional hubs like in the fronto-parietal networks would be particularly susceptible to any manipulation that challenges energy consumption (Tomasi et al., 2013). Fronto-parietal regions play multiple functional roles involved in facilitating attention, language, memory, and visual consciousness (Naghavi and Nyberg, 2005; Zhu et al., 2014). In functional connectivity studies, fronto-parietal networks are considered as control networks found to mediate DAN-DMN anticorrelations in a task-dependent manner (Gao and Lin, 2012; Spreng et al., 2013). In fact, the left fronto-parietal control network seems particularly susceptible to perturbations and has been shown to break down in neurological diseases such as Lewy body dementia (Peraza et al., 2015) and aphasic stroke (Zhu et al., 2014), in which the degree of network disruption is associated with the deficit's severity and recovery. In addition, previous studies have shown modulation of the amplitude of the BOLD signal or functional connectivity of fronto-parietal regions due to tACS or transcranial magnetic stimulation, respectively (Cabral-Calderin et al., 2016; Gratton et al., 2013). The flexibility of the left fronto-parietal control network might explain its sensitivity to tACS modulation.

We previously showed that tACS over Cz-Oz increased the BOLD signal in fronto-parietal regions (most strongly in the left hemisphere) but not in the areas close to the electrodes, such as occipital cortex (Cabral-Calderin et al., 2016). We hypothesized that this modulation of distant areas could be explained by changes in functional connectivity between these areas and the directly stimulated regions. In the present study, we found that the functional connectivity between the l-FP (which includes the regions reported in our previous study, such as MFG and IPL) and occipital regions was modulated by tACS in a frequency-dependent manner. These results partially match our previous hypothesis. However, when the seed region for the functional connectivity analysis was placed over Oz (for tACS over Cz-Oz), which would match our previous design, no significant functional connectivity changes were observed with similar fronto-parietal areas. We would like to point out, however, that our seed region for Oz only included the voxels where the strongest electric field was observed for most of the subjects and not the entire stimulated area. It could still be possible that stimulated areas outside our Oz seed are changing functional connectivity with the left fronto-parietal control network. Results from this and our previous study suggest that the l-FP is a network that is easy to perturb with tACS. Future studies could expand on the possibility of using tACS for modulating l-FP functional connectivity in patient populations where decreased l-FP functional connectivity has been reported (Zhu et al., 2014; Peraza et al., 2015).

Implications for behavioral studies

We previously showed that tACS effects on the BOLD signal were not typically observed in the areas under the electrodes but mainly in more distant fronto-parietal regions (Cabral-Calderin et al., 2016). In agreement with those findings, the present study showed that tACS effects are not limited to the directly stimulated brain regions, i.e., tACS also modulates spontaneous BOLD signal fluctuations in distant regions (e.g., medial frontal gyrus) as well as functional connectivity between spatially distant networks/regions (e.g., between the l-FP and the visual network). These results suggest that tACS effects are influenced by network interactions, which should be considered when interpreting behavioral effects of tACS. Behavioral consequences of tACS cannot be interpreted based only on the role of the directly stimulated regions, and the roles of functional networks should also be considered. For instance, when applying tACS over the occipital cortex, the logical aim is to modulate the activity in visual areas, and, in consequence, the performance in a given visual task. However, our results suggest that using this stimulation protocol, the activity of fronto-parietal areas – as well as their functional connectivity with more distant brain regions – is also being modulated. Therefore, any change in visual task performance could be influenced by attentional or executive control processes, more than by local changes in visual areas. However, it is important to note that the results shown in the present study pertain to resting-state conditions. Since tACS effects on the BOLD signal are strongly task dependent (Cabral-Calderin et al., 2016), inference from resting state to task-related tACS effects should be made carefully. Future studies could evaluate functional connectivity changes induced by tACS under the task condition of interest, e.g., with fMRI or electrophysiological measurements cleared from tACS-induced artifacts, and implement causational analysis techniques like psychophysiological interactions or dynamic causal modeling.

Limitations

Resting-state functional connectivity in a single subject varies over time (Chang and Glover, 2010; Hutchison et al., 2013). In addition, some studies reported the effect of stimulation with oscillatory currents to be variable over time (Veniero et al., 2015). Our functional connectivity analyses were done with average measures across 8 min periods; therefore, dynamic fluctuations in functional connectivity due to tACS below that time window are not evaluated. Another factor to take into account when examining tACS effects is the inter-subject variability

(in terms of anatomy, RSN spatial distributions and brain stimulation response), which might contribute to different tACS effects (Opitz et al., 2015a; Mennes et al., 2011; Mueller et al., 2013; Cohen et al., 2008). Future studies could expand on the use of subject-specific electric field simulations and RSNs to investigate the influence of individual differences on tACS effects.

Conclusions

In the present study we evaluated the effect of tACS on spontaneous low frequency BOLD signal fluctuations by applying tACS over the posterior cortex of healthy subjects at three different frequencies and with two different electrode montages. We offer a detailed description of the impact of tACS on spontaneous activity during and after stimulation. Stimulation frequency-dependent effects were given by opposite effects induced by 10 Hz (alpha) and 40 Hz (gamma). Most tACS effects were observed as modulation of inter-network functional connectivity (e.g., l-FP to the visual network), while intra-network functional connectivity changes were modest and only observed in the DAN, motor and visual networks. The left fronto-parietal control network showed the most extensive frequency-dependent modulation in functional connectivity, mainly with occipito-parietal areas. Our results suggest that tACS effects are not limited to regions below the electrodes but are influenced by network interactions, which should be taken into account when using tACS for studying brain function and behavior in health and disease.

Acknowledgements

We thank Ilona Pfahlert and Britta Perl for technical assistance during functional imaging experiments, Severin Heumüller and Hendrik Eichenauer for computer support, and Carsten Schmidt-Samoa for advice on statistical analysis. This work was supported by the Hermann and Lilly Schilling Foundation (to M. W.) and the European Neuroscience Campus Network, an Erasmus Mundus Joint Doctoral Program (to M.W. and K.W.).

Appendix A. Supplementary data

Supplementary data to this article can be found online at http://dx.doi.org/10.1016/j.neuroimage.2016.07.005.

References

Alekseichuk, I., Diers, K., Paulus, W., Antal, A., 2015. Transcranial electrical stimulation of the occipital cortex during visual perception modifies the magnitude of BOLD activity: a combined tES-fMRI approach. NeuroImage. http://dx.doi.org/10.1016/j.neuroimage.2015.11.034 (PubMed PMID: 26608246).

Ali, M.M., Sellers, K.K., Frohlich, F., 2013. Transcranial alternating current stimulation modulates large-scale cortical network activity by network resonance. J. Neurosci. 33 (27), 11262–11275. http://dx.doi.org/10.1523/JNEUROSCI.5867-12.2013 (PubMed PMID: 23825429).

Amadi, U., Ilie, A., Johansen-Berg, H., Stagg, C.J., 2013. Polarity-specific effects of motor transcranial direct current stimulation on fMRI resting state networks. NeuroImage 88C, 155–161. http://dx.doi.org/10.1016/j.neuroimage.2013.11.037 (PubMed PMID: 24287440; PubMed Central PMCID: PMCPMC3991849).

Antal, A., Bikson, M., Datta, A., Lafon, B., Dechent, P., Parra, L.C., et al., 2014. Imaging artifacts induced by electrical stimulation during conventional fMRI of the brain. NeuroImage 85 (Pt 3), 1040–1047. http://dx.doi.org/10.1016/j.neuroimage.2012.10.026 (PubMed PMID: 23099102; PubMed Central PMCID: PMC3759658).

Beckmann, C.F., DeLuca, M., Devlin, J.T., Smith, S.M., 2005. Investigations into resting-state connectivity using independent component analysis. Philos. Trans. R. Soc. Lond. Ser. B Biol. Sci. 360 (1457), 1001–1013. http://dx.doi.org/10.1098/rstb.2005.1634 (PubMed PMID: 16087444; PubMed Central PMCID: PMCPMC1854918).

Biswal, B., Yetkin, F.Z., Haughton, V.M., Hyde, J.S., 1995. Functional connectivity in the motor cortex of resting human brain using echo-planar MRI. Magn. Reson. Med. 34 (4), 537–541 (PubMed PMID: 8524021).

Brignani, D., Ruzzoli, M., Mauri, P., Miniussi, C., 2013. Is transcranial alternating current stimulation effective in modulating brain oscillations? PLoS One 8 (2), e56589. http://dx.doi.org/10.1371/journal.pone.0056589 (PubMed PMID: 23457586; PubMed Central PMCID: PMC3573000).

Brittain, J.S., Probert-Smith, P., Aziz, T.Z., Brown, P., 2013. Tremor suppression by rhythmic transcranial current stimulation. Curr. Biol. 23 (5), 436–440. http://dx.doi.org/10.1016/j.cub.2013.01.068 (PubMed PMID: 23416101; PubMed Central PMCID: PMC3629558).

Cabral-Calderin, Y., Anne Weinrich, C., Schmidt-Samoa, C., Poland, E., Dechent, P., Bahr, M., et al., 2016. Transcranial alternating current stimulation affects the BOLD signal in a frequency and task-dependent manner. Hum. Brain Mapp. 37 (1), 94–121. http://dx.doi.org/10.1002/hbm.23016 (PubMed PMID: 26503692).

Cabral-Calderin, Y., Schmidt-Samoa, C., Wilke, M., 2015. Rhythmic gamma stimulation affects bistable perception. J. Cogn. Neurosci. 27 (7), 1298–1307. http://dx.doi.org/10.1162/jocn_a_00781 (PubMed PMID: 25603029).

Canolty, R.T., Knight, R.T., 2010. The functional role of cross-frequency coupling. Trends Cogn. Sci. 14 (11), 506–515. http://dx.doi.org/10.1016/j.tics.2010.09.001 (PubMed PMID: 20932795; PubMed Central PMCID: PMCPMC3359652).

Chang, C., Glover, G.H., 2010. Time-frequency dynamics of resting-state brain connectivity measured with fMRI. NeuroImage 50 (1), 81–98. http://dx.doi.org/10.1016/j.neuroimage.2009.12.011 (PubMed PMID: 20006716; PubMed Central PMCID: PMCPMC2827259).

Cohen, A.L., Fair, D.A., Dosenbach, N.U., Miezin, F.M., Dierker, D., Van Essen, D.C., et al., 2008. Defining functional areas in individual human brains using resting functional connectivity MRI. NeuroImage 41 (1), 45–57. http://dx.doi.org/10.1016/j.neuroimage.2008.01.066 (PubMed PMID: 18367410; PubMed Central PMCID: PMC2705206).

Corbetta, M., Shulman, G.L., 2002. Control of goal-directed and stimulus-driven attention in the brain. Nat. Rev. Neurosci. 3 (3), 201–215. http://dx.doi.org/10.1038/nrn755 (PubMed PMID: 11994752).

Cox, R.W., 1996. AFNI: software for analysis and visualization of functional magnetic resonance neuroimages. Comput. Biomed. Res. 29 (3), 162–173 (PubMed PMID: 8812068).

Ehm, W., Bach, M., Kornmeier, J., 2011. Ambiguous figures and binding: EEG frequency modulations during multistable perception. Psychophysiology 48 (4), 547–558. http://dx.doi.org/10.1111/j.1469-8986.2010.01087.x (Epub 2010/08/28. PubMed PMID: 20796247).

Ekstrom, L.B., Roelfsema, P.R., Arsenault, J.T., Bonmassar, G., Vanduffel, W., 2008. Bottom-up dependent gating of frontal signals in early visual cortex. Science 321 (5887), 414–417. http://dx.doi.org/10.1126/science.1153276 (PubMed PMID: 18635806; PubMed Central PMCID: PMC3011100).

Fedorov, A., Chibisova, Y., Szymaszek, A., Alexandrov, M., Gall, C., Sabel, B.A., 2010. Non-invasive alternating current stimulation induces recovery from stroke. Restor. Neurol. Neurosci. 28 (6), 825–833. http://dx.doi.org/10.3233/RNN-2010-0580 (PubMed PMID: 21209497).

Feurra, M., Bianco, G., Santarnecchi, E., Del Testa, M., Rossi, A., Rossi, S., 2011b. Frequency-dependent tuning of the human motor system induced by transcranial oscillatory potentials. J. Neurosci. 31 (34), 12165–12170. http://dx.doi.org/10.1523/JNEUROSCI.0978-11.2011 (PubMed PMID: 21865459).

Feurra, M., Pasqualetti, P., Bianco, G., Santarnecchi, E., Rossi, A., Rossi, S., 2013. State-dependent effects of transcranial oscillatory currents on the motor system: what you think matters. J. Neurosci. 33 (44), 17483–17489. http://dx.doi.org/10.1523/JNEUROSCI.1414-13.2013 (PubMed PMID: 24174681).

Feurra, M., Paulus, W., Walsh, V., Kanai, R., 2011a. Frequency specific modulation of human somatosensory cortex. Front. Psychol. 2, 13. http://dx.doi.org/10.3389/fpsyg.2011.00013 (Epub 2011/06/30. PubMed PMID: 21713181; PubMed Central PMCID: PMC3111335).

Fox, M.D., Raichle, M.E., 2007. Spontaneous fluctuations in brain activity observed with functional magnetic resonance imaging. Nat. Rev. Neurosci. 8 (9), 700–711. http://dx.doi.org/10.1038/nrn2201 (PubMed PMID: 17704812).

Fox, M.D., Buckner, R.L., Liu, H., Chakravarty, M.M., Lozano, A.M., Pascual-Leone, A., 2014. Resting-state networks link invasive and noninvasive brain stimulation across diverse psychiatric and neurological diseases. Proc. Natl. Acad. Sci. U. S. A. 111 (41), E4367–E4375. http://dx.doi.org/10.1073/pnas.1405003111 (PubMed PMID: 25267639; PubMed Central PMCID: PMC4205651).

Fox, M.D., Halko, M.A., Eldaief, M.C., Pascual-Leone, A., 2012. Measuring and manipulating brain connectivity with resting state functional connectivity magnetic resonance imaging (fcMRI) and transcranial magnetic stimulation (TMS). NeuroImage 62 (4), 2232–2243. http://dx.doi.org/10.1016/j.neuroimage.2012.03.035 (PubMed PMID: 22465297; PubMed Central PMCID: PMC3518426).

Fox, M.D., Snyder, A.Z., Vincent, J.L., Corbetta, M., Van Essen, D.C., Raichle, M.E., 2005. The human brain is intrinsically organized into dynamic, anticorrelated functional networks. Proc. Natl. Acad. Sci. U. S. A. 102 (27), 9673–9678. http://dx.doi.org/10.1073/pnas.0504136102 (PubMed PMID: 15976020; PubMed Central PMCID: PMC1157105).

Gao, W., Lin, W., 2012. Frontal parietal control network regulates the anti-correlated default and dorsal attention networks. Hum. Brain Mapp. 33 (1), 192–202 (10.1002/hbm.21204. PubMed PMID: 21391263; PubMed Central PMCID: PMCPMC3131466).

Gratton, C., Lee, T.G., Nomura, E.M., D'Esposito, M., 2013. The effect of theta-burst TMS on cognitive control networks measured with resting state fMRI. Front. Syst. Neurosci. 7, 124. http://dx.doi.org/10.3389/fnsys.2013.00124 (PubMed PMID: 24416003; PubMed Central PMCID: PMC3874542).

Helfrich, R.F., Knepper, H., Nolte, G., Struber, D., Rach, S., Herrmann, C.S., et al., 2014b. Selective modulation of interhemispheric functional connectivity by HD-tACS shapes perception. PLoS Biol. 12 (12), e1002031. http://dx.doi.org/10.1371/journal.pbio.1002031 (PubMed PMID: 25549264; PubMed Central PMCID: PMC4280108).

Helfrich, R.F., Schneider, T.R., Rach, S., Trautmann-Lengsfeld, S.A., Engel, A.K., Herrmann, C.S., 2014a. Entrainment of brain oscillations by transcranial alternating current stimulation. Curr. Biol. 24 (3), 333–339. http://dx.doi.org/10.1016/j.cub.2013.12.041 (PubMed PMID: 24461998).

Helfrich, R.F., Herrmann, C.S., Engel, A.K., Schneider, T.R., 2015. Different coupling modes mediate cortical cross-frequency interactions. NeuroImage. http://dx.doi.org/10.1016/j.neuroimage.2015.11.035 (PubMed PMID: 26608244).

Hutchison, R.M., Womelsdorf, T., Gati, J.S., Everling, S., Menon, R.S., 2013. Resting-state networks show dynamic functional connectivity in awake humans and anesthetized macaques. Hum. Brain Mapp. 34 (9), 2154–2177. http://dx.doi.org/10.1002/hbm.22058 (PubMed PMID: 22438275).

Jenkinson, M., Beckmann, C.F., Behrens, T.E., Woolrich, M.W., Smith, S.M., 2012. Fsl. NeuroImage 62 (2), 782–790. http://dx.doi.org/10.1016/j.neuroimage.2011.09.015 (PubMed PMID: 21979382).

Jensen, O., Mazaheri, A., 2010. Shaping functional architecture by oscillatory alpha activity: gating by inhibition. Front. Hum. Neurosci. 4, 186. http://dx.doi.org/10.3389/fnhum.2010.00186 (PubMed PMID: 21119777; PubMed Central PMCID: PMC2990626).

Jensen, O., Bonnefond, M., Marshall, T.R., Tiesinga, P., 2015. Oscillatory mechanisms of feedforward and feedback visual processing. Trends Neurosci. 38 (4), 192–194. http://dx.doi.org/10.1016/j.tins.2015.02.006 (PubMed PMID: 25765320).

Joundi, R.A., Jenkinson, N., Brittain, J.S., Aziz, T.Z., Brown, P., 2012. Driving oscillatory activity in the human cortex enhances motor performance. Curr. Biol. 22 (5), 403–407. http://dx.doi.org/10.1016/j.cub.2012.01.024 (Epub 2012/02/07. PubMed PMID: 22305755; PubMed Central PMCID: PMC3343257).

Kanai, R., Chaieb, L., Antal, A., Walsh, V., Paulus, W., 2008. Frequency-dependent electrical stimulation of the visual cortex. Curr. Biol. 18 (23), 1839–1843. http://dx.doi.org/10.1016/j.cub.2008.10.027 (Epub 2008/11/26. PubMed PMID: 19026538).

Kar, K., Krekelberg, B., 2012. Transcranial electrical stimulation over visual cortex evokes phosphenes with a retinal origin. J. Neurophysiol. 108 (8), 2173–2178. http://dx.doi.org/10.1152/jn.00505.2012 (PubMed PMID: 22855777; PubMed Central PMCID: PMC3545027).

Kar, K., Krekelberg, B., 2014. Transcranial alternating current stimulation attenuates visual motion adaptation. J. Neurosci. 34 (21), 7334–7340. http://dx.doi.org/10.1523/JNEUROSCI.5248-13.2014 (PubMed PMID: 24849365; PubMed Central PMCID: PMCPMC4028503).

Laakso, I., Tanaka, S., Koyama, S., De Santis, V., Hirata, A., 2015. Inter-subject variability in electric fields of motor cortical tDCS. Brain Stimul. 8 (5), 906–913. http://dx.doi.org/10.1016/j.brs.2015.05.002 (PubMed PMID: 26026283).

Laczo, B., Antal, A., Niebergall, R., Treue, S., Paulus, W., 2012. Transcranial alternating stimulation in a high gamma frequency range applied over V1 improves contrast perception but does not modulate spatial attention. Brain Stimul. 5 (4), 484–491. http://dx.doi.org/10.1016/j.brs.2011.08.008 (Epub 2011/10/04. PubMed PMID: 21962982).

Lowe, M.J., Mock, B.J., Sorenson, J.A., 1998. Functional connectivity in single and multislice echoplanar imaging using resting-state fluctuations. NeuroImage 7 (2), 119–132. http://dx.doi.org/10.1006/nimg.1997.0315 (PubMed PMID: 9558644).

Mantini, D., Perrucci, M.G., Del Gratta, C., Romani, G.L., Corbetta, M., 2007. Electrophysiological signatures of resting state networks in the human brain. Proc. Natl. Acad. Sci. U. S. A. 104 (32), 13170–13175. http://dx.doi.org/10.1073/pnas.0700668104 (PubMed PMID: 17670949; PubMed Central PMCID: PMC1941820).

Mennes, M., Zuo, X.N., Kelly, C., Di Martino, A., Zang, Y.F., Biswal, B., et al., 2011. Linking inter-individual differences in neural activation and behavior to intrinsic brain dynamics. NeuroImage 54 (4), 2950–2959. http://dx.doi.org/10.1016/j.neuroimage.2010.10.046 (PubMed PMID: 20974260; PubMed Central PMCID: PMC3091620).

Mo, J., Liu, Y., Huang, H., Ding, M., 2013. Coupling between visual alpha oscillations and default mode activity. NeuroImage 68, 112–118. http://dx.doi.org/10.1016/j.neuroimage.2012.11.058 (PubMed PMID: 23228510; PubMed Central PMCID: PMC3557590).

Moeller, S., Yacoub, E., Olman, C.A., Auerbach, E., Strupp, J., Harel, N., et al., 2010. Multiband multislice GE-EPI at 7 tesla, with 16-fold acceleration using partial parallel imaging with application to high spatial and temporal whole-brain fMRI. Magn. Reson. Med. 63 (5), 1144–1153. http://dx.doi.org/10.1002/mrm.22361 (PubMed PMID: 20432285; PubMed Central PMCID: PMC2906244).

Mueller, S., Wang, D., Fox, M.D., Yeo, B.T., Sepulcre, J., Sabuncu, M.R., et al., 2013. Individual variability in functional connectivity architecture of the human brain. Neuron 77 (3), 586–595. http://dx.doi.org/10.1016/j.neuron.2012.12.028 (PubMed PMID: 23395382; PubMed Central PMCID: PMC3746075).

Murphy, K., Birn, R.M., Bandettini, P.A., 2013. Resting-state fMRI confounds and cleanup. NeuroImage 80, 349–359. http://dx.doi.org/10.1016/j.neuroimage.2013.04.001 (PubMed PMID: 23571418; PubMed Central PMCID: PMCPMC3720818).

Muthukumaraswamy, S.D., Singh, K.D., 2009. Functional decoupling of BOLD and gamma-band amplitudes in human primary visual cortex. Hum. Brain Mapp. 30 (7), 2000–2007. http://dx.doi.org/10.1002/hbm.20644 (PubMed PMID: 18729078).

Naghavi, H.R., Nyberg, L., 2005. Common fronto-parietal activity in attention, memory, and consciousness: shared demands on integration? Conscious. Cogn. 14 (2), 390–425. http://dx.doi.org/10.1016/j.concog.2004.10.003 (PubMed PMID: 15950889).

Nettekoven, C., Volz, L.J., Leimbach, M., Pool, E.M., Rehme, A.K., Eickhoff, S.B., et al., 2015. Inter-individual variability in cortical excitability and motor network connectivity following multiple blocks of rTMS. NeuroImage 118, 209–218. http://dx.doi.org/10.1016/j.neuroimage.2015.06.004 (PubMed PMID: 26052083).

Neuling, T., Rach, S., Herrmann, C.S., 2013. Orchestrating neuronal networks: sustained after-effects of transcranial alternating current stimulation depend upon brain states. Front. Hum. Neurosci. 7, 161. http://dx.doi.org/10.3389/fnhum.2013.00161 (PubMed PMID: 23641206; PubMed Central PMCID: PMC3639376).

Neuling, T., Ruhnau, P., Fusca, M., Demarchi, G., Herrmann, C.S., Weisz, N., 2015. Friends, not foes: magnetoencephalography as a tool to uncover brain dynamics during transcranial alternating current stimulation. NeuroImage 118, 406–413. http://dx.doi.org/10.1016/j.neuroimage.2015.06.026 (PubMed PMID: 26080310; PubMed Central PMCID: PMC4686537).

Neuling, T., Wagner, S., Wolters, C.H., Zaehle, T., Herrmann, C.S., 2012. Finite-element model predicts current density distribution for clinical applications of tDCS and tACS. Front. Psychiatr. 3, 83. http://dx.doi.org/10.3389/fpsyt.2012.00083 (PubMed PMID: 23015792; PubMed Central PMCID: PMC3449241).

Opitz, A., Fox, M.D., Craddock, R.C., Colcombe, S., Milham, M.P., 2015a. An integrated framework for targeting functional networks via transcranial magnetic stimulation. NeuroImage 127, 86–96. http://dx.doi.org/10.1016/j.neuroimage.2015.11.040 (PubMed PMID: 26608241).

Opitz, A., Paulus, W., Will, S., Antunes, A., Thielscher, A., 2015b. Determinants of the electric field during transcranial direct current stimulation. NeuroImage 109, 140–150. http://dx.doi.org/10.1016/j.neuroimage.2015.01.033 (PubMed PMID: 25613437).

Ozen, S., Sirota, A., Belluscio, M.A., Anastassiou, C.A., Stark, E., Koch, C., et al., 2010. Transcranial electric stimulation entrains cortical neuronal populations in rats. J. Neurosci. 30 (34), 11476–11485. http://dx.doi.org/10.1523/JNEUROSCI.5252-09.2010 (PubMed PMID: 20739569; PubMed Central PMCID: PMC2937280).

Park, H.J., Friston, K., 2013. Structural and functional brain networks: from connections to cognition. Science 342 (6158), 1238411. http://dx.doi.org/10.1126/science.1238411 (PubMed PMID: 24179229).

Parkes, L.M., Fries, P., Kerskens, C.M., Norris, D.G., 2004. Reduced BOLD response to periodic visual stimulation. NeuroImage 21 (1), 236–243 (PubMed PMID: 14741661).

Peraza, L.R., Taylor, J.P., Kaiser, M., 2015. Divergent brain functional network alterations in dementia with Lewy bodies and Alzheimer's disease. Neurobiol. Aging 36 (9), 2458–2467. http://dx.doi.org/10.1016/j.neurobiolaging.2015.05.015 (PubMed PMID: 26115566).

Polania, R., Nitsche, M.A., Korman, C., Batsikadze, G., Paulus, W., 2012. The importance of timing in segregated theta phase-coupling for cognitive performance. Curr. Biol. 22 (14), 1314–1318. http://dx.doi.org/10.1016/j.cub.2012.05.021 (Epub 2012/06/12. PubMed PMID: 22683259).

Raco, V., Bauer, R., Olenik, M., Brkic, D., Gharabaghi, A., 2014. Neurosensory effects of transcranial alternating current stimulation. Brain Stimul. 7 (6), 823–831. http://dx.doi.org/10.1016/j.brs.2014.08.005 (PubMed PMID: 25442154).

Raichle, M.E., 2010. Two views of brain function. Trends Cogn. Sci. 14 (4), 180–190. http://dx.doi.org/10.1016/j.tics.2010.01.008 (PubMed PMID: 20206576).

Raichle, M.E., 2015. The restless brain: how intrinsic activity organizes brain function. Philos. Trans. R. Soc. Lond. Ser. B Biol. Sci. 370 (1668). http://dx.doi.org/10.1098/rstb.2014.0172 (PubMed PMID: 25823869; PubMed Central PMCID: PMCPMC4387513).

Raichle, M.E., MacLeod, A.M., Snyder, A.Z., Powers, W.J., Gusnard, D.A., Shulman, G.L., 2001. A default mode of brain function. Proc. Natl. Acad. Sci. U. S. A. 98 (2), 676–682. http://dx.doi.org/10.1073/pnas.98.2.676 (PubMed PMID: 11209064; PubMed Central PMCID: PMCPMC14647).

Reato, D., Rahman, A., Bikson, M., Parra, L.C., 2013. Effects of weak transcranial alternating current stimulation on brain activity — a review of known mechanisms from animal studies. Front. Hum. Neurosci. 7, 687. http://dx.doi.org/10.3389/fnhum.2013.00687 (PubMed PMID: 24167483; PubMed Central PMCID: PMC3805939).

Salomons, T.V., Dunlop, K., Kennedy, S.H., Flint, A., Geraci, J., Giacobbe, P., et al., 2014. Resting-state cortico-thalamic-striatal connectivity predicts response to dorsomedial prefrontal rTMS in major depressive disorder. Neuropsychopharmacology 39 (2), 488–498. http://dx.doi.org/10.1038/npp.2013.222 (PubMed PMID: 24150516; PubMed Central PMCID: PMCPMC3870791).

Santarnecchi, E., Polizzotto, N.R., Godone, M., Giovannelli, F., Feurra, M., Matzen, L., et al., 2013. Frequency-dependent enhancement of fluid intelligence induced by transcranial oscillatory potentials. Curr. Biol. 23 (15), 1449–1453. http://dx.doi.org/10.1016/j.cub.2013.06.022 (PubMed PMID: 23891115).

Scheeringa, R., Petersson, K.M., Kleinschmidt, A., Jensen, O., Bastiaansen, M.C., 2012. EEG alpha power modulation of fMRI resting-state connectivity. Brain Connect. 2 (5), 254–264. http://dx.doi.org/10.1089/brain.2012.0088 (PubMed PMID: 22938826; PubMed Central PMCID: PMC3621304).

Schutter, D.J., 2015. Cutaneous retinal activation and neural entrainment in transcranial alternating current stimulation: a systematic review. NeuroImage. http://dx.doi.org/10.1016/j.neuroimage.2015.09.067 (PubMed PMID: 26453929).

Setsompop, K., Gagoski, B.A., Polimeni, J.R., Witzel, T., Wedeen, V.J., Wald, L.L., 2012. Blipped-controlled aliasing in parallel imaging for simultaneous multislice echo planar imaging with reduced g-factor penalty. Magn. Reson. Med. 67 (5), 1210–1224. http://dx.doi.org/10.1002/mrm.23097 (PubMed PMID: 21858868; PubMed Central PMCID: PMC3323676).

Shmuel, A., Leopold, D.A., 2008. Neuronal correlates of spontaneous fluctuations in fMRI signals in monkey visual cortex: implications for functional connectivity at rest. Hum. Brain Mapp. 29 (7), 751–761. http://dx.doi.org/10.1002/hbm.20580 (PubMed PMID: 18465799).

Spaak, E., Bonnefond, M., Maier, A., Leopold, D.A., Jensen, O., 2012. Layer-specific entrainment of gamma-band neural activity by the alpha rhythm in monkey visual cortex. Curr. Biol. 22 (24), 2313–2318. http://dx.doi.org/10.1016/j.cub.2012.10.020 (PubMed PMID: 23159599; PubMed Central PMCID: PMCPMC3528834).

Spreng, R.N., Sepulcre, J., Turner, G.R., Stevens, W.D., Schacter, D.L., 2013. Intrinsic architecture underlying the relations among the default, dorsal attention, and frontoparietal control networks of the human brain. J. Cogn. Neurosci. 25 (1), 74–86. http://dx.doi.org/10.1162/jocn_a_00281 (PubMed PMID: 22905821; PubMed Central PMCID: PMCPMC3816715).

Struber, D., Rach, S., Neuling, T., Herrmann, C.S., 2015. On the possible role of stimulation duration for after-effects of transcranial alternating current stimulation. Front. Cell. Neurosci. 9, 311. http://dx.doi.org/10.3389/fncel.2015.00311 (PubMed PMID: 26321912; PubMed Central PMCID: PMC4530587).

Struber, D., Rach, S., Trautmann-Lengsfeld, S.A., Engel, A.K., Herrmann, C.S., 2014. Antiphasic 40 Hz oscillatory current stimulation affects bistable motion perception. Brain Topogr. 27 (1), 158–171. http://dx.doi.org/10.1007/s10548-013-0294-x (PubMed PMID: 23709044).

Tagliazucchi, E., von Wegner, F., Morzelewski, A., Brodbeck, V., Laufs, H., 2012. Dynamic BOLD functional connectivity in humans and its electrophysiological correlates. Front. Hum. Neurosci. 6, 339. http://dx.doi.org/10.3389/fnhum.2012.00339 (PubMed PMID: 23293596; PubMed Central PMCID: PMC3531919).

Thielscher, A., Antunes, A., Saturnino, G.B., 2015. Field modeling for transcranial magnetic stimulation: a useful tool to understand the physiological effects of TMS? Conference Proceedings : Annual International Conference of the IEEE Engineering in Medicine and Biology Society IEEE Engineering in Medicine and Biology Society Annual Conference Vol. 2015, pp. 222–225. http://dx.doi.org/10.1109/EMBC.2015.7318340 (PubMed PMID: 26736240)

Thielscher, A., Opitz, A., Windhoff, M., 2011. Impact of the gyral geometry on the electric field induced by transcranial magnetic stimulation. NeuroImage 54 (1), 234–243. http://dx.doi.org/10.1016/j.neuroimage.2010.07.061 (PubMed PMID: 20682353).

Tomasi, D., Wang, G.J., Volkow, N.D., 2013. Energetic cost of brain functional connectivity. Proc. Natl. Acad. Sci. U. S. A. 110 (33), 13642–13647. http://dx.doi.org/10.1073/pnas.1303346110 (PubMed PMID: 23898179; PubMed Central PMCID: PMC3746878).

Turi, Z., Ambrus, G.G., Janacsek, K., Emmert, K., Hahn, L., Paulus, W., et al., 2013. Both the cutaneous sensation and phosphene perception are modulated in a frequency-specific manner during transcranial alternating current stimulation. Restor. Neurol. Neurosci. 31 (3), 275–285. http://dx.doi.org/10.3233/RNN-120297 (PubMed PMID: 23478342).

Van Dijk, K.R., Hedden, T., Venkataraman, A., Evans, K.C., Lazar, S.W., Buckner, R.L., 2010. Intrinsic functional connectivity as a tool for human connectomics: theory, properties, and optimization. J. Neurophysiol. 103 (1), 297–321. http://dx.doi.org/10.1152/jn.00783.2009 (PubMed PMID: 19889849; PubMed Central PMCID: PMC2807224).

Veniero, D., Vossen, A., Gross, J., Thut, G., 2015. Lasting EEG/MEG aftereffects of rhythmic transcranial brain stimulation: level of control over oscillatory network activity. Front. Cell. Neurosci. 9, 477. http://dx.doi.org/10.3389/fncel.2015.00477 (PubMed PMID: 26696834; PubMed Central PMCID: PMC4678227).

Vincent, J.L., Kahn, I., Snyder, A.Z., Raichle, M.E., Buckner, R.L., 2008. Evidence for a frontoparietal control system revealed by intrinsic functional connectivity. J. Neurophysiol. 100 (6), 3328–3342. http://dx.doi.org/10.1152/jn.90355.2008 (PubMed PMID: 18799601; PubMed Central PMCID: PMCPMC2604839).

von Stein, A., Sarnthein, J., 2000. Different frequencies for different scales of cortical integration: from local gamma to long range alpha/theta synchronization. Int. J. Psychophysiol. 38 (3), 301–313 (PubMed PMID: 11102669).

Vossen, A., Gross, J., Thut, G., 2015. Alpha power increase after transcranial alternating current stimulation at alpha frequency (alpha-tACS) reflects plastic changes rather than entrainment. Brain Stimul. 8 (3), 499–508. http://dx.doi.org/10.1016/j.brs.2014.12.004 (PubMed PMID: 25648377; PubMed Central PMCID: PMC4464304).

Vosskuhl, J., Huster, R.J., Herrmann, C.S., 2015. BOLD signal effects of transcranial alternating current stimulation (tACS) in the alpha range: a concurrent tACS-fMRI study. NeuroImage. http://dx.doi.org/10.1016/j.neuroimage.2015.10.003 (PubMed PMID: 26458516).

Wach, C., Krause, V., Moliadze, V., Paulus, W., Schnitzler, A., Pollok, B., 2013. Effects of 10 Hz and 20 Hz transcranial alternating current stimulation (tACS) on motor functions and motor cortical excitability. Behav. Brain Res. 241, 1–6. http://dx.doi.org/10.1016/j.bbr.2012.11.038 (PubMed PMID: 23219965).

Wang, J., Yang, Y., Fan, L., Xu, J., Li, C., Liu, Y., et al., 2015. Convergent functional architecture of the superior parietal lobule unraveled with multimodal neuroimaging approaches. Hum. Brain Mapp. 36 (1), 238–257. http://dx.doi.org/10.1002/hbm.22626 (PubMed PMID: 25181023; PubMed Central PMCID: PMC4268275).

Windhoff, M., Opitz, A., Thielscher, A., 2013. Electric field calculations in brain stimulation based on finite elements: an optimized processing pipeline for the generation and usage of accurate individual head models. Hum. Brain Mapp. 34 (4), 923–935. http://dx.doi.org/10.1002/hbm.21479 (PubMed PMID: 22109746).

Witkowski, M., Garcia-Cossio, E., Chander, B.S., Braun, C., Birbaumer, N., Robinson, S.E., et al., 2015. Mapping entrained brain oscillations during transcranial alternating current stimulation (tACS). NeuroImage http://dx.doi.org/10.1016/j.neuroimage.2015.10.024 (PubMed PMID: 26481671).

Xu, J., Moeller, S., Auerbach, E.J., Strupp, J., Smith, S.M., Feinberg, D.A., et al., 2013. Evaluation of slice accelerations using multiband echo planar imaging at 3 T. NeuroImage 83, 991–1001. http://dx.doi.org/10.1016/j.neuroimage.2013.07.055 (PubMed PMID: 23899722; PubMed Central PMCID: PMC3815955).

Zaehle, T., Rach, S., Herrmann, C.S., 2010. Transcranial alternating current stimulation enhances individual alpha activity in human EEG. PLoS One 5 (11), e13766. http://dx.doi.org/10.1371/journal.pone.0013766 (PubMed PMID: 21072168; PubMed Central PMCID: PMC2967471).

Zang, Y.F., He, Y., Zhu, C.Z., Cao, Q.J., Sui, M.Q., Liang, M., et al., 2007. Altered baseline brain activity in children with ADHD revealed by resting-state functional MRI. Brain and Development 29 (2), 83–91. http://dx.doi.org/10.1016/j.braindev.2006.07.002 (PubMed PMID: 16919409).

Zhan, Z., Xu, L., Zuo, T., Xie, D., Zhang, J., Yao, L., et al., 2014. The contribution of different frequency bands of fMRI data to the correlation with EEG alpha rhythm. Brain Res. 1543, 235–243. http://dx.doi.org/10.1016/j.brainres.2013.11.016 (PubMed PMID: 24275197).

Zhu, D., Chang, J., Freeman, S., Tan, Z., Xiao, J., Gao, Y., et al., 2014. Changes of functional connectivity in the left frontoparietal network following aphasic stroke. Front. Behav. Neurosci. 8, 167. http://dx.doi.org/10.3389/fnbeh.2014.00167 (PubMed PMID: 24860452; PubMed Central PMCID: PMC4026698).

Zou, Q.H., Zhu, C.Z., Yang, Y., Zuo, X.N., Long, X.Y., Cao, Q.J., et al., 2008. An improved approach to detection of amplitude of low-frequency fluctuation (ALFF) for resting-state fMRI: fractional ALFF. J. Neurosci. Methods 172 (1), 137–141. http://dx.doi.org/10.1016/j.jneumeth.2008.04.012 (PubMed PMID: 18501969; PubMed Central PMCID: PMC3902859).

Zuo, X.N., Di Martino, A., Kelly, C., Shehzad, Z.E., Gee, D.G., Klein, D.F., et al., 2010. The oscillating brain: complex and reliable. NeuroImage 49 (2), 1432–1445. http://dx.doi.org/10.1016/j.neuroimage.2009.09.037 (PubMed PMID: 19782143; PubMed Central PMCID: PMC2856476).